The luminescence properties of multinuclear platinum complexes†

Emma V. Puttock, Melissa T. Walden and J. A. Gareth Williams*

Department of Chemistry, Durham University, Durham, DH1 3LE, U.K.

† Invited contribution to special issue for 22nd ISPPCC, edited by A. Vlcek

* Author to whom correspondence should be addressed: j.a.g.williams@durham.ac.uk

Abstract

Platinum(II) complexes featuring conjugated aromatic ligands are widely studied in the context of luminescence. Many such compounds have been discovered that display intense phosphorescence from triplet excited states, offering potential applicability to numerous areas of contemporary interest, including as phosphors for light-emitting devices and imaging agents in cell biology. Aside the large number of mononuclear Pt(II) complexes that have been reported in the context of luminescence, there are several examples of multinuclear systems – ones that incorporate two or more Pt(II) ions or Pt(II) in combination with other platinum group metal ions. The introduction of a second metal ion can lead to very different luminescence properties compared to the mononuclear analogues. This review aims to provide an overview of some of the key features of multinuclear Pt(II) complexes and their luminescence. It proves to be convenient to subdivide the examples into three classes, according to whether or not there are significant intramolecular interfacial interactions between the square-planar units. In some cases (Class A), for example with aromatic bridging ligands, the units are rigidly held apart from one another and no such intramolecular interactions are possible. In some such complexes, however, the presence of a second metal ion can nevertheless lead to very different properties compared to mononuclear analogues. In particular, recent work has shown that large red shifts in absorption and emission can be accompanied by an increase in the phosphorescence radiative rate constant, offering a way to efficient red and near-infrared emitters. In Class B, on the other hand, the planar Pt(II) units are rigidly held in a conformation that facilitates interfacial interactions. In many cases they involve overlap of Pt $5d_{z2}$ and $6p_z$ orbitals, leading to the generation of low-energy ^{3}MMLCT excited states similar to those seen in aggregates of mononuclear Pt(II) complexes. Finally, complexes in Class C – of which there are very many and we cover only a selection of examples – are those in which there is some flexibility in the linkers between the Pt(II) units. They may display dual emission both from excited states that resemble those of the isolated units, and from lower-energy excited states similar to aggregates or excimers, owing to the ability of the Pt(II) moieties to approach one another in the appropriate conformation.

Keywords

Dinuclear complex; binuclear complex; multimetallic; phosphorescence; organic light-emitting device (OLED).

1. Introduction

The past 20 years has seen a huge increase in research into the luminescence properties of platinum(II) complexes and the synthesis of new complexes designed to display intense emission [1,2,3,4,5,6]. Prior to the 1990s, most studies had focused on complexes with diimine ligands such as bipyridine. Complexes such as $Pt(bpy)Cl_2$ were known to be luminescent in the solid state, but few were significantly so in solution. The development of cyclometallated complexes, for example those based on phenylpyridine (ppy) and related multidentate ligands, opened up more brightly luminescent systems with respectable quantum yields in deoxygenated solution at ambient temperature [2,4]. Owing to the high spin-orbit coupling (SOC) constant of platinum, intersystem crossing in low-molecular-weight Pt(II) complexes is typically much faster than fluorescence, and the triplet state T_1 is populated with high efficiency. Subsequent phosphorescence requires efficient SOC pathways to promote the formally forbidden $T_1 \rightarrow S_0$ process [7]. High quantum yields are also favoured by a high degree of rigidity to disfavour non-radiative decay [8]. These principles have been reviewed elsewhere, illustrated by numerous examples of mononuclear complexes [1–6].

Much of the research in this field since 2000 has been driven by applications such as triplet phosphors for organic light-emitting diodes (OLEDS) [9,10,11,12]; probes and labels for biological imaging, including time-resolved emission microscopy [13,14,15,16]; triplet sensitizers for triplet-triplet annihilation upconversion [17,18]; and optical sensors for molecular oxygen which rely on quenching of long-lived excited states [19].

In this contribution, we focus on the luminescence properties of *multinuclear* platinum(II) complexes – those which feature two or more Pt atoms per molecule, or which contain Pt(II) and one (or more) other platinum group metal centres such as Ir(III) or Ru(II). Interest in such systems has begun to increase rapidly over the past few years, and the majority of the examples included

here date since 2010, though not to the exclusion of pioneering earlier studies which underpin the recent work. We are not aware of any other reviews that deal specifically with this topic.

One of the ways in which Pt(II) complexes differ from those of other metals popular in the field of luminescence {*viz.*, the d^6 metal ions Re(I), Ru(II), Os(II), Rh(III), Ir(III)} is that they are normally 4-coordinate square-planar as opposed to 6-coordinate pseudo-octahedral. Planarity opens up the possibility of face-to-face interactions between complexes, which often play an important role in the photophysics of Pt(II) complexes. In the case of mononuclear Pt(II) complexes, such interactions may occur in the ground state, leading to aggregates, or in the excited state, leading to excimers, or both. Aggregates and excimers may display different emission properties – normally red-shifted – from those of the isolated monomers (see Section 3.1 for further discussion), and indeed the combination of monomer and excimer / aggregate emission has been the subject of much interest with regard to white light generation in OLEDs using a single phosphor [20,21]. In a *multinuclear* complex incorporating two or more distinct Pt(II) units that are covalently bound, such interactions may be possible *within* the molecule – *i.e.*, intramolecular versus intermolecular. Of course, whether they do occur will depend upon the separation and relative disposition of the units – whether they are linked in such a way that the necessary interactions can occur.

We have chosen to sub-divide the subject matter broadly according to whether or not such interactions occur in the complexes discussed, as illustrated schematically in Fig. 1. In the first section, we focus on systems with rigid linking units between the metal centres that do *not* offer the appropriate geometries for face-to-face interactions between the metal complex units (represented by case **A** in Fig. 1). The second section also deals with rigidly linked systems, but in this case, the rigid molecular conformation is one that *does* strongly favour ground and/or excited-state interactions between the metals and/or their aromatic ligands (case **B**). In these examples, aggregate-like or excimer-like emission predominates. Finally, in the third section, we describe a

representative selection of examples that feature flexible linkers between the metal units (case **C**). Many of the complexes in this category feature dual emission from mononuclear and binuclear excited states, and the ratio between them may be influenced by a range of environmental factors such as temperature and polarity.

< Figure 1 >

We should stress that our objective is not to produce an exhaustive survey of all luminescent multinuclear Pt(II) complexes reported to date, but rather to provide a survey of the different types of behaviour that may be observed, using a selection of representative examples. The discussion is confined to complexes featuring platinum in oxidation state +2, except for a few specific cases where conversion to +3 analogues occurs readily. Finally, it should be noted that we have restricted our coverage to complexes featuring at least one conjugated aromatic ligand. In such systems, crucial excited states are typically ones with a high degree of metal-to-ligand charge transfer (MLCT) character, owing to the presence of relatively low-energy π^* orbitals on the aromatic ligand. Purely "inorganic" materials, such as the famous dinuclear complex known as "platinum POP" – $[Pt_2(P_2O_5H_2)_4]^{4-}$ with bridging pyrophosphate ligands – and its relatives (e.g. with bridging phosphine ligands) are not discussed in detail here, but they have been extensively studied over many years [22,23,24]. Their photophysical and photochemical properties are dominated by metal-centred excited states, albeit unusual ones that involve molecular orbitals spanning both metal ions (see Section 3.1).

2. Complexes with rigid linkers unsuited to intramolecular face-to-face interactions

The common feature between the complexes discussed in this section is that the bridging units lead to an extended planar conformation, such that the metal units are held too far apart and in the incorrect disposition for face-to-face interactions to occur. Although aggregate- and/or excimer-

like properties are thus ruled out, the photophysical properties may nevertheless be very different from those of mononuclear analogues. Of particular interest in such systems is the question as to whether an increase in the efficiency of SOC may arise as a result of the introduction of a second metal ion. Although a definitive answer remains elusive, some of the systems show exciting potential for efficient red and NIR emission.

2.1 Complexes in which the metal ions are bound to a rigid, bridging bis-chelating heterocycle

Bis(2-pyridyl)pyrazines were used by a number of researchers in the 1990s to prepare multinuclear Ru(II) complexes [25,26,27]. They can act as bridging bis-chelating ligands that can offer *N^N* coordination simultaneously to two metal ions. In most examples, the remaining coordination sites were typically simple diimines such as bipyridine. In such systems, however, fast non-radiative decay was generally found to be problematic, typically leading to inferior emission compared to $[Ru(bpy)_3]^{2+}$. Structurally related bridging cyclometallating ligands that can offer bis-*N^C* as opposed to bis-*N^N* chelation have been developed much more recently, particularly by Kozhevnikov and co-workers. In their initial work, 4,6-di-(4-*tert*-butylphenyl)pyrimidine **1** was employed to provide such a bridging *N^C*-coordinating ligand [28]. The proligand **1** can undergo cycloplatination with one or two equivalents of K_2PtCl_4 to give a mono or dinuclear Pt(II) complex, **2** or **3** respectively, after treatment with sodium acetylacetonate (Fig. 2). Reaction of two equivalents of the mononuclear complex **2** with $IrCl_3.3H_2O$ allows access to a heterometallic complex **5** of composition Pt_2Ir, the properties of which may be compared with the analogous mononuclear iridium complex **4**.

< Figure 2 >

< Figure 3 >

The UV-visible absorption and emission spectra of the four complexes are shown in Fig. 3. The absorption spectrum of the dinuclear platinum complex **3** is quite different from its mononuclear counterpart **2**. It displays a very strong absorption band ($\varepsilon \sim 25\,000$ M^{-1} cm^{-1}) at substantially longer wavelength than the longest wavelength band of **2**, whilst a weak but well-defined low-energy band emerges at 530 nm, attributed to direct excitation to the triplet state. It is immediately clear that the dinuclear system does not behave simply as two interconnected, discrete mononuclear platinum units: if that were the case, the band positions would be expected to be similar to those of **2** albeit with higher ε values. A similar red-shift in absorption is observed for the heterometallic Pt_2Ir complex **5** compared to the mononuclear Pt and Ir models **2** and **4**.

All four of the complexes are highly luminescent in deoxygenated solution at room temperature, with Φ_{lum} in the range of 0.3 – 0.5 [*op. cit.*]. The trend of lower-energy emission upon introduction of additional metal ions – λ_{max} in the order **2** (Pt) < **3** (Pt_2) < **4** (Ir) < **5** (Pt_2Ir) – mirrors that observed for the lowest-energy absorption bands. Neither the dinuclear Pt_2 complex **3** nor the Pt_2Ir complex **5** shows any detectable emission bands corresponding to the mononuclear unit. As in absorption, then, the multinuclear systems are thus seen to behave as emitters that are intrinsically different from their constituent units. A combination of electrochemistry and time-dependent density functional theory (TD-DFT) calculations reveals that the trend to lower energy absorption / emission upon introduction of additional metal ions can be attributed primarily to stabilisation of the LUMO, to which the bridging pyrimidine ring makes a substantial contribution. The presence of *two* metal ions bound to the pyrimidine lowers the LUMO energy.

Of particular interest is the observation that the quantum yields do not fall off as the emission shifts to the red (see Table 1). The efficiency of most metal-based phosphors tends to decrease towards the red end of the spectrum, owing to increased non-radiative decay processes through coupling to low-energy vibrations, and often also to a lower degree of metal character in the excited state and

hence less efficient SOC. Some insight into the high emission efficiencies is offered through consideration of the radiative k_r and non-radiative Σk_{nr} decay constants estimated from the phosphorescence lifetimes τ and the Φ_{lum} values. It can be seen from a comparison of these data for **2** and **3** (Table 1) that the k_r value increases upon introduction of the second metal centre, despite the emission energy decreasing. Similarly, the presence of the platinum centres in the Pt_2Ir complex **5** is seen to enhance k_r compared to that of mono-iridium complex **4**, despite the emission energy of the former being lower. The value of k_r roughly doubles on going from **2** to **3** and likewise from **4** to **5**. Evidently, the $T_1 \rightarrow S_0$ radiative process is indeed promoted by the presence of the additional metal centres. Though it may be tempting to attribute this effect to the SOC associated with the extra metal ions relaxing the spin-selection rule, the researchers urge caution with such an interpretation. From a consideration of the extinction coefficients, it is clear that the $S_0 \rightarrow S_1$ process also increases in intensity from **2** to **3** and from **4** to **5** (by a similar 2-fold factor to the increase in k_r in each case), suggesting that the oscillator strength increases for spin-allowed transitions as well. TD-DFT calculations support this conclusion. An increase in the oscillator strength of ^{1}MLCT transitions to which the triplet state couples will increase the allowedness of the phosphorescent transition as will a decrease in the energy separation between the two states [7].

Table 1 Luminescence data for complexes **2**–**5**[(a)]

Compound (composition)	**Emission** λ_{max} **/ nm**	Φ_{lum}	τ **/ ns**	k_r **/ 10^5 s^{-1}**	Σk_{nr} **/ 10^5 s^{-1}**
2 (Pt)	513, 536sh	0.31	2100	1.5	3.3
3 (Pt_2)	550, 591, 647	0.54	1700	3.2	2.7
4 (Ir)	585	0.39	1000	3.9	6.1
5 (Pt_2Ir)	626	0.45	580	7.1	10

(a) In deoxygenated CH_2Cl_2 at 298 K; data from reference [28].

The same researchers have since reported on a related tetranuclear complex of composition Pt_3Ir, **7** (Fig. 4), which can be regarded as a tris-platinated derivative of the archetypal luminescent iridium(III) complex *fac*-$Ir(ppy)_3$ [29]. Compound **7** was obtained from the same proligand **1** as complex **5**, but in this case the synthetic procedure involved introduction of the iridium centre before the platinum, as opposed to the opposite sequence used in the preparation of **5**. The mononuclear iridium complex **6** was prepared and reacted with K_2PtCl_4 followed by treatment with sodium acetylacetonate to generate **7**. The absorption and emission bands of **7** are substantially red-shifted compared to those of *fac*-$Ir(ppy)_3$ – the emission λ_{max} from 508 to 611 nm in CH_2Cl_2 solution. The measured quantum yield of 0.76 for **7** renders it one of the most brightly emissive red phosphors reported to date. The high efficiency is favoured by an exceptionally high radiative decay constant $k_r > 10^6$ s^{-1}, almost double that of *fac*-$Ir(ppy)_3$. The trend thus mirrors that found for the earlier set of complexes, again with an increase in molar absorptivity, and similar trends for homo-multinuclear iridium(III) complexes investigated in related studies [30,31].

< Figure 4 >

The above complexes are based on the use of bis(phenyl)pyrimidines, where there is a *meta* relationship between the nitrogen atoms of the central heterocycle. Ligands based on bis(2-pyridyl)pyrazines – with a *para* relationship between the nitrogen atoms of the central ring – offer an alternative bridging unit. In a detailed study, Kozhevnikov, Williams and co-workers prepared and investigated a series of five dinuclear platinum(II) complexes based on such ligands (**9**–**13**), together with their mono-platinum counterparts and bis(phenyl)pyrimidine analogues (**8** and its mononuclear counterpart) for comparison (Fig. 5) [32]. The main observations and conclusions from the work can be summarised as follows.

(i) All of the complexes are significantly luminescent in deoxygenated solution at ambient temperature, with the dinuclear complexes emitting in the orange, red, or near-infrared (NIR) regions of the spectrum.

(ii) In the case of each bridging ligand, the emission of the dinuclear complex is red-shifted relative to its mononuclear counterpart, as observed for the pyrimidine complexes discussed above. Analysis of redox potentials and TD-DFT calculations again suggests that the lowering in energy of the excited state arises primarily from a stabilisation of the LUMO as opposed to any significant effect in the HOMO. Indeed, the emission energies correlate well with the reduction potential (Fig. 6) as do the energies of the lowest-energy absorption maxima.

(iii) For all of the systems in which k_r can be estimated with confidence, its value increases upon introduction of the second metal ion, despite the red shift.

(iv) Amongst the three isomeric complexes **8**, **9** and **10**, the two pyrazine-based systems **9** and **10** emit at lower energy than the pyrimidine-based complex **8**, with the 2,5-diphenylpyrazine complex slightly lower than its 2,3-diphenylpyrazine isomer.

(v) Extension of the conjugation in the heterocycle of **12** and **13**, and planarization of the aromatic system favoured by interannular bond formation in **11** and **13**, leads to further red shifts of the absorption and emission spectra to wavelengths in the deep-red / NIR that are unusually long for cyclometallated platinum(II) complexes.

Irrespective of the mechanism by which the additional metal ions exert their effect, it is clear from these studies that multinuclear Pt(II) and/or Ir(III)-containing complexes can offer an attractive route to efficient red and NIR emitters.

<Fig. 5>

<Fig. 6>

Carbene-based analogues of cyclometallating arylpyridine ligands have generated some interest for the development of luminescent platinum(II) complexes [33,34,35]. Strassner and co-workers made use of N-heterocyclic carbene ligands that coordinate in a C^C* fashion, where C* represents a charge-neutral N-heterocyclic carbene donor (equivalent to the pyridyl ring in ppy for example) [33]. The mononuclear complexes presented in their initial study showed luminescence in poly(methyl methacrylate) (PMMA) films with lifetimes of tens of microseconds, attributed to excited states of primarily ligand-centred character. A series of dinuclear complexes were subsequently presented (Fig. 7), in which the two Pt(II) centres are bound to the same, central phenyl ring, either in *para*-related positions (**14**–**17**) or *meta* to one another (**18**) [34]. The structures contrast with those of Kozhevnikov discussed above – where it is the heterocycle, rather than the metallated aryl ring, to which the two metal ions are both bound. The solubility of the acac derivatives **14** and **18** was too poor for study, but **15**–**17** were found to be intensely luminescent in PMMA films at room temperature, with λ(0–0) around 487 nm and quantum yields in excess of 0.75 in each case. Radiative rate constants were found to be around an order of magnitude higher than those of the previously investigated mononuclear complexes, which the authors suggest could again arise from "an additive effect of two heavy metal ions" enhancing SOC. No data were reported for the complexes in solution, however, so a direct comparison with conventional cyclometallated complexes cannot readily be made. An OLED incorporating **15** doped at 30% by mass into 2,8-bis(triphenylsilyl)-dibenzo[*b,d*]furan as the emitting layer displayed a maximum quantum efficiency of 8.5% [*op. cit.*].

<Fig. 7>

Crassous and co-workers have been pioneering the chemistry of luminescent complexes of d-block metal ions with helicene ligands, in which the chelate ring incorporating the metal ion becomes incorporated into the helicene [36,37]. Conventional helicenes are fascinating *ortho*-linked

polycyclic aromatics that are helically chiral owing to the twist induced by steric hindrance between aromatic rings; they may display very strong chiroptical properties (optical rotation and circular dichroism in the UV-visible region). Cyclometallated platinum(II) derivatives of helicences have been developed recently [38,39,40]. Normally, of course, Pt(II) complexes have planar conformations and so they are achiral, unlike complexes of d^6 metal ions with two or more bidentate ligands. But, upon binding to a helicene, the complexes become helically chiral. As with chiral systems in general, the challenge is to find a successful method to resolve the enantiomers. An elegant method involving the introduction of homochiral sulfoxide ligands has been described by Crassous' team, including the case of a dinuclear Pt(II) complex **21** generated using 1,8-di(2-pyridyl)naphthalene as a bridging, bis-*N^C*-coordinating ligand **19** (Fig. 8) [39]. Platination of **19** using (R_S,R_S)-$PtCl_2$(*p*-tolyl-MeSO)$_2$ (i.e. *R* chirality at the sulphur centres) leads to a pair of diastereomeric complexes **20** in which two Pt(II) ions are coordinated to the bridging ligand, with the coordination sphere of each metal ion being completed by a chloride and sulfoxide. The diastereoisomers (*P*,R_S,R_S)-**20** and (*M*,R_S,R_S)-**20** were formed in a 1 : 1.5 ratio, suggesting that the cycloplatination is diastereoselective. The former could be resolved from the mixture by crystallisation, whilst the latter could be obtained in pure form by chromatography of the supernatant. The crystal structure of (*P*,R_S,R_S)-**20** confirms the helical topology, with a helicity angle between the pyridyl rings of 58.8˚, similar to carbo[6]helicenes. Thus, the two almost planar platinacycles are incorporated into the helical backbone. In a final step, the chloride and sulfoxide ligands could be replaced by acac, without racemisation, giving the pair of enantiomers *P*-**21** and *M*-**21**.

The complexes, **21**, are luminescent in the red region of the spectrum: λ_{max} = 633 nm in CH_2Cl_2, Φ_{lum} = 0.13 and τ = 19.7 μs [*op. cit.*]. The quantum yield is a little higher than that of a comparable mono-platinahelicene but the difference is not much more than the uncertainty on the values. Of most interest are the chiroptical properties. The complexes display circularly polarised luminescence, with the *P* and *M* enantiomers displaying luminescence dissymmetry factors g_{lum} of

+0.0005 and –0.0005 respectively (Fig. 9). Though the values are small, their opposite signs confirm that the emitted light is polarised in opposite directions for the two enantiomeric forms.

<Fig. 8>

<Fig. 9>

Many platinum(II) salen complexes of the form Pt(O^N^N^O) are known to be luminescent [41]. Houjou *et al.* have recently described the synthesis, crystal structure and optical properties of a dinuclear fused salen complex **23**, incorporating a naphthalene-based *bis*-N^O-coordinating bridging ligand, **22**, prepared as shown in Fig. 10 [42]. The complex displays substantially red-shifted absorption and emission compared to the closely related mononuclear complexes **24** and **25**, tailing well into the NIR (Fig. 11). The authors suggest that "a virtual expansion of the π-conjugated system" upon coordination of the two Pt(II) ions generates a fused quasi-aromatic ring system analogous to chrysene. Despite the presence of short Pt···Pt interactions of 3.43 Å in its crystal structure, the close resemblance of the emission of **23** in the solid state compared to solution (only a small red-shift) suggests that there is no emission from aggregate-like states in the solid (*cf.* Section 3). Unfortunately, no quantum yield data were presented that might have allowed comparison of the efficiency with the mononuclear complexes or with other dinuclear structures.

< Figure 10 >

< Figure 11 >

Platinum(II) complexes with tridentate N^N^C-coordinating phenylbipyridine (phbpy) derivatives have become a popular class with respect to luminescence, following pioneering work of Che and co-workers in the late 1990s [43,44]. In complexes of the form Pt(N^N^C)Cl, the monodentate chloride can be replaced by a variety of mondentate ligating units. The introduction of an acetylide

in place of chloride augments the ligand field strength and serves to raise the energy of potentially deactivating d-d states, leading to increases in emission efficiency. Yao and co-workers have synthesised an interesting bridging ligand – 2,3-di(2-pyridyl)-5-phenylpyrazine, **26** – which can simultaneously offer a bidentate N^N and a tridentate N^N^C binding site for two metal ions (Fig. 12) [45]. Reaction of **26** with *cis*-$Ru(bpy)_2Cl_2$ leads to coordination through the N^N site to generate **27**, leaving the N^N^C site available for complexation to Pt(II) upon treatment with K_2PtCl_4 giving **28**, subsequently converted to the acetylide adduct **29**. The Ru(II) complex **27** shows emission typical of the ^{3}MLCT excited states of tris-bipyridyl ruthenium complexes, red-shifted to λ_{max} 695 nm compared to about 630 nm for homoleptic $[Ru(bpy)_3]^{2+}$; the shift can be readily understood in terms of the lower π^* orbitals expected for a pyrazine compared to a pyridine ring. In the heterometallic dinuclear complex **28**, on the other hand, the emission is further red-shifted to λ_{max} = 750 nm. DFT studies suggest that the lowest MLCT transitions are mainly associated with the platinum-acetylide moiety, and so the NIR emission is attributed to excited states largely localised on this unit, with essentially quantitative energy transfer from the Ru-based ^{3}MLCT excited state. The emission is strongly red-shifted compared to Py(phbpy)(-C≡C-Ph), which is again readily understood in terms of the π^* orbitals of the bis-coordinated bridging ligand being lower in energy than those of phbpy. In contrast to the Kozhevnikov complexes, though, the red shift is accompanied by a large decrease in Φ_{lum} to 0.4% for **28** (MeCN at room temperature).

< Figure 12 >

As noted at the beginning of Section 2.1, bis(2-pyridyl)pyrazine (dpp) has previously been popular for the generation of multinuclear Ru(II) complexes, acting as a *bis*-N^N-coordinating ligand. But, in Pt(II) chemistry, N^N-coordinated complexes typically have inferior emission properties compared to those of cyclometallated analogues. Nevertheless, Pt(II) moieties of the form $Pt(N^N)Cl_2$ have long been of interest as redox catalytic sites, for example, in reduction of water to

oxygen [46]. In this field, the objective of coupling of such units to light-absorbing diimine-ruthenium units for photocatalysis has inspired the synthesis of a number of elegant multinuclear Ru-Pt multinuclear complexes. Much of the work dates back to the 1980s and 1990s [47,48,49], and has been the subject of an excellent review in 2013 in this journal by the late Karen Brewer [50]. The continued interest in photocatalysed water splitting means that further examples continue to appear. Indeed, attention is turning increasingly to cyclometallated Ir(III) complexes in place of Ru(II)-based sensitizers, owing in part to the rational tunability of their excited states through ligand modification. A recent example is provided by the work of Kang and co-workers, who prepared $[Ir(ppy)_2(\mu\text{-dpp})PtCl_2]PF_6$ **31** (together with its analogue with F_2ppy in place of ppy; Figure 13) and corresponding homodinuclear Ir complexes [51]. The strong luminescence typically observed for $[Ir(N^C)_2(N^N)]^+$ complexes is quenched in these dinuclear complexes by thermally activated population of Pt and/or Ir-based d-d states, which results in cleavage of the Pt–dpp and/or Ir–dpp bonds and thus to photoinduced dissociation of the bimetallic complexes. The Ir-based ^{3}d-d states appear to be lowered in energy upon complexation of the Pt centre to the dpp. The researchers accounted for this effect with reference to the crystal structures, which show that the torsion angle between the uncoordinated pyridine and the pyrazine ring in the mononuclear Ir(III) complex **30** is reduced upon binding to Pt(II); *i.e.*, the interannular bond twists towards a more coplanar conformation of the dpp. This is thought to exert a steric constraint at each metal centre that leads to the observed photochemical instability. At 77 K, the complexes are luminescent, and the emission properties are then typical of $[Ir(N^C)_2(N^N)]^+$ complexes having a low-energy $\pi^*_{N^N}$ ligand (λ_{max} = 670 nm, τ = 1.6 μs in 2-MeTHF) [*op. cit.*].

< Figure 13 >

2.2 Complexes in which the metal ions are bound to a bridging ligand where rotation is possible around connecting bonds

Like its near neighbours in the periodic table, such as gold and mercury, Pt(II) is "soft" in its coordination chemistry, and has a strong affinity for sulphur ligands. Numerous dinuclear Pt(II) complexes bridged by thiol-containing ligands have been known for many years. In several of these systems, the Pt(II) centres are brought into close proximity in such a conformation that intramolecular Pt···Pt interactions are strongly favoured; examples of those are discussed in Section 3. Uosaki and co-workers obtained a trinuclear platinum complex **33** upon treatment of $[Pt(tpy)OH]^+$ with the commodity chemical 1,3,5-triazine-2,4,6-trithiol (Fig. 14) [52]. They also prepared three related dinuclear complexes **32a-c** in a similar way using 2-substituted triazine-dithiols. No base was required to deprotonate the thiols. The multinuclear complexes were obtained in significant proportions even when using sub-stoichiometric amounts of the Pt(II) precursor (*e.g.,* as low as 1:1 for **33**, compared to the stoichiometric ratio of 3:1), reflecting the high affinity of Pt(II) for the thiolate ligand. X-ray crystallography of **32a** and **32c** revealed that a mutually *syn* conformation of the Pt(tpy) units is adopted in the solid state. But, although the PtN_3S planes are quite close to being parallel to one another, the intramolecular Pt···Pt distances {4.350(1) and 4.255(1) Å for **32a** and **32c**, respectively} are too long to allow any significant intermetallic interactions within the molecules. Indeed, intermolecular distances are shorter: in **32c** they are 3.663(1) Å and in **32a** there are alternate short and long distances of 3.641 and 4.352 Å (Fig. 15). The complexes are weakly emissive in deoxygenated solution at ambient temperature: quantum yields are reported to be < 0.01, with emission maxima between 620 and 640 nm. The combination of electrochemical and DFT data suggests that the emission may be assigned to charge-transfer states from the Pt/triazine unit to the terpyridines, in line with well-established conclusions on mononuclear platinum complexes featuring the combination of diimine and thiolate ligands [53]. Yet, despite the lack of a major influence of the substituents in the triazine ring on the absorption and emission, two distinct reduction waves at around –0.70 V are observed in the binuclear complexes associated with sequential terpyridine reduction, indicating that the triazine dithiolates do mediate a degree of electronic coupling between the Pt(II) centres.

< Figure 14 >

< Figure 15 >

Phosphines are also good ligands for Pt(II) and, just as for thiolates, binuclear complexes can be obtained by using bis-phosphines. Many examples have sufficient flexibility in the bis-phosphine backbone to allow interfacial interactions and MMLCT (see Section 4), but a recent study made use of a rigid phosphine, bis(diphenylphosphine)acetylene (dppac), which enforces a linear structure [54]. The binuclear complexes studied have the structure $\{Pt(N^C)Ar\}_2(\mu$-dppac), where N^C is cyclometallated ppy or benzo[*h*]quinoline (bzq), and Ar is *para*-tolyl or *para*-anisyl. All four complexes display structured luminescence in the solid state with λ(0-0) around 480 nm; the bzq complexes are also emissive in CH_2Cl_2 solution at room temperature, and the emission is attributed to excited states of d(Pt)/π(N^C) $\rightarrow$ π^*(N^C) character. Such an assignment would suggest that the presence of the second metal ion might have rather little effect, but no direct mononuclear analogues were reported in the study that might have allowed the influence – if any – of the second metal to be probed. Dppac was also used in an earlier study to generate some unusual binuclear complexes of composition $\{Pt(S^S)\}_2(\mu$-dppac$)_2$, featuring *two* bridging dppac ligands [55]. Here, S^S represents a chelating aromatic dithiolate, *viz.*, 1,2-benzenedithiolate, 3,4-toluenedithiolate or 1,4-dichlorobenzene-2,3-dithiolate; only in the third case was any detectable luminescence observed (λ_{max} = 610 nm in the solid state at 298 K).

A pair of heterodimetallic Pt–Ir complexes linked through a pyridyl ring have been reported by Bronner *et al.* [56]. The Ir moiety is an Ir(ppy)$_2$(*N^N*-dipyrrin) complex with a pendant 4-pyridyl ring at the central position of the dipyrrin, which is available to bind to a Pt(*C^N^C*-dppy) unit (dppy = 2,6-diphenylpyridine) (Fig. 16). The monoanionic dipyrrin unit features in the well-known class of bright and tunable fluorophores known as BODIPYs (boron dipyrromethenes) wherein it is

bound to a BF_2 group; rotation of centrally-appended rings is established as an important non-radiative decay pathway in such molecules [57]. The two complexes, **34** and **35**, differ from one another in that **35** features flanking methyl groups that will inhibit such interannular rotation relative to **34**.

Study of the corresponding mononuclear Ir(III) complexes without the coordinated Pt unit and of Pt(dppy)(DMSO), used as models, reveals that there is good spectral overlap of the emission of the latter with a strong absorption band of the former. The photophysical study of the binuclear complexes confirms that energy transfer from the Pt(II) unit to the Ir(III) unit occurs, with an efficiency estimated to be > 90%. The Ir-based emission in **34** is red-shifted compared to **35** (λ_{max} = 741 and 705 nm respectively in dichloromethane), which is attributed to the fact that a more planar conformation of the pyridyl ring with the dipyrrin unit will be possible in **34**, extending the conjugation and possibly introducing more ^{3}ILCT character into the excited state. Moreover, the quantum yield and lifetime of the Ir-based emission of **34** are around 30 times smaller than for the methylated analogue **35** (for which Φ_{lum} = 0.0029 and τ = 337 ns) owing to a two-orders-of-magnitude increase in the non-radiative decay constant k_{nr}. This is attributed to the efficiency of interannular rotation in **34** as a source of non-radiative decay, just as for BODIPYs.

< Figure 16 >

Acetylacetonate ($acac^-$) has been widely used as a monoanionic "ancillary" ligand in both Pt(II) and Ir(III) complexes for luminescence, for example, in complexes such as Pt(ppy)(acac) and $Ir(ppy)_2(acac)$ and derivatives thereof. The term "ancillary" indicates that the ligand's role is largely to complete the coordination sphere of the metal: it does not have a significant effect on the photophysics, since the excited states are localised on the metal and N^C ligand. Thompson and co-workers used a C–C-linked "back-to-back" bis-*O^O*-coordinating version of $acac^-$, namely sym-

tetraacetylethane (tae), to prepare a range of dinuclear Pt(II) complexes of the general composition (*N^C*)Pt(μ-tae)(*N^C**), represented as **36** in Fig. 17 [58]. The two N^C ligands may be the same as one another (homodyads) or different from one another (heterodyads). In the former case, the emission energies were very similar to those of corresponding mononuclear Pt(*N^C*)(acac) complexes, but with *N^C* = 2,6-difluorophenylpyridine (dfppy), there was evidence for an increase in k_r, attributed to an increase in the oscillator strength of ^{1}MLCT state to which the triplet is coupled and/or a decrease in the energy separation between the two states. In the heterodyads, efficient energy transfer is observed from the higher-energy Pt(*N^C*) unit to the lower one, probably in a Dexter-mediated process. The same ligand was also used by Bruce and co-workers in the synthesis of a heterometallic Pt-Ir complex, **37** (Fig. 17), designed for liquid crystalline properties [59]. It displays Ir-based emission, irrespective of the excitation wavelength, indicative of fast energy transfer from the higher-energy Pt(*N^C*) excited state to that associated with the Ir(*N^C*)$_2$ unit.

< Figure 17 >

3. Complexes in which intramolecular face-to-face interactions are rigidly maintained by the bridging unit

Face-to-face interactions between square planar Pt(II) complexes play an important role in defining the properties of many Pt(II) compounds, especially in the solid state and in aggregates. They may involve Pt···Pt interactions and/or π-π interactions between conjugated ligands. A molecule incorporating two (or more) planar Pt(II) units may be subject to such interactions intramolecularly – as opposed to intermolecularly – but only if the geometry is suitable to bring the units into the required disposition with respect to one another. In this section, we summarise some examples in which a rigid conformation either enforces or at least favours the attainment of such a geometry.

We first briefly review the underlying molecular orbital theory that accounts for the tendency of square-planar Pt(II) complexes to form dimers or aggregates.

3.1 Molecular orbital description of Pt···Pt interfacial interactions

The stabilisation arising from bringing two Pt(II) units together is attributable (in part) to the σ overlap of $5d_{z^2}$ and $6p_z$ orbitals of adjacent metal centres. The two $5d_{z^2}$ orbitals generate a pair of bonding and antibonding MOs of a_{1g} and a_{2u} symmetries respectively, both of which are filled by a pair of electrons (Fig. 18a). Configuration interaction with MOs of the same symmetry formed by overlap of the vacant $6p_z$ orbitals results in stabilisation of the $5d_{z^2}$ MOs, decreasing the total energy (Fig. 18b). In the case of dinuclear complexes without any aromatic ligands that introduce low-energy π* orbitals, the MO diagram of Fig 18b is largely sufficient for an appreciation of the photophysical properties. For example, the archetypal pyrophosphate-bridged compound $[Pt_2(P_2O_5H_2)_4]^{4-}$ (PtPOP), mentioned at the end of Section 1, displays a strong ground-state absorption band at around 370 nm, due to the spin-allowed $a_{2u} \rightarrow a_{1u}$ ($d\sigma^* \rightarrow p\sigma$) transition, together with a weaker band at about 460 nm assigned to the corresponding spin-forbidden transition.[22–24] The resulting $^1A_{2u}$ and $^3A_{2u}$ excited states display, respectively, weak, short-lived fluorescence at around 400 nm, and intense green phosphorescence on the microsecond timescale centred at around 520 nm (in deoxygenated aqueous solution). An experimentally observed increase in the frequency of the Pt–Pt symmetric stretching vibration in the excited states is consistent with the MO picture of promotion of an electron from an antibonding dσ* orbital into a bonding pσ orbital and, indeed, recent experiments have dramatically demonstrated the shortening of the Pt···Pt distance in the excited state.[24]

When dealing with the intermolecular interactions between mononuclear Pt(II) complexes featuring aromatic ligands, the same molecular orbital approach can be employed. But the presence of aromatic ligands introduces additional π and π* orbitals into the MO description (Fig. 18c). The

relative energies of the orbitals compared to those based on metal will depend on the identity of the complex. It is clear, though, that the gap between highest occupied and lowest unoccupied orbitals is reduced compared to isolated molecules, accounting for the red-shifted absorption and emission of aggregates relative to the isolated molecules. The low-energy absorption that is introduced in this way is typically described as a metal-metal-to-ligand charge transfer transition (MMLCT or dσ*–π*), as in the example of Fig. 18c, though π-π* transitions may equally well account for such effects, according to the relative energies of the MOs.

< Figure 18 >

Excimers differ from aggregates and excimers in that the favourable interactions occur only in the excited state: an excited monomer is stabilised through interaction with a ground-state monomer. Upon return to the ground state, the dimeric species is unstable relative to the isolated molecules, so it instantaneously dissociates. Excimer emission is red-shifted compared to the monomer, broad and structureless. Since the excimer does not pre-exist in the ground state, there are no additional ground-state absorption bands in this case. Excimer formation in Pt(II) complexes with conjugated ligands is probably little different from that of well-known planar organic molecules such as pyrene, and mostly likely involves contributions from π / π and π */ π* interactions: Pt···Pt interactions are not necessarily required.

3.2 Sulphur-containing bridging ligands

As noted in Section 2, thiolates are good ligands for Pt(II) and Eisenberg examined the photophysics of complexes of the form Pt(N^N)$(SR)_2$ in the mid-1990s [53]. By using a 1:1 as opposed to 2:1 RS^- : Pt ratio in the synthesis, Che and co-workers subsequently showed that pyridine-2-thiolate (pyS^-) could act as a bridging ligand between two bpy-coordinated Pt(II) ions, generating $[Pt(N^{\wedge}N\text{-}^{t}Bubpy)(\mu\text{-}pyS)]_2^{2+}$ [60], similar to earlier work on thiolate-bridged Pt(en) units

by Ooi and colleagues [61]. The theme was taken up by Kato *et al.*, who isolated two different forms of [Pt(bpy)(μ-pyS)]$_2$(PF$_6$)$_2$, **38**, *viz.*, an *anti* isomer – with a head-to-tail arrangement of the two pyS$^-$ bridging ligands and an N$_3$S coordination environment around each Pt centre – and a *syn* isomer – with head-to-head pyridinethiolates, where one Pt ion is bonded to four nitrogen atoms whilst the other has N$_2$S$_2$ coordination (Fig. 19) [62]. Crystals of the *anti* isomer – which has a Pt–Pt distance of 2.997(1) Å – display intense orange emission at room temperature (λ_{max} = 603 nm, τ = 240 ns), whilst the *syn* form is red-shifted (λ_{max} = 644 nm) and has a shorter Pt–Pt distance of 2.923(1) Å. The red-shift that accompanies the shortening of the intermetallic distance is consistent with a ^{3}MMLCT assignment, since the highest filled dσ* orbitals will be raised as the interaction between the Pt ions becomes stronger.

< Figure 19 >

More recently, a number of groups have turned their attention to related bridged dinuclear structures featuring cyclometallated Pt(N^C) units in place of Pt(N^N), which has led to some brightly emissive systems in solution. A selection of these compounds are shown in Fig. 20 with key photophysical data [63,64,65,66,67,68,69,70].‡ They have generally been prepared from the readily accessible chloro-bridged precursors of type [Pt(*N^C*)(μ-Cl)]$_2$ or from Pt(N^C)Cl(HN^C) mononuclear complexes. They invariably have a head-to-tail arrangement of the bridging ligands (in contrast to *syn*-**38** for example), which can be attributed to the strong *trans* influence of the carbanion of the cyclometallating ligand. All show deep red luminescence in solution, attributable to the dσ* $\rightarrow$ π*$_{N^C}$ MMLCT excited states, in many cases with high quantum yields, perhaps reflecting the high degree of molecular rigidity which will serve to inhibit non-radiative decay. Compounds **46** and **47** have been successfully tested as red emitters in phosphorescent OLEDs.

‡ The complexes **42** and **44** were depicted in the original articles by Balashev and colleagues with inclusion of a Pt–Pt bond and explicitly described as comprising a metal–metal bond [63–64]. Our view is that such a description is not fully compatible with the MO description of the Pt(II)···Pt(II) interaction (Section 3.1) that suggests a formal bond order of zero (notwithstanding the influence of configuration interaction).

< Figure 20 >

The complexes are readily oxidised, leading to Pt(III)–Pt(III) systems featuring a Pt–Pt bond (*cf.* Fig. 18a: removal of electrons from the dσ* orbital leads to a bond order of 1). For example, **39** and **40** form **48** and **49** respectively [65], whilst **41** reacts with halogens Cl_2, Br_2 or I_2 to give the corresponding dihalodiplatinum(III) compounds **50** with the sixth coordination site of each Pt occupied by a monodentate halide [67] (Fig. 21). The Pt(III) dinuclear complexes are not luminescent in the visible region, though it may be noted that studies by Yam and colleagues have shown that structurally related dinuclear Pt(III) complexes emit in the NIR region from metal-centred dσ-dσ* states with some CT character [71].

< Figure 21 >

3.3 Acetamidate, amidinate and pyrazolate bridging ligands

Kato and co-workers have isolated some intriguing binuclear structures related to those of **38**, but featuring head-to-tail acetamidate bridges, and including a fascinating mixed valence "trimer of dimers" **51** (Fig. 22) in which the formal oxidation state of Pt is 2.33 [72]. This compound was isolated following a procedure in which the well-known chloro-bridged dimer $[Pt(ppy)(\mu\text{-}Cl)]_2$ was first treated with Ag^+ in CH_3CN to generate $[Pt(ppy)(MeCN)_2]^+$ and then subject to base hydrolysis of the nitrile ligands using aqueous NaOH in the presence of oxygen. It has a bowed structure and its formation is apparently favoured by the synergistic combination of Pt···Pt interactions, π-π interactions and hydrogen bonding between the acetamidate ligands (dotted lines in Fig. 22). The Pt–Pt distances at the ends are around 0.2 Å shorter than the others, suggesting that the most appropriate formulation of oxidation states is Pt(III)–Pt(II)–Pt(II)–Pt(II)–Pt(II)–Pt(III). Electrochemical or chemical reduction (with Cp^*_2Co) allows the $Pt(II)_2$ compound **52** to be

obtained, whilst the $Pt(III)_2$ form with terminal chlorides **53** has also been isolated and structurally characterised. Only the $Pt(II)_2$ form is luminescent, showing a broad emission band centred at 643 nm in the solid state at room temperature, $\Phi_{lum} = 0.14$, $\tau = 1.4$ μs.

< Figure 22 >

Meanwhile, amidinate ligands, formed by deprotonation of Ph–N=CH–NH–Ph, have been used to prepare related $Pt(II)_2$ structures featuring charge-neutral C^C*-coordinating N-heterocyclic carbenes as opposed to anionic phenylpyridines. The compounds **54** and **55** (Fig. 23) emit at 561 and 596 nm respectively in PMMA film (2 wt %) at room temperature, with high quantum yields > 0.8 and very high radiative decay rates, although as for the carbene complexes of Section 2, there is no data on solution-state emission [73].

< Figure 23 >

A series of dinuclear complexes of the composition $[Pt(dfppy)(\mu\text{-}pz')]_2$ **56**, featuring a pair of deprotonated pyrazole rings *pz′* as anionic bridging ligands, were studied by Thompson and co-workers [74]. Four pyrazoles of increasing steric bulk were used: pyrazole, 3,5-dimethylpyrazole, 3-methyl-5-*tert*-butylpyrazole and 3,5-bis(*tert*-butyl)pyrazole. Their crystal structures reveal a boat-like conformation that brings the two Pt atoms relatively close together (Fig. 24). The bulky substituents on the pyrazoles force the Pt(dfppy) units even closer: the Pt–Pt distances range from 3.3763(7) Å for *pz′* = pyrazole to 2.8343(6) Å for 3,5-bis(*tert*-butyl)pyrazolate. The extent of Pt···Pt interactions are enhanced accordingly, as evident from the effect on the photophysical properties. The complexes with one and two *tert*-butyl substituents are orange and red, respectively, with low-energy absorption bands between 400 and 500 nm that have no counterpart in the other two dimers or in model mononuclear analogues, which are yellow. The additional bands are assigned to

$d\sigma^* \rightarrow \pi^*_{N^C}$ MMLCT transitions. Similarly, in the 77 K emission spectra, these two complexes display a broad, structureless low-energy band, typical of emission from such an excited state, whereas the other two have vibrationally structured bands at higher energy, more typical of the mononuclear complexes. In fluid solution, all four complexes are able to access the MMLCT excited state, giving the red emission. More recent studies on the unsubstituted pyrazole system have highlighted the activation barrier for accessing the MMLCT state from the initially formed excited state in a process that has been compared to the flapping of a butterfly's wings [75, 76].

< Figure 24 >

3.4 Rigid aromatic bridges: xanthenes and related polycyclic units

Cárdenas and co-workers described a dinuclear Pt(II) complex **58** in which two Pt(N^N^C) units were tethered by a 4,5-diethynylxanthene bridge (Fig. 25) [77]. The synthesis is facilitated by the previsouly mentioned ease with which Pt(N^N^C)Cl complexes undergo metathesis with alkynyl ligands. The emission of **58** is strongly red-shifted compared to the mononuclear counterpart **57**; λ_{max} = 626 and 817 nm respectively, in CH_2Cl_2 at room temperature (Fig. 26a). Emission from **58** is tentatively attributed to a MMLCT state; its excitation spectrum does show some enhanced absorption to long wavelength of the lowest energy absorption band, compared to **57**, suggesting some weak ground-state interaction between the Pt units. The quantum yield of **58** is reduced compared to **57**, primarily owing to the expected increased non-radiative decay rate as the excited state energy decreases. There is no evidence in this case of a beneficial effect of the second metal ion in augmenting k_r. A heterometallic Pt-Au version was also prepared, **59**, incorporating a Au(C^N^C) unit in place of one of the Pt(N^N^C) units. The emission properties of this compound closely resemble those of **58** (Fig. 26b), and there is no evidence of higher-energy emission associated with the Au(C^N^C) unit (for which λ_{max} = 490 nm in the corresponding mononuclear complex), irrespective of the excitation wavelength. It is concluded that excitation of the

Au(C^N^C) unit is followed by fast energy transfer to the Pt(N^N^C) unit, no doubt favoured by good spectral overlap and the close proximity of two units.

< Figure 25 >

< Figure 26 >

A xanthene backbone had previously been used by Develay and Williams to bring together two Pt(N^C^N) units, in this case *via* C–C bond formation to the 4-position of the central aryl ring of 1,3-dipyridylbenzene (dpyb) as an N^C^N unit, compound **61** (Fig. 27) [78]. The mononuclear complex Pt(dpyb)Cl and many of its derivatives are well known to form brightly luminescent excimers [79]. On the other hand, there is no evidence for propensity to MMLCT formation in such complexes (in contrast to isomeric complexes with phenylbipyridines), nor are there close Pt···Pt contacts in their crystal structures. It is interesting in this context to note the behaviour of **61**. It displays a broad, low-energy emission band centred at 690 nm in CH_2Cl_2 at room temperature, Φ_{lum} = 0.20, compared to λ(0-0) = 491 nm for Pt(dpyb)Cl and 510 nm for the mononuclear model **60**. The emission is similar to the excimeric emission of Pt(dpyb)Cl observed at elevated concentrations. Upon cooling to 77 K, the red emission band of **61** disappears and a structured green emission is seen, resembling that of Pt(dpyb)Cl. Such behaviour is inconsistent with an MMLCT state, since a decrease in temperature should normally favour the Pt···Pt interaction. The authors interpreted the results in terms of an excimer-like excited state being responsible for the room-temperature red emission, the attainment of which requires some conformational change relative to the ground state in a process that is inhibited at 77 K.

Work by Chan and colleagues compared xanthene, as a backbone for linking Pt(salphen) units, to dibenzofuran and biphenylene, structures **62**, **63** and **64** respectively (Fig. 28) [80]. Crystal structures of **62** and **64** showed that the Pt(salphen) units are twisted relative to the plane of the

bridging aromatic unit (torsion angles of 43º and 36º respectively). In **62**, despite the intramolecular interplanar separation (defined as the mean separation between Pt and the adjacent N_2O_2 plane) being only 3.22 Å, the twist leads to the Pt atoms being displaced relative to one another, leading to a much longer Pt–Pt distance of 5.012(2) Å. In **64**, on the other hand, the Pt atoms are held closer to one another, with an intramolecular Pt–Pt distance of 3.359 Å. Though shorter, this is only short enough for weak Pt···Pt interaction. No crystal data was available for **63**, but a larger interplanar distance can be expected, given the shape of the dibenzofuran bridge. All three complexes emit at similar energies in solution at room temperature (around 635 nm): there is no evidence of MMLCT excited states. The quantum yield of **63** is, however, an order of magnitude higher than **62** and **64**, which is attributed to π-π quenching processes in the latter two complexes, facilitated by the closer separations of the Pt(N_2O_2) units.

< Figure 28 >

4. Dinuclear complexes with flexible bridging ligands

Dinuclear complexes with flexible bridging ligands may feature intramolecular Pt–Pt and/or π-π interactions if an appropriate conformation is attained. An early example is provided by the work of Che, who explored the use of bidentate and terdentate phosphines, of varying length, to bridge between two or three Pt(N^N^C) units (Fig. 29) [81]. When bis(diphenylphosphino-methane) (dppm) is used as the bridge (one carbon spacer, complex **65**), low-energy, structureless emission is observed in solution. The bridge holds the two Pt units sufficiently close and in the appropriate face-to-face conformation for Pt···Pt interactions in solution: emission is assigned to the ^{3}MMLCT excited state. When longer bridges are used (3 or 5 carbon spacers, complexes **66** and **67** respectively), emission characteristic of the ^{3}MLCT state is restored. The length and nature of the

linking unit is seen to be crucial in determining the scope for intramolecular interactions and thus the nature of the emission. More recent work has examined how environmental factors can affect the equilibrium between the monomer-like and dimer-like excited states, examples of which are addressed in the sub-sections that follow.

<Figure 29>

4.1 Gelation and Aggregation

Aggregation and self-assembly through intermolecular interactions in dinuclear complexes can give rise to gelation-induced phosphorescence (GIP) and aggregation-induced emission (AIE). Gels have solid-like rheology and do not flow, despite being predominantly liquid in composition [82]. They are typically formed by slow cooling from a solution above the sol-gel transition temperature (T_{gel}) where a material changes from a liquid to a gel. Recently there has been increased interest in the photophysical properties of mononuclear metallogellating Pt complexes on the sol-gel phase transition [83,84,85], but there are very few examples of binuclear Pt(II) complexes which display the same phenomenon.

Ultrasound-induced aggregation resulting in the GIP of dinuclear Pt complexes has been investigated by Naota *et al.* [86]. This phenomenon describes materials which readily form gels when subject to sonication. They synthesised a series of chiral, peg-shaped *trans*-bis(salicylaldiminato)Pt(II) complexes doubly linked with polymethylene spacers. Synthesis of these complexes was achieved by reflux of $PtCl_2(CH_3CN)_2$ with the corresponding N,N'-bis(salicylidene)-1,n-alkanediamine (n = 5–7, corresponding to complexes **68a**, **b** and **c** respectively) in dimethyl sulfoxide (DMSO) and toluene to afford achiral *syn* and racemic mixtures of chiral *anti* isomers (Fig. 30). These were separated readily by silica gel column chromatography. Optically pure (100% ee) complexes, (+) *anti*-**68a**, (-) *anti*-**68a**, (+) *anti*-**68c** and (-) *anti*-**68c** were

obtained from racemic mixtures using a HPLC chiral column. All solutions of complex **68** in organic solvents were non-emissive at room temperature, but ultrasound-induced gels from racemic mixtures of chiral (±)*anti*-**68a**, (±) *anti*-**68c**, and (+) *anti*-**68c** displayed intense yellow phosphorescence.

<Figure 30>

The emissive gels which formed were stable at room temperature but could be reverted to their original non-emissive solution on heating above their t_{gel}. Moreover, extended sonication resulted in more intense emission for complexes (±) *anti*-**68a** and (+) *anti*-**68c**. Quantum yields for complexes (±) *anti*-**68a** and (+) *anti*-**68c** were found to be highest measured at 77 K with values of 20 % and 34 % respectively.

<Figure 31>

Emission was only observed after ultrasound-induced aggregation whilst complexes which formed spontaneous gels displayed no emission (Fig. 31). Scanning electron microscopy (SEM) revealed the formation of colloidal aggregates for solutions of racemic *anti*-**68a** and *anti*-**68c** (Fig. 32). Following ultrasound irradiation, this spherical morphology changed to long and thin fibres (ca. 50 nm wide) which became higher ordered nano-structures after lengthy sonication. The ultrasound irradiation is thought to form interpenetrating microcrystals which results in highly rigidified complexes and suppresses energy loss for phosphorescent emission. Hence, control of emission has been demonstrated by the ultrasound-controllability of the sol-gel transition, providing fast and precise OFF/ON switching.

<Figure 32>

A mononuclear analogue of these complexes has also been studied by the group (complex **69**) and was found to be non-emissive in solution but emissive in the crystal form [87]. Complex **69** has a long linker and forms dimeric arrays which are supported by intermolecular Pt···Pt interactions when in the crystal form (Fig. 33). The bridge which connects the two N atoms within the complex – as opposed to in the dinuclear complex where two N atoms on separate sites of the complex are connected – allows for intermolecular H-bonding which can stabilise the intermolecular structures in the crystal and supress mobility of the structure which would otherwise lead to a loss of luminescence efficiency.

<Figure 33>

In the dinuclear crystals, strong intermolecular interactions are present in the racemic mixture of (±) *anti*-**68a** compared with very weak offset π-π stacking interactions in the optically pure (+) *anti*-**68a** crystals. Meanwhile, intermolecular interactions in the racemic (±) *anti*-**68c** crystals are much weaker than those in the optically pure (+) form which has strong Pt···Pt interactions of 3.3 Å (Fig. 34). No intramolecular Pt-Pt interactions are present for any of the dinuclear complexes which explains the lack of ^{3}MMLCT emission.

<Figure 34>

Compared to the dinuclear complex, no evidence of gelation was discussed for the mononuclear complexes. Crystals of complex **69** were found to have a quantum yield of 38 % at 298 K and 52 % at 77 K. The mononuclear complex is seen to possess higher quantum yields than those of the dinuclear complexes at 77 K but both present an ON/OFF switching mechanism for luminescence.

GIP has also been demonstrated by Xiang *et al.*, who designed dinuclear cyclometallated Pt(II) complexes **70**–**72** of the form [(ppy)Pt(μ-SA)Pt(ppy)] (ppy: 2-phenyl pyridine, SA: salicylaldehyde azine) (Fig. 35) [88]. The choice of the SA bridging ligand was based on its highly conjugated and rotatable nature which could aid in AIE. Synthesis of the complexes involved cleavage of the $[(ppy)Pt(\mu\text{-}Cl)]_2$ dimer with the corresponding SA bridging ligand in 2-ethoxyethanol at 120ºC for 24 h with the addition of Na_2CO_3 as base.

<Figure 35>

Complexes **70**–**72** were non-emissive in solution owing to the intramolecular rotations of the bridging SA bond which allowed non-radiative decay of the phosphorescence. However, as aggregates in tetrahydrofuran (THF)/water or in the solid state, room temperature emission was observed (Fig. 36).

<Figure 36>

Only crystals of complexes **71** and **72** were obtained and enantiomers were observed for both complexes. The crystal structure of complex **71** revealed the presence of many strong intermolecular interactions of less than 3.0 Å in the enantiomers including: H_{Ar}–C_{Ar} (2.7085 Å), H_{Ar}–$C_{C=N}$ (2.7844 Å), H_{Ar}–Pt (2.9459 Å), H_{Ar}–O_{phenol} (2.7803 Å), H_{OMe}–H_{Ar} (2.5737, 2.6169, and 2.9639 Å), H_{OMe}–C_{Ar} (2.8314 and 2.9393 Å), and H_{OMe}–O_{phenol} (2.9647 Å) (Fig. 37). These restrict the rotation of the N–N single bond as well as the OMe groups. The propeller type structure of the complex (Fig. 37a with dihedral angles 73.3° and 106.7°) did, however, ensure that no intermolecular π-π stacking / Pt···Pt interactions or intramolecular Pt···Pt interactions were present, which benefits the complex emission owing to the absence of dimer formation.

<Figure 37>

The enantiomers of complex **72** were seen to pack together more tightly than those of **71**: they are seen to induce strong face-to-face intermolecular stacking interactions that are not present in complex **71**. Complex **72** was more soluble than the other complexes owing to its two -NEt_2 groups. As a result, it can form metallogels in organic solvents which are emissive and thus it could be a promising GIP-active material for photoactive nanostructured devices. The mechanism of gel formation in complex **72** was thought to proceed via self-assembly through strong enantiomer-induced intermolecular interactions (H–C, H–O, H–H and π-π stacking), which grow to form nano-fiber structures during gelation. Compared to the dinuclear complexes with quantum yields ranging from 7.5 to 14 %, the mononuclear analogue [Pt(ppy)SA] (Fig. 38, complex **73**) was shown to have a quantum yield of 38 % in the crystal form stemming from AIE. This was thought to originate from "restricted distortion of the excited-state structure by weak C–H---π interactions" with a contact distance of 2.875 Å in 3D structures [89]. Similarly, with the dinuclear complex, the mononuclear complex was non-emissive in solution due to the intramolecular rotations.

<Figure 38>

The Pt···Pt and π-π stacking interactions which affect the self-assembly of dinuclear Pt complexes to form metallogels in organic solvents have been recently investigated by Xing *et al*. [90]. New dinuclear alkynylplatinum (II) terpyridyl complexes with flexible bridging ligands (-$O(CH_2)_nO$, n=4 or 6, complexes **74** and **75**) have been designed where long alkyl chains were chosen as bridging units owing to their propensity to aid self-assembly into gels (Fig. 39). Amide groups on the complexes facilitated hydrogen bonding between molecules to further encourage gelation properties.

<Fig. 39>

FT-IR studies of solution, solid and xerogel samples (xerogels were prepared by casting gels of complexes in toluene onto a KBr plate and drying in the air) revealed intermolecular interactions which enabled the self-assembly of molecules of **74** and **75** into long fibres in organic solvents and further entanglement to form gels. Intermolecular hydrogen bonds in xerogels were revealed by the presence of the urea N–H stretching vibrations at around 3250 cm^{-1} in xerogels **74** and **75** which were absent in chloroform solution. Moreover, the C=O stretching and N–H bending bands shifted to lower wavenumber (1690 cm^{-1}) and higher wavenumber (1560 cm^{-1}), respectively, in the xerogel compared to chloroform solution. Van der Waals interactions were evidenced by the lower frequency absorption bands of the asymmetric and symmetric CH_2 stretching vibrations of xerogels **74** and **75**, observed at 2922 and 2854 cm^{-1} respecively (Fig. 40).

<Figure 40>

These dinuclear complexes were non-emissive in DMSO solution at room temperature. In their UV-vis absorption spectra in DMSO, it was found that **74** and **75** showed a weak absorption at 500–550 nm, tentatively assigned as to ^{1}MMLCT [(dσ*-π*)] owing to intermolecular interactions between the complexes in solution (Fig. 41a). Concentration-dependent UV-vis spectra revealed an enhancement of this band with increasing concentration, indicative of aggregate formation (Fig. 41b). This contrasts with typical mononuclear cationic terpyridyl Pt complexes which have been shown to obey Beer's law in the 10^{-5} – 10^{-2} M range and which are weakly emissive in solution at 298 K, independent of concentration (Φ_{lum} values ranging from 0.1 to 1.2 %) [91, 92].

<Figure 41 >

The results presented by this group demonstrate effective fabrication of metallogels based on Pt(II) complexes with the aid of the cooperative multiple intermolecular interactions. GIP is shown to be very dependent on the flexible linker of the dinuclear complex. Depending on the susceptibility of the flexible linker to external stimuli such as solvent and mechanical stress, the conformation of the complex can be altered. This can result in significant changes in the photophysical properties of the complex as discussed in the next section.

4.2 Conformational changes induced by external factors, e.g. solvent and mechanical stress

Mechanochromic materials display a change in colour with the application of mechanical stimuli/stress. The tolerance of the molecule to the stress is determined by the molecular design. Many groups have attempted to probe the mechanism of mechanochromism. The Houjou group synthesised a dinuclear complex with a flexible linker to try to allow a greater range of motion for the complex units to efficiently undergo mechanochromism [93]. They designed a novel, tweezer-type dinuclear N,N'-disalicyldiene-1,2-ethylenediaminato platinum Pt(salen) complex with isobutylene as the linker (complex **76**) which was compared to the mononuclear complex (**77)** (Fig. 42). The use of isobutylene as a flexible linker to give several stable conformers has previously been demonstrated [94]. The dinuclear Pt complex was synthesised by reaction of the ligand with K_2PtCl_4 in THF/DMSO with the addition of sodium acetate as base.

<Figure 42>

The NMR spectra of **76** and **77** show similar chemical shifts, revealing that the dinuclear complex has the same structure as the isolated Pt(salen) unit in solution. Moreover, the solution state UV-Vis spectra, emission and excitation of **76** and **77** were very similar, which suggests a lack of interactions between the Pt centres. In the solid state, as microcrystals, both **76** and the **77** are emissive. However, when these microcrystals were smeared into thin films, the emission of

complex **76** was significantly weakened and turned orange whilst complex **77** emission intensity did not change and the colour was only slightly changed from yellow to yellow-green (Fig. 43).

<Figure 43>

For both complexes the Pt···Pt distances ranged from 3.5 – 4.0 Å which are too long to be classed interactions between metal centres, but van der Waals interactions were present between the aromatic rings in the salen leading to a stacking conformation of the mononuclear complex units being adopted in both complexes. In complex **76**, this stacking led to a zig-zag network connected by the flexible linkers (Fig. 44) whilst a columnar stack prevailed in complex **77**. The semi-flexible linker in complex **76** was thus thought to be responsible for forming a networked structure of the dinuclear complexes, which was more easily broken down than the stacked mononuclear complexes and hence showed greater mechanochromic properties.

<Figure 44>

Similar to mechanochromism, where the external stimulus of mechanical stress can cause a change in complex emission, solvatochromism can be observed on changing the solvent. Zhong *et al.* synthesised diplatinum complexes with a N,N-dimethylurea bridge (Fig. 45) [95]. The different forms of the crystals and their susceptibility to solvent were studied. Diarylureas were chosen as the linker unit between the metal centres owing to the versatile conformations that they can adopt. Diarylureas with two N,N-methyl substituents adopt a dominant U shaped *cis,cis* conformation. This is known to allow through-space interactions and manipulation of the conformation can give rise to changes in the intermolecular stacking which in turn can affect the photophysical properties of the emissive materials [96,97].

<Figure 45>

Three forms of the same complex, **78a**–**c**, were synthesised by reaction of K_2PtCl_4 with the known ligand in different solvents **78a** = CH_2Cl_2 / $CHCl_3$, **78b** = CH_2Cl_2 / MeOH and **78c** = PhCl. The choice of solvent for each complex played a crucial role in determining the conformation of the molecules. In the crystal of complex **78a**, the chloroform molecules of the solvent showed hydrogen bonding to the Cl atoms of the complex. In the crystal of **78c**, the PhCl solvent sits above a pyridine ring of the [Pt(NCN)] unit with a distance between the two Pt centres of 4.36 Å. These effects in **78a** and **78c** enforce an open conformation by pushing the two [Pt(NCN)] units away from each other. These solvent molecules can be lost upon heating which enables a switching mechanism of the complex conformation from open to closed. In **78c**, no solvent molecules are present. MeOH acts as a hydrophilic and polar solvent which brings the Pt centres closer together and makes the complex adopt a closed conformation (Fig. 46).

<Figure 46 >

From the crystal structures, no Pt···Pt interactions were observed for **78a** and **78b** but a short intermetallic distance of 3.226 Å was observed in **78c**. In **78b** there is a short face-face distance of 3.16 Å and overlap of the two Pt(N^C^N) planes which provides strong intramolecular π-π interactions. All conformations are emissive in the solid state. The emissive properties of each complex are shown below in Table 2. Complex **78c** is promising as a deep red emitter with λ_{max} of 650 nm and a respectable quantum yield of 36 %.

Table 2. Photophysical data for complexes **78a**, **b** and **c** in the solid state.

Crystal	**$\lambda_{max\ emission}$ / nm**	**Quantum Yield / %**	**Lifetime/ ns**
78a	555	8.4	306

78b	560, 650 sh	2.0	283
78c	650	36	846

<Figure 47>

The emissive properties of complex **78** in solution were also measured using different solvents at different concentrations (Fig. 47). The emission in chloroform only exhibited one band across the selected concentration range of 1×10^{-6} to 1×10^{-4} M, which suggests a lack of intramolecular and intermolecular π-π interactions even at high concentration. Conversely, in MeOH solution, bands at 540 nm and 660 nm were observed even in dilute concentrations which support a closed conformation with π-π interactions. The emission in PhCl displayed a typical monomeric emission in dilute solution and intermolecular stacking in concentrated solution. As a result, by using different solvents at different concentrations, the emissive properties of these molecules can be modulated. The generation of different emission colours can be achieved, stemming from the flexible linker being able to adopt different conformations to give different interactions between the complex and the corresponding solvent.

Similar to Zhong, the Hirao group have demonstrated how different external stimuli can cause a complex to change conformation and thus change its photophysical properties [98]. They synthesised a Pt(II)–pyridinedicarboxamide analogue which has short metal–metal and π-π interactions that were able to be tuned by temperature and solvent. Conformational switching between MLCT and MMLCT emission under the influence of methanol was also demonstrated. The dinuclear complex **79** and its mononuclear analogue **80** (Fig. 48) were synthesised by Sonogashira coupling of the terminal alkyne ligand with the chloro Pt complex in the presence of $CuI/Et_3N/CH_2Cl_2$. Alkynes in the 6 position were used to provide a suitable platform for Pt···Pt interaction.

<Figure 48 >

Structural changes of Hirao's complex **79** induced by addition of methanol were confirmed by ^{1}H NMR. The complex structure is held intact by a network of intermolecular interactions between the linker and H_2O and intramolecular H-bonded interactions along the linker between the amide groups as inferred from the ligand's crystal structure (Fig. 49).

<Figure 49>

Increasing methanol content decreases the π–π interaction resulting in the downfield shift of most protons of the phenylbipyridine ligand. Furthermore, weakening of the H-bonds in the inside of the cavity was found, which is indicated by the chemical shift changes of the amide protons from 11.65 ppm in $CDCl_3$ to 11.55ppm in MeOH–$CDCl_3$ (1:1). This indicates a weaker interaction between the Pt–phenylbipyridine moieties resulting in the elongation of the Pt(II)–Pt(II) distance. These conformational changes show that methanol is likely to compete with the intramolecular H-bonds, resulting in H-bond distortion.

The absorption spectrum of complex **79** in comparison to the ligand and mononuclear complex **80** were measured in DCM. Both complexes **79** and **80** show an intense ^{1}IL absorption band below 400 nm, a moderate MLCT absorption at 400–450 nm and an absorption tail above 450 nm. The slightly higher intensity of the absorption tail of complex **79** is an indication of MMLCT transition brought about by the close proximity of the metals. This is supported by the broad, unstructured, low-energy emission band of complex **79** with a maximum of 750 nm that accompanies the slightly higher energy emission band at 600 nm. This lower energy band is not present in complex **80** (Fig. 50). Tuning of the complex emission was proven possible by altering the emission temperature and

type of solvent. Lowering the temperature of complex **79** in CH_2Cl_2 from 293 K to 193 K led to a red-shift of the ^{3}MMLCT emission band from λ_{max} =743 nm to λ_{max} = 771 nm, from which a shortening and strengthening of the Pt···Pt interaction is inferred. Moreover, on addition of MeOH, this low-energy ^{3}MMLCT transition decreased in intensity whilst the ^{3}MLCT emission intensity increased. These conformational changes were enhanced by increasing the temperature of complex **79** in the presence of 10% methanol, implying temperature-induced elongation of the Pt(II)···Pt(II) distance. Quantum yields for complex **79** were lower than for the mononuclear complex **80** but increased with increasing MeOH content.

<Figure 50>

Similarly, Yam's group synthesised dinuclear complexes in which the Pt(II)–terpyridine moieties are connected through flexible bridges of various oligo(oxyethylene) groups or meta-phenylene–ethylene oligomers (complex **81**, Fig. 48) [99]. They too showed increasing ^{3}MMLCT emission upon introduction of external stimuli such as CH_3CN and reduction of temperature and were able to form interesting structures via their self-assembly. The highest quantum yield value achieved for these complexes was 0.3 %.

4.3 Conformational changes resulting in self-assembly stemming from H-bonding, stacking, M-M interactions etc.

Yam *et al*. have shown many examples of dinuclear Pt complexes with self-assembly into a vast array of nanostructures mainly stemming from H-bonding, π-π stacking and M-M interactions that lend the resulting complexes interesting photophysical properties [91, 99]. Their synthesis of

dinuclear alkynylplatinum (II) terpyridyl complexes with oligomeric bridges has led to a vast array of further research.

Some earlier work by the group focused on the synthesis of complexes linked via *meta* phenylene ethynylene (*m*PE) units [100]. These units are classed as foldamers owing to their strong tendency to fold back onto themselves forming short helical strands. Yam's group were able to exploit the use of metal-metal interactions present in the dinuclear Pt complexes which can stabilise these foldamers in helical conformations (Fig. 51). This opens up the possibility of their roles as spectroscopic reporters for the probing of the folded or unfolded state in spectroscopic and luminescence studies.

<Figure 51>

Synthesis of the complexes **82–87** was achieved by Sonogashira reaction to form the *m*PE oligomers and subsequent reaction of these oligomers with [(^{t}Bu$_3$trpy)PtCl]OTf in dry DMF containing NEt_3 with a catalytic amount of CuI stirring at room temperature overnight (Fig. 52).

<Figure 52>

From the UV-Vis absorption spectra complexes **82**–**87** gave pale yellow solutions in DCM with intense IL transitions [$\pi\rightarrow\pi^*$] of the terpyridyl and alkynyl ligands at 302-340 nm and low energy absorptions at 412-470 nm assigned as MLCT [$d\pi(Pt)\rightarrow\pi^*(tpy)$] with mixed alkynyl-to-terpyridine LLCT [$\pi(C\equiv C)\rightarrow\pi^*(tpy)$] character. By increasing CH_3CN content in DCM, the dinuclear complex **84** showed a decrease in the IL absorption band and the appearance of a MMLCT absorption tail at 500 nm (Fig. 53). Conversely, for complexes **82** and **83** only negative solvatochromism was observed, representative of the shorter length of the oligomers which prohibit

the two terminal Pt moieties to construct a turn. Complex **86**, in which a ^{t}Bu terpyridine moiety is replaced with a sterically less demanding triethyl terpyridine moiety, was seen to exhibit a more pronounced MMLCT absorption increase which indicates that the variation on the steric bulk of the terpyridine ligands has some effect on the extent of Pt···Pt interactions able to stabilise the short helical strand in solution.

<Figure 53 >

^{3}MMLCT emission was observed in complexes **84**–**86**, especially in **84** and **85** (Fig. 54), and is possibly a result of the tethering together of the two Pt-^{t}Bu$_3$trpy units via *m*PE linkers of the appropriate chain length that aided the bringing together of the two end-groups into close proximity for Pt-Pt and π-π interactions to occur. This low-energy ^{3}MMLCT emission band in complexes **84-86** was present even in solution concentrations as dilute as 10^{-7} M, which supports the involvement of an intramolecular association.

<Figure 54>

Complexes **82**, **83**, and **87** show no evidence of ^{3}MMLCT emission in the concentration range of 10^{-6} to 10^{-4} M, indicating a lack of intramolecular interactions. It was complex **86** that showed the most stable helical arrangement owing to a red shift in the ^{3}MMLCT at low temperature with no sign of monomeric ^{3}MLCT/^{3}LLCT emission bands even at high temperature. As a result complex **86**, with asymmetric terpyridyl Pt moieties (one with lower steric demand) linked by *m*PE of length 5, had the best molecular arrangement to increase Pt···Pt and π-π interactions in order for stable helices to form.

In an extension of this work, Yam *et al*. went on to synthesise dinuclear terpyridyl Pt complexes **88**–**90** with a modified *m*PE bridge containing a central binapthol with triethylene glycol monoethyl ether groups (Fig. 55) [101].

<Figure 55>

Three complexes with extending *m*PE chain lengths were synthesised in the same manner as previously. The binapthol moiety provided a handle in which to control the spatial arrangement for the formation of both right-handed (P) and left-handed (M) helices in the self-assembly process. It was found that complexes **89** and **90** formed helical strands in increasingly polar solvents owing to the longer *m*PE chains as evidenced by ^{3}MMLCT absorption tails at 500 nm (Fig. 56). This absorption tail was not present in complex **88** which adopts an unfolded conformation in pure CH_3CN to exist as a random coil without the presence of intramolecular metal–metal interactions.

<Figure 56>

The presence of long hydrophilic triethylene glycol monomethyl ether chains allowed for the solubilisation of complexes in both water and CH_3CN. By increasing the water content of the solvent for UV-vis absorption for complexes **89** and **90**, a significant decrease in the ILCT was observed at 284-337 nm. Moreover when the temperature is increased from 293 K to 353 K in a 70 % water-CH_3CN solution of complex **89** a disappearance of the MMLCT band is observed. This suggests a thermal equilibrium where stacked helices would dissociate from the supramolecular cylindrical columns upon an increase in temperature due to the destruction of the intermolecular Pt-Pt and π-π interactions.

Luminescence enhancement has also been demonstrated in these complexes. Upon excitation at $\lambda >$ 400 nm, complexes **88**–**90** exhibit emission bands in DCM at 572–580 nm, assigned as ^{3}MLCT/^{3}LLCT typical of monomeric platinum(II) terpyridine complexes, and thus indicative of the random coil state without the formation of metal–metal interactions (Fig. 57). When the acetronitrile content is increased there is a decrease in the intensity of these bands in complexes **89** and **90** with an increase in ^{3}MMLCT bands at 703 and 688 nm respectively, indicative of helical formations stabilised by Pt-Pt and π-π interactions. However this is not the case for complex **88** which retains the intensity of its ^{3}MLCT/^{3}LLCT band. Complex **89** was seen to adopt the most stable helical strand owing to its lower energy emission compared to complex **90**. The emission of this complex was thus chosen to investigate further in varying amounts of water in CH_3CN solution from 0 to 70 %. On increasing the water content, luminescence enhancement is observed.

<Figure 57>

Complex **89** is thought to co-operatively stack to self-assemble into the hierarchical helix of helices with the enhancement of the emission intensity orginating from the tight stacking of the helical columns, together with the increase in the rigidity of the tertiary structure of foldamers. Yam's group also synthesised dinuclear Pt terpyridyl complexes **91** and **92** containing hydrophilic oligo(*para*-phenylene ethynylene) (OPE) moieties with two 3,6,9-trioxadec-1-yloxy chains (Fig. 58) [102]. OPEs containing π-π stacking interactions are known to self assemble into an array of various nanostructures and hence were chosen to form part of the bridge for these Pt complexes.

<Figure 58>

The complexes were studied via different means of microscopy and it was discovered that the mononuclear complex **93** formed irregular networks of molecular tapes with lamellar packing,

complex **91** formed well defined nanotubes with directional metal-metal interactions, and complex **92** formed helical ribbons with staggered π-π interactions (Fig. 59).

<Figure 59>

UV-vis studies were conducted on complexes **91** and **92** and compared to the mononuclear complex **93** in order to help elucidate the mechanism for the self assembly into the various nanostructures (Fig. 60). At 326 K, the UV-vis absorption spectrum of **93** in DMSO solution shows the emergence of a low-energy MMLCT absorption tail at 525 nm, together with the depletion of the MLCT/LLCT band at 479 nm. The absorption of complex **93** appears linear with respect to concentration. Complex **91**, end-capped with the unsubstituted terpyridine ligand, experiences stronger metal−metal interactions, evidenced by the more significant growth and red shift of the MMLCT absorption band (550 nm) on decreasing temperature together with the significant deviation of the MMLCT absorption band from the linear relationship of Beer's law at various concentrations.

<Figure 60>

Complex **92** which contains the bulky *tert*-butyl substituents, however, does not show a temperature dependence on the low-energy absorption band and the UV-Vis absorption spectra show a good agreement with Beer's law at various concentrations (Fig. 61). This suggests a lack of metal−metal interactions in the self-assembly process owing to the sterically bulky *tert*-butyl groups.

<Figure 61>

The authors did not report emission data for these complexes but the complex structures are similar to the dinuclear Pt terpyridyl complexes **94**-**97** with extended bridges containing *p*-phenylene

ethynylene oligomers reported by *Du et al* (Fig. 62) [103]. As a result, similar emission may be expected. The quantum yield values for Du's reported complexes ranged from 0.007 % to 0.24 % in CH_3CN and from 0.19 % to 15 % in DCM.

<Figure 62>

Aggregation behaviour was observed for complex **97** on increasing the concentration from 1 x 10^{-6} to 1 x 10^{-5} M in CH_3CN solution where the intensity of its emission band from 520-670 nm dropped dramatically and a new band at 650-850 nm appeared (Fig. 63). Conversely, complexes **94–96** showed no sign of aggregation at 1 × 10^{-5} M in either CH_3CN/DCM, which is thought to be due to the sterically demanding *tert*-butyl groups, supportive of Yam's findings. The low energy band at a high concentration in complex **97** is assigned as the MMLCT band and indicates that the longer *p*-phenylene ethynylene oligomers in complex **97**, compared to shorter bridges in complexes **94-96**, facilitate stronger intermolecular interactions. This effect is seen to increase the quantum yield significantly compared to the other complexes in DCM solution.

<Figure 63>

Similar to the helical arrangements of complexes synthesised by Yam, stacking of complexes to form networked structures through self-assembly has been observed in luminescent clamshell-like dinuclear complexes containing two aromatic imine ligands and bridging ligands which promote intermolecular and intramolecular interactions [43, 62, 104].

Influenced by this, Fujihara and co-workers synthesised three novel clamshell-like dinuclear Pt complexes with tartrate as the chiral bridging ligand (complexes **98-100**) [105]. The chirality of the tartrate was proposed to aid in altering the emission colours of the materials through its effect on the

crystal and molecular structures of each complex. The complexes synthesised with $_L$- and *meso*-tartH_2^{2-} were: [{Pt^{II}(bpy)}$_2$(μ-x-tart)], (x = $_L$ (**98**), *meso*- (**99**)), and racemic mixture [{Pt^{II}(bpy)}$_2$(μ-$_D$-tart)] [{Pt^{II}(bpy)}$_2$(μ-$_L$-tart)] (**100**). A mononuclear complex **101** was also synthesised. The synthesis of these complexes was achieved via reaction of [Pt(bpy)$(NO_3)_2$] with the corresponding sodium tartrate, Na_2(x-tartH_2)(x = $_L$, *meso*), in the molar ratio of 2 : 1 in aqueous solution (Fig. 64).

<Figure 64>

Complex **98** crystallised as two polymorphs, **98α** and **98β**, and intramolecular Pt···Pt and π-π interactions were evident in these complexes leading to a right handed helical arrangement with a rotation angle of 120° along the b-axis. In the crystal structure of **98α**, Pt-Pt distances of 3.23–3.49 Å were revealed as well as bpy–bpy separations of 3.24–3.31 Å which also indicated the presence of weak π-π interactions between the pyridyl moieties (Fig. 65). Hydrogen bonding aided by water molecules enabled dinuclear complexes to bridge and form this right handed helical arrangement.

<Figure 65>

All crystals displayed luminescence with broad emission bands when excited at 365 nm. Mononuclear complex **101** showed an emission band at 535 nm and Φ_{lum} = 0.05, attributed to ^{3}LC and ^{3}MLCT excited states. The other complexes gave lower-energy emission, with complex **100** showing a band at 569 nm, complex **99** at 621 nm and **98α** at 656 nm (Fig. 66). The quantum yields of these complexes were in the range of 0.05–0.07 and emission was assigned to ^{3}MMLCT states.

<Figure 66>

Shortening of the Pt···Pt separations (**100**·4H_2O, 3.54 Å > **99**·12.5H_2O, 3.34 Å > **98α**, 3.23–3.49 Å), giving stronger Pt–Pt interactions, led to a red-shift in the low-energy emission band (**100** = 569 nm → **98** = 656 nm). This is because the strong interaction generates a large splitting between the d_{z2} σ* antibonding and d_{z2} σ bonding orbitals. In comparison, the mononuclear parent complex Pt(bpy)Cl_2 exists in yellow and red polymorphs with emission being ascribed to metal centred d-d states and MMLCT respectively. The switch in the nature of the emissive excited state between the two forms is attributed to Pt···Pt interactions in the red form, which has a linear-chain structure with a Pt···Pt distance of 3.45 Å. The emission maxima of both polymorphs are centred around 640 nm, similar to complex **99** and **98α**, but unlike the clamshell-like dinuclear complexes, Pt(bpy)Cl_2 is non-emissive owing to rapid non-radiative decays.

Acknowledgements

We thank EPSRC and Durham University for funding. We are grateful to our collaborators – Dr Valery Kozhevnikov and his team at Northumbria University, Dr Jeanne Crassous at the Université de Rennes, and Prof. Diego Cárdenas at Universidad Autónoma de Madrid – for stimulating collaborations in the field of multinuclear complexes incorporating platinum.

Captions to Figures

Figure 1 Schematic illustration of the three subdivisions of binuclear complexes as used in this review. **(A)** Complexes featuring rigid bridges that hold the Pt units in such a way that they cannot come together through *intramolecular* face-to-face interactions. **(B)** Complexes in which the Pt units are rigidly held in a conformation that favours face-to-face interactions between them,

either in the ground state and/or the excited state. **(C)** Complexes with flexible bridges where the Pt units may behave as essentially independent units or interact with each other.

Figure 2 Structures and synthetic routes to the mono- and dinuclear Pt(II) complexes **2** and **3**, mononuclear iridium complex **4**, and the heterotrimetallic Pt_2Ir complex **5,** from the *bis*-N^C-cyclometallating proligand **1** [28].

Figure 3 UV-visible absorption (left) and emission spectra (right) of **2**–**5** in CH_2Cl_2 at room temperature [28].

Figure 4 Structures of the Pt_3Ir complex **7** and the corresponding mononuclear iridium complex **6** [29].

Figure 5 Structures of the dinuclear platinum(II) complexes **9–13** featuring diphenylpyrazine units, together with a diphenylpyrimidine analogue **8** [32].

Figure 6 Left: plot of the lowest-energy absorption maximum in CH_2Cl_2 at 298 K (derived from λ_{max}) versus the reduction potential (values versus $Fc|Fc^+$) obtained by cyclic voltammetry for **8**–**13** (red squares), and for the corresponding mononuclear complexes (blue circles). Dashed line represents the best fit of the data for all 12 complexes; gradient = 6410 cm^{-1}/V. Right: corresponding plot for the emission maxima, under the same conditions; gradient of best-fit line = 6460 cm^{-1}/V [32].

Figure 7 Diplatinum complexes **14**–**18** featuring N-heterocyclic carbene ligands [34].

Figure 8 Enantiopure bis-platinahelicence **21** isolated following the resolution of diastersomeric complexes **20** containing chiral sulfoxide ligands, starting from 1,8-bis(2-pyridyl)naphathalene **19** [39].

Figure 9 Cicurlarly polarized luminescence and total luminescence (upper and lower panels respectively) of *M*-**21** and *P*-**21** (red and black data points respectively) in degassed CH_2Cl_2 solution at 295 K. Reproduced from [39] by permission of The Royal Society of Chemistry.

Figure 10 Structures of the *bis*-N_2O_2-coordinating bridging ligand **22** and its Pt_2 complex 23, with mononuclear models **24** and **25** [41].

Figure 11 Emission and excitation spectra of **23**, **24**, and **25** in *o*-dichlorobenzene solution. Reprinted from [41] with permission of Elsevier.

Figure 12 The NN–NNC bridging ligand **26** and the heterometallic RuPt complexes **28** and **29** isolated via the mononuclear Ru complex **27** [45].

Figure 13 The bimetallic Ir-Pt complex **31** and its mono-iridium analogue **30** [51].

Figure 14 Multinuclear Pt(II) complexes **32a-c** and **33**, with triazine thiolate linkers [52].

Figure 15 (a) Structure of **32a** in the crystal. (b) Crystal packing diagram of the cations in **32a**, with intermolecular Pt···Pt distances that are alternately short, 3.641(1) Å, and long, 4.352(1) Å. (c) Structure of **32c** in the crystal. (d) Crystal packing diagram of the cations in **32c**, with intermolecular Pt···Pt distances of 3.663(1) Å. Hydrogen atoms are omitted for clarity; thermal

ellipsoids in (a) and (c) are shown at the 50% probability level. Reproduced from [52] by permission of The Royal Society of Chemistry.

Figure 16 Heterometallic Ir-Pt complexes **34** and **35** featuring a dipyrrin ligand bound to the $Ir(ppy)_2$ unit [56].

Figure 17 Complexes with a *bis*-O^O-coordinating bridging ligand. Symmetrical (N^C* = N^C) and asymmetrical (N^C* ≠ N^C) complexes of type **36** reported by Thompson and co-workers [58], and the heterometallic Ir-Pt **37** synthesised by Bruce and co-workers for liquid crystalline properties [59].

Figure 18 Molecular orbital scheme for a "dimer" consisting of two Pt(II) complexes interacting through Pt···Pt face-to-face interactions. (a) The interaction of the Pt centres through [vacant] $5d_{z2}$ and [filled] $6p_z$ orbitals without taking into account configuration interaction. (b) When configuration interaction between MOs of the same symmetry is taken into account, the resulting stabilisation becomes clear. (c) When conjugated aromatic ligands are present with low-energy π* orbitals, the lowest-energy excited states are typically dσ*-π* (MMLCT), but note that π-π* transitions may also be significant.

Figure 19 Isomers of $[Pt(bpy)(\mu\text{-pyS})]_2^{2+}$ **38** featuring an *anti* (top) or *syn* (bottom) arrangement of the bridging N^S ligands. Reproduced from [62] by permission of John Wiley & Sons Ltd.

Figure 20 A selection of complexes of the type $[Pt(N^C)(\mu\text{–}N^S)]_2$, together with luminescence λ_{max} and Φ_{lum} values in degassed CH_2Cl_2, except where indicated by an asterisk, for which the data

refer to the complex doped into a thin film; **39**, **40** [65], **41** [67], **42** [63,64], **43** [68], **44** [63,64], **45** [68], **46** [69], **47** [70].

Figure 21 Examples of Pt(III)–Pt(III) dimers incorporating a Pt–Pt bond, formed through oxidation of corresponding *N*^*S*-bridged $Pt(II)_2$ complexes [65,67].

Figure 22 Molecular structures of **51**, **52**, and **53** in their respective crystals, in which the oxidation states of platinum are formally +2.33, +2, and +3 respectively. Ellipsoids are shown at the 50% probability level and hydrogen atoms are omitted for clarity. Reproduced from [72] by permission of John Wiley & Sons Ltd.

Figure 23 Amidinate-bridged $Pt(II)_2$ complexes with carbene ligands [73].

Figure 24 Two views of the molecular structure of $[Pt(dfppy)(\mu\text{-pz})]_2$ (**56** with *pz'* = pyrazole) in the crystal, showing the boat-like conformation that leads to short metal-metal separations. Reproduced with permission from [74]. Copyright 2005 American Chemical Society.

Figure 25 Dinuclear Pt(N^N^C) complex **58** with a bridging xanthene ligand and the structurally similar heterometallic Au-Pt complex **59**, together with the mononuclear model complex **57** [77].

Figure 26 *Left:* Absorption spectrum of **58** and the emission and excitation spectra of **58** (solid lines) and **57** (dashed lines) in CH_2Cl_2 at room temperature. *Right:* Absorption and emission spectra of the heterometallic Au-Pt complex **59** (solid lines) together with the corresponding spectra of the homo-dimetallic gold complex (dashed lines, labelled $\mathbf{Au_2}$) in CH_2Cl_2 at room temperature [77].

Figure 27 Mono- and diplatinum complexes **60** and **61**, their emission spectra in CH_2Cl_2 at room temperature, and the emission spectrum of **61** at 77 K (in diethyl ether / isopentane / ethanol, 2:2:1 v/v) [78].

Figure 28 Dinuclear platinum(II) complexes **62**, **63** and **64** featuring Pt(salphen) units bridged by xanthene, dibenzofuran and biphenylene respectively. Reproduced from [80] by permission of John Wiley & Sons Ltd.

Figure 29 Structure of Pt complexes **65-67** linked by phosphino bridges.

Figure 30 ORTEP representation of (a) (R) anti-**68a** and (b) (R) anti-**68c** as their racemic (left) and optically pure (right), (+) form crystals. Thermal ellipsoids are shown at the 50% probability level. Reproduced with permission from [86]. Copyright 2011 American Chemical Society.

Figure 31 Emission spectra of gels of (a) (±) anti-**68a** (1.50×10^{-3} M) and (b) (+) anti-**68c** (2.20×10^{-3} M) in cyclohexane generated by sonication (44 kHz, 0.31 W/cm^2) for various sonication times ($\lambda_{ex} = 420$ nm, 293 K). Dashed line: a spontaneous gel formed by standing at room temperature for 1 h without sonication. Reproduced with permission from [86]. Copyright 2011 American Chemical Society.

Figure 32 SEM images of dried ((±) anti-**68a** aggregates prepared from a 1.50×10^{-3} M solution in cyclohexane by various methods. (a) Solution prepared freshly; (b) gel just after brief sonication (44 kHz, 0.31W/cm^2, 3 s). Reproduced with permission from [86]. Copyright 2011 American Chemical Society.

Figure 33 Molecular structure and packing of mononuclear complex **69**. Reproduced with permission from [87]. Copyright 2011 American Chemical Society.

Figure 34 Packing of dinuclear complexes (a) (±) anti-**68a**, (b) (+) (R) anti-**68a**.C_6H_{12}, (c) (±) anti-**68c**, and (d) (+) (R) anti-**68c**.$2.5C_6H_{12}$ in the crystalline state. Reproduced with permission from [86]. Copyright 2011 American Chemical Society.

Figure 35 Synthesis of [(ppy)Pt(μ-SA)Pt(ppy)] complexes **70**-**72**. Quantum yield and lifetimes in powder form.

Figure 36 Normalized emission spectra of complex **70**–**72** powders. Reproduced from [88] by permission of John Wiley & Sons Ltd.

Figure 37 Single-crystal X-ray diffraction structure and packing of molecules of **71**: (a) side view; (b) packing (H atoms are omitted); (c,d) intermolecular interactions of the two closest enantiomers where a= 2.7844 Å, b= 2.9459 Å, c = 2.8566 Å, d= 2.7803 Å, e= 2.7085 Å, f= 2.6169 Å, g= 2.5737 Å, h = 2.9393 Å, i= 2.9639 Å, j= 2.9647 Å, k= 2.8314 Å; (e) enantiomers of **71**. Reproduced from [88] by permission of John Wiley & Sons Ltd.

Figure 38 Structure of complex **73**.

Figure 39 Chemical structures and synthesis routes of **74** and **75**. (a) 1,6- Hexanediol or 1,4-butanediol, DMSO, KOH; (b) K_2PtCl_4,CH_3CN, H_2O; (c) dodecyloxy-terminal alkyne, CuI, DMF, TEA.

Figure 40 The FT-IR spectra **74** (a) and **75** (b) in solid, xerogel (obtained from toluene) and chloroform solution. Reproduced from [90] by permission of The Royal Society of Chemistry.

Figure 41 UV-vis absorption (a) comparison of **74** and **75** in DMSO solution at 2.2×10^{-5} M concentration (b) spectral changes of **74** in different concentrations of DMSO solution. Reproduced from [90] by permission of The Royal Society of Chemistry.

Figure 42 Synthesis of the dinuclear bis-salen complex **76** and the structure of the mononuclear complex **77**.

Figure 43 Microscopic fluorescence images of **77** (a–c) and **76** (d–f). (a, d) Microscale single crystals, (b, e) crushed microcrystals, and (c, f) samples smeared on a glass slide. Reproduced from [93] by permission of Elsevier.

Fig. 44 Crystal structure of complex **76**. (a) The zigzag network composed of the stacked salen pair. A close-up of the (b) short contact and (c) long contact around the stacked pairs. Reproduced from [93] by permission of Elsevier.

Figure 45 Diplatinum complex **78** that switches between the closed and the open form. Reproduced from [95] by permission of The Royal Society of Chemistry.

Figure 46 Thermal ellipsoid plots (a-c) and crystal packing (d-f) of three different single-crystal forms of complex **78** at 30 % probability. Reproduced from [95] by permission of The Royal Society of Chemistry.

Figure 47 Emission spectral changes of complex **78** in (a) $CHCl_3$, (b) MeOH, and (c) PhCl, as a function of concentration. Reproduced from [95] by permission of The Royal Society of Chemistry.

Figure 48 Pt complexes **79**-**81**.

Figure 49 Crystal structure of the ligand for complex **79**. Reproduced from [98] by permission of The Royal Society of Chemistry.

Figure 50 (a) UV-vis spectra of complexes **79** and **80** at different concentrations and (b) emission spectra of complexes **79** and **80** at different concentrations, all measured in DCM at 298 K. Reproduced from [98] by permission of The Royal Society of Chemistry.

Figure 51 Folding and unfolding of complexes based on solvent and temperature modulation. Reproduced with permission from [100]. Copyright 2012 American Chemical Society.

Figure 52 Structures of the dinuclear Pt complexes **84**-**86** and mononuclear Pt complex **87**.

Figure 53 UV-vis absorption spectra of (a) complex **84** and (b) complex **86** with increasing CH_3CN content in DCM solution. The inset shows the absorbance ratio $A_{500\ nm}/A_{422\ nm}$ as a function of solvent compositions. Reproduced with permission from [100]. Copyright 2012 American Chemical Society.

Figure 54 Emission spectra of CH_3CN for **84** (black), **85** (blue), and **86** (red) at 298 K in DCM. Reproduced with permission from [100]. Copyright 2012 American Chemical Society.

Figure 55 Structure of dinuclear Pt complexes **88-90** with modified mPE bridges.

Figure 56 Helical arrangement of complexes **89** and **90**. Reproduced from [101] by permission of The Royal Society of Chemistry.

Figure 57 Luminescence enhancement of complex **89** on increasing the water content of solutions. Reproduced from [101] by permission of The Royal Society of Chemistry.

Figure 58 Structures of complexes **91-93**.

Figure 59 AFM images of complex **91** (upper) and complex **92** (lower). Reproduced from [102] by permission of Proceedings of the National Academy of Sciences of the United States of America.

Figure 60 **(**a) UV-vis absorption spectral traces of **93** in DMSO ([Pt]=843 μM) on increasing temperature. (b) UV-vis absorption spectral changes of **93** in DMSO as the concentration is increased from 69 to 1,005 μM. (Inset) A plot of the apparent absorbance of **93** at 525 nm as a function of concentration. (c) UV-vis absorption spectral changes of **91** in DMSO as the concentration is increased from 17 to 1,442μM. (d) A plot of the apparent absorbance of **27** at 550 nm as a function of concentration. Reproduced from [102] by permission of Proceedings of the National Academy of Sciences of the United States of America.

Figure 61 **(**a) UV-vis absorption spectral traces of **92** in DMSO ([Pt]=360 μM) on decreasing temperature and (b) plot of absorbance at 463 nm vs. Temperature from 353 to 297 K. (c) UV-vis absorption spectral changes of **92** in DMSO as the concentration is increased from 28 to 510μM. (d) A plot of the apparent absorbance at 530 nm as a function of concentration. Reproduced from

[102] by permission of Proceedings of the National Academy of Sciences of the United States of America.

Figure 62 Synthesis of Pt terpyridyl complexes **94-97** reported by Du et al.

Figure 63 Emission spectra of complexes **94–97** in CH_3CN at 298 K (concentration 1×10^{-5} M, λ_{ex} 500 nm. Reproduced with permission from [103]. Copyright 2012 American Chemical Society.

Figure 64 Synthesis of complexes **98-101**.

Figure 65 (a) Clamshell-like form of the dinuclear complex **98**, (b) crystal structures of the right-handed helical structure **98α**. Reproduced from [105] by permission of The Royal Society of Chemistry.

Figure 66 Luminescence spectra (λ_{ex} = 365 nm) of **98α**, **98β**, **99**·12.5H_2O, **100**·4H_2O, and **101**·H_2O at room temperature. Reproduced from [105] by permission of The Royal Society of Chemistry.

References

[1] D.R. McMillin, J.J. Moore, Luminescence that lasts from Pt(trpy)Cl^+ derivatives (trpy = 2,2':6',2"-terpyridine), Coord. Chem. Rev. 229 (2002) 113–121.

[2] J.A.G. Williams, Photophysics and photochemistry of coordination compounds: Platinum, Top. Curr. Chem. 281 (2007) 205–268.

[3] R. McGuire, M.C. McGuire, D.R. McMillin, Platinum(II) polypyridines: A tale of two axes, Coord. Chem. Rev. 254 (2010) 2574–2583.

[4] L. Murphy, J.A.G. Williams, Luminescent platinum compounds: From Molecules to OLEDs, Top. Organomet. Chem. 28 (2010) 75–111.

[5] Y. Chi, P.T. Chou, Transition metal phosphors with cyclometalating ligands: fundamentals and applications, Chem. Soc. Rev. 39 (2010) 638–655.

[6] K. Li, G.S.M. Tong, Q.Y. Wan, G. Cheng, W.Y. Tong, W.H. Ang, W.L. Kwong, C.M. Che, Highly phosphorescent platinum(II) emitters: photophysics, materials and biological applications, Chem. Sci. 7 (2016) 1653.

[7] H. Yersin, A.F. Rausch, R. Czerwieniec, T. Hofbeck, T. Fischer, The triplet state of organo-transition metal compounds. Triplet harvesting and singlet harvesting for efficient OLEDs, Coord. Chem. Rev. 255 (2011) 2622–2652.

[8] A. Rausch, L. Murphy, J.A.G. Williams, H. Yersin, Improving the performance of Pt(II) complexes for blue light emission by enhancing the molecular rigidity, Inorg. Chem. 51 (2012) 312–319.

[9] W.Y. Wong and C.L. Ho, Heavy metal organometallic electrophosphors derived from multi-component chromophores, Chem. Soc. Rev. 253 (2009) 1709–1758.

[10] J. Kalinowski, V. Fattori, M. Cocchi, J.A.G. Williams, Light-emitting devices based on organometallic complexes as emitters, Coord. Chem. Rev. 255 (2011) 2401–2425.

[11] C.M. Che, C.C. Kwok, S.W. Lai, A.F. Rausch, W.J. Finkenzeller, N.Y. Zhu, H. Yersin, Photophysical properties and OLED applications of phosphorescent platinum(II) Schiff base complexes, Chem. Eur. J. 16 (2010) 233–247.

[12] S.Q. Huo, J. Carroll and D.A.K. Vezzu, Desigen, synthesis, and applications of highly phosphorescent cyclometalated platinum complexes, Asian J. Org. Chem. 4 (2015) 1210–1245.

[13] Q. Zhao, C. Huang and F. Li, Phosphorescent heavy-metal complexes for bioimaging, Chem. Soc. Rev. 40 (2011) 2508–2524.

[14] K.K.W. Lo, A.W.T. Choi and W.H.T Law, Applications of luminescent inorganic and organometallic transition metal complexes as biomolecular and cellular probes, Dalton Trans. 41 (2012) 6021–6047.

[15] E. Baggaley, J.A. Weinstein and J.A.G. Williams, Lighting the way to see inside the live cell with luminescent transition metal complexes, Coord. Chem. Rev. 256 (2012) 1762–1785.

[16] E. Baggaley, J. A. Weinstein and J. A. G. Williams, Time-resolved emission imaging microscopy using phosphorescent metal complexes: Taking FLIM and PLIM to new lengths, Struct. Bond. 165 (2015) 205–256.

[17] J.Z. Zhao, W.H. Wu, J. F. Sun, S. Guo, Triplet photosensitizers: from molecular design to applications, Chem. Soc. Rev. 42 (2013) 5323–5351.

[18] F.N. Castellano, Altering molecular photophysics by merging organic and inorganic chromophores, Acc. Chem. Res. 48 (2015) 828–839.

[19] G. Liebsch, I. Klimant, B. Field, G. Holst, O.S. Wolfbeis, Luminescence lifetime imaging of oxygen, pH, and carbon dioxide distribution using optical sensors, Appl. Spectrosc. 54 (2000) 548–559.

[20] M. Cocchi, J. Kalinowksi, V. Fattori, J.A.G. Williams, L. Murphy, Color-variable highly efficient organic electrophosphorescent diodes manipulating molecular exciton and excimer emissions, 94 (2009) 073309.

[21] L. Murphy, P. Brulatti, V. Fattori, M. Cocchi, J.A.G. Williams, Blue-shifting the monomer and excimer phosphorescence of tridentate cyclometallated platinum(II) complexes for optimal white-light OLEDs, Chem. Commun. 48 (2012) 5817–5819.

[22] D.M. Roundhill, H.B. Gray, C.M. Che, Pyrophosphite-bridged diplatinum chemistry, Acc. Chem. Res. 22 (1989) 55–61.

[23] R.M. van der Veen, C.J. Milne, A. El Nahhas, F.A. Lima, V.T. Pham, J. Best, J.A. Weinstein, C.N. Borca, R. Abela, C. Bressler, M. Chergui, Structural determination of a photochemically active diplatinum molecule by time-resolved EXAFS spectroscopy, Angew. Chem. Int. Ed. 48 (2009) 2711–2714; M. Christensen, K. Haldrup, K. Bechgaard, R. Feidenhans'l, Q. Kong, M. Cammarata, M. Lo Russo, M. Wulff, N. Harrit, M.M. Nielsen, J. Am. Chem. Soc. 131 (2009) 502–508.

[24] R. M. van der Veen, A. Cannizzo, F. van Mourik, A. Vlcek, M. Chergui, J. Am. Chem. Soc. 133 (2011) 305–315; S. Zalis, Y.C. Lam, H.B. Gray, A. Vlcek, Spin-orbit TDDFT electronic structure of diplatinum(II,II) complexes, Inorg. Chem. 54 (2015) 3491–3500.

[25] J.B. Cooper, D.B. MacQueen, J.D. Petersen, D.W. Wertz, Role of the LUMO in determining redox stability for 2,3-dipyridylpyrazine-bridged and 2,3-dipyridylquinoxaline-bridged ruthenium(II) bimetallic complexes, Inorg. Chem. 29 (1990) 3701–3705.

[26] G. Denti, S. Campagna, L. Sabatino, S. Serroni, M. Ciano, V. Balzani, Luminescent and redox-reactive building blocks for the design of photochemical molecular devices – mononuclear, dinuclear, trinuclear, and tetranuclear ruthenium(II) polypyridine complexes, Inorg. Chem. 39 (1990) 4750–4758.

[27] S. Serroni, A. Juris, S. Campagna, M. Venturi, G. Denti, V. Balzani, Tetranuclear bimetallic complexes of ruthenium, osmium, rhodium, and iridium – synthesis, absorption spectra, luminescence, and electrochemical properties, J. Am. Chem. Soc. 116 (1994) 9086–9091.

[28] V.N. Kozhevnikov, M.C. Durrant, J.A.G. Williams, Highly luminescent mixed-metal Pt(II)/Ir(III) Complexes: bis-cyclometalation of 4,6-diphenylpyrimidine as a versatile route to rigid multimetallic assemblies, Inorg. Chem. 50 (2011) 6304–6313.

[29] G. Turnbull, J.A.G. Williams, V.N. Kozhevnikov, Rigidly linking cyclometallated Ir(III) and Pt(II) centres: an efficient approach to strongly absorbing and highly phosphorescent red emitters, Chem. Commun. 53 (2017) 2729–2732.

[30] P.H. Lanoë, C.M. Tong, R.W. Harrington, J.A.G. Williams, V.N. Kozhevnikov, Ditopic bis-terdentate cyclometallating ligands and their highly luminescent dinuclear iridium(III) complexes, Chem. Commun. 50 (2014) 6831–6834.

[31] R.E. Daniels, S. Culham, M.C. Durrant, M. Probert, W. Clegg, J.A.G. Williams, V. Kozhevnikov, When two are better than one: bright phosphorescence from non-stereogenic dinuclear iridium(III) complexes, Dalton Trans. 45 (2016) 6949–6962.

[32] S. Culham, P.H. Lanoë, V.L. Whittle, M.C. Durrant, J.A.G. Williams, V.N. Kozhevnikov, Highly luminescent dinuclear platinum(II) complexes incorporating bis-cyclometallating pyrazine-based ligands: a versatile approach to efficient red phosphors, Inorg. Chem. 52 (2013) 10992–11003.

[33] Y. Unger, D. Meyer, O. Molt, C. Schildknecht, I. Münster, G. Wagenblast, T. Strassner, Green-blue emitters: NHC-based cyclometalated [Pt(C^C*)(acac)] complexes, Angew. Chem. Int. Ed. 49 (2010) 10214–10216.

[34] A. Tronnier and T. Strassner, (C^C*) Cyclometalated binuclear N-heterocyclic biscarbene platinum(II) complexes – highly emissive phosphorescent emitters, Dalton Trans. 42 (2013) 9847–9851.

[35] J. Moussa, K. Haddouche, L.M. Chamoreau, H. Amouri, J.A.G. Williams, New N^C^N-coordinated Pd(II) and Pt(II) complexes of a tridentate N-heterocyclic carbene ligand featuring a 6-membered central ring: synthesis, structure and luminescence, Dalton Trans. 45 (2016) 12644–12648.

[36] M.E.S. Moussa, H. Chen, Z. Wang, M. Srebro-Hooper, N. Vanthuyne, S. Chevance, C. Roussel, J.A.G. Williams, J. Autschbach, R. Réau, Z. Duan, C. Lescop, J. Crassous, Bimetallic gold(I) complexes with ethynyl-helicene and bis-phosphole ligands: understanding the role of aurophilic interactions in their chiroptical properties, Chem. Eur. J. 22 (2016) 6075–6086.

[37] N. Hellou, M. Srebro-Hooper, L. Favereau, F. Zinna, E. Caytan, L. Toupet, V. Dorcet, M. Jean, N. Vanthuyne, J.A.G. Williams, L. Di Bari, J. Autschbach, J. Crassous, Enantiopure cycloiridiated complexes bearing a pentahelicenic N-heterocyclic carbene and displaying long-lived circularly polarized phosphorescence, Angew. Chem. Int. Ed. 56 (2017) 8236–8239.

[38] E. Anger, M. Rudolph, L. Norel, S. Zrig, C. Shen, N. Vanthuyne, L. Toupet, J.A.G. Williams, C. Roussel, J. Autschbach, J. Crassous, R. Réau, Multifunctional and reactive enantiopure organometallic helicenes: Tuning chiroptical properties by structural variations of mono- and bis-(platinahelicene)s, Chem. Eur. J. 17 (2011) 14178–14198.

[39] C. Shen, E. Anger, M. Srebro, N. Vanthuyne, K.K. Deol, T.D. Jefferson, Jr., G. Muller, J.A.G. Williams, L. Toupet, C. Roussel, J. Autschbach, R. Réau, J. Crassous, Straightforward access to mono- and bis-cycloplatinated helicenes displaying circularly polarized phosphorescence by using crystallization resolution methods, Chem. Sci. 5 (2014) 1915–1927.

[40] N. Saleh, B. Moore, II, M. Srebro, N. Vanthuyne, L. Toupet, J.A.G. Williams, C. Roussel, K.K. Deol, G. Muller, J. Autschbach, J. Crassous, Acid/base-triggered switching of circularly polarized luminescence and electronic circular dichroism in organic and organometallic helicenes, Chem. Eur. J. 21 (2015) 1673–1681.

[41] L.P. Ardasheva, G.A. Shagisultanova, Concentration and aggregation effects on luminescence properties of Pt(II) complexes with N.N'-bis(salicylidene)-1,3-propanediamine, Russ. J. Inorg. Chem. 43 (1998) 85–91.

[42] H. Houjou, Y. Hoga, Y.L. Ma, H. Achira, I. Yoshikawa, T. Mutai, K. Matsumara, Dinuclear fused salen complexes of group-10 metals: peculiarity of the crystal structure and near-infrared luminescence of a bis(Pt-salen) complex, Inorg. Chim. Acta, 461 (2017) 27–34.

[43] T.C. Cheung, K.K. Cheung, S.M. Peng, C.M. Che, Photoluminescent cyclometallated diplatinum(II,II) complexes: photophysical properties and crystal structures of $[PtL(PPh_3)]ClO_4$ and $[Pt_2L_2(\mu\text{-dppm})][ClO_4]_2$ (HL = 6-phenyl-2,2'-bipyridine, dppm = $Ph_2PCH_2PPh_2$) J. Chem. Soc. Dalton Trans. (1996) 1645–1651.

[44] W. Lu, B.X. Mi, M.C.W. Chan, Z. Hui, C.M. Che, N. Zhu, S.T. Lee, Light-emitting tridentate cyclometalated platinum(II) complexes containing sigma-alkynyl auxiliaries: tuning of photo- and electrophosphorescence, J. Am. Chem. Soc. 126 (2004) 4958–4971.

[45] S. H. Wu, Y.W. Zhong, J. Yao, 2,3-Di(2-pyridyl)-5-phenylpyrazine: a NN–CNN-type bridging ligand for dinuclear transition-metal complexes, Chem. Asian J. 8 (2013) 1504–1513.

[46] H. Ozawa, M. A. Haga, K. Sakai, A photo-hydrogen-evolving molecular device driving visible-light-induced EDTA-reduction of water into molecular hydrogen, J. Am. Chem. Soc. 128 (2006) 4926–4927.

[47] R. Sahai, D.A. Baucom, D.P. Rillema, Strongly luminescing ruthenium(II)/ruthenium(II) and ruthenium(II)/platinum(II) binuclear complexes, Inorg, Chem. 25 (1986) 3843–3845.

[48] V.W.W. Yam, V.W.M. Lee, K.K. Cheung, Synthesis, photophysics and electrochemistry of a novel luminescent organometallic ruthenium(II) platinum(II) binuclear complex and its ruthenium(II) dichloro-platinum(II) and palladium(II) counterparts – X-ray crystal structure of $[Ru(bpy)_2(\mu\text{-}2,3\text{-dpp})PtCl_2]^{2+}$ [2,3-dpp = 2,3-bis(2-pyridyl)pyrazine], J. Chem. Soc. Chem. Commun. (1994) 2075.

[49] M. Milkevitch, E. Brauns, K.J. Brewer, Spectroscopic and electrochemical properties of a series of mixed-metal d^6, d^8 bimetallic complexes of the form $[(bpy)_2M(BL)PtCl_2]^{2+}$ (bpy = 2,2'-bipyridine; BL = dpq (2,3-bis(2-pyridyl)quinoxaline) or dpb (2,3-bis(2-pyridyl)benzoquinoxaline); M = Os^{II} or Ru^{II}), Inorg, Chem. 35 (1996) 1737–1739.

[50] G.F. Manbeck, K.J. Brewer, Photoinitiated electron collection in polyazine chromophores coupled to water reduction catalysts for solar H_2 production, Coord. Chem. Rev. 257 (2013) 1660–1675.

[51] Y.J. Cho, S.Y. Kim, C.M. Choi, N.J. Kim, C.H. Kim, D.W. Cho, H.J. Son, C. Pac, S.O. Kang, Photophysics and excited-state properties of cyclometalated iridium(III)–platinum(II) and iridium(III)–iridium(III) bimetallic complexes bridged by dipyridylpyrazine, Inorg. Chem. 56 (2017) 5305–5315.

[52] H.X. Zhang, M. Kato, Y. Sasaki, T. Ohba, H. Ito, A. Kobayashi, H.-C. Chang and K. Uosaki, Terpyridine platinum(II) complexes conatining triazaine di-or tri-thiolate bridges: structures, luminescence, electrochemistry, and aggregation, Dalton Trans. **41** (2012) 11497–11506.

[53] S.D. Cummings and R. Eisenberg, Tuning the excited-state properties of platinum(II) diimine dithiolate complexes, J. Am. Chem. Soc. 118 (1996) 1949–1960.

[54] M. Jamshidi, S. M. Nabavizadeh, H. Sepehrpour, F. Niroomand, R. Kia and M. Rashidi, Cycloplatinated(II) complexes containing bridging bis(diphenyl[hosphine)acetylene: Photophysical study, *J Lumin.*, 2016, **179**, 222–229.

[55] K.S. Shin, K.I. Son, J.I. Kim, C.S. Hong, M. Suh, D.Y. Noh, Heteroleptic binuclear palladium(II) and platinum(II) complexes containing 1,2-bis(diphenylphosphine)acetylene and 1,2-benzenedithiolates: syntheses, crystal structures, electrochemistry and photoluminescence properties, Dalton Trans. (2009) 1767–1775.

[56] C. Bronner, M. Veiga, A. Guenet, L. De Cola, M. W. Hosseini, C. A. Strassert and S. A. Baudron, Excited state properties and energy transfer within dipyrrin-based binuclear iridium/platinum dyads: the effect of ortho-methylation on the spacer, Chem. Eur. J. **18** (2012) 4041–4050.

[57] E. Bahaidarah, Harriman, P. Stachelek, S. Rihn, E. Heyer, R. Ziessel, Fluorescent molecular rotors based on the BODIPY motif: effect of remote substituents, Photochem. Photobiol. Sci. 13 (2014) 1397–1401.

[58] B. Ma, P.I. Djurovich, M. Yousufuddin, R. Bau, M.E. Thompson, Phosphorescent platinum dyads with cyclometalated ligands: synthesis, characterization, and photophysical studies, J. Phys. Chem. C 112 (2008) 8022–8031.

[59] A.M. Prokhorov, A. Santoro, J.A.G. Williams, D.W. Bruce, Phosphorescent mesomorphic dyads based on tetraacetylethane complexes of iridium(III), Angew. Chem. Int. Ed. 51 (2012) 95–98.

[60] B.C. Tzeng, W.F. Fu, C.M. Che, H.Y. Chao, K.K. Cheung, S.M. Peng, Structures and photoluminescence of dinuclear platinum(II) and palladium(II) complexes with bridging thiolates and 2,2'-bipyridine or 2,2':6',2"-terpyridine ligands, J. Chem. Soc., Dalton Trans. (1999) 1017–1023.

[61] K. Umakoshi, I. Kinoshita, Y. Fukui-Yasuba, K. Matsumoto, S. Ooi, H. Nakai, M. Shiro, Binuclear platinum(II) complexes bridged by pyridine-2-thiolate and related ligands. Synthesis and crystal structure, J. Chem. Soc., Dalton Trans. (1989) 815–819.

[62] M. Kato, A. Omura, A. Toshikawa, S. Kishi, Y. Sugimoto, Vapor-induced luminescence switching in crystals of the syn isomer of a dinculear (bipyridine)platinum(II) complex bridged with pyridine-2-thiolate ions, Angew. Chem. Int. Ed. 41 (2002) 3183–3185.

[63] E.A. Katlenok, A.A. Zolotarev, K.P. Balashev, Binuclear complexes of Pt(II) with platinated 2-phenylbenzothiazole and bridged derivatives of pyridine- and benzothiazol-2-thiols, Russ. J. Gen. Chem. 84 (2014) 1593–1598.

[64] E.A. Katlenok, K.P. Balashev, The effect of the nature of peripheral platinated and bridging mercapto ligands on the optical and electrochemical properties of binuclear Pt(II) complexes with a metal-metal chemical bond, Opt. Spectrosc. 117 (2014) 374–380.

[65] Z. Wang, L. Jiang, Z.P. Liu, C.R.R. Gan, Z. Liu, X.H. Zhang, J. Zhao, T.S.A. Hor, Facile formation and redox of benzoxazole-2-thiolate-bridged dinuclear Pt(II/III) complexes, Dalton Trans. 41 (2012) 12568–12576.

[66] V. Sicilia, P. Borja, J. M. Casas, S. Fuertes, A. Martin, Selective synthesis of new half-lantern benzoquinolate platinum complexes. DFT and photophysical studies on the platinum(II,II) derivative, J. Organomet. Chem. 731 (2013) 10–17.

[67] V. Sicilia, P. Borja, J. M. Casas, S. Fuertes, A. Martin, Highly luminescent half-lantern cyclometalated platinum(II) complex: structure, luminescence studies, and reactivity, Inorg. Chem. 51 (2012) 3427–3435.

[68] Y. Zhu, K. Luo, L. Zhao, H. Ni, Q. Li, Binuclear platinum(II) complexes based on 2-mercaptobenzthiazole, 2-mercaptobenzimidazole and 2-hydroxypyridine as bridging ligands: red and near-infrared luminescence originated from MMLCT transition, Dyes and Pigments 145 (2017) 144–151.

[69] X. Wu, Y. Liu, Y. Wang, L. Wang, H. Tan, M. Zhu, W. Zhu, Y. Cao, Highly efficient near-infrared emission from binuclear cyclo-metalated platinum complexes bridged with 5-(4-octyloxyphenyl)-1,3,4-oxadiazole-2-thiol in PLEDs, Org. Electron. 13 (2012) 932–937.

[70] W. Xong, F. Meng, H. Tan, Y. Wang, P. Wang, Y. Zhang, Q. Tao, S. Su, W. Zhu, Dinuclear platinum complexes containing aryl-isoquinoline and oxadiazole-thiol with an efficiency of over 8.8%: in-depth investigation of the relationship between their molecular structure and near-infrared electroluminescent properties in PLEDs, J. Mater. Chem. C 4 (2016) 6007–6015.

[71] M.A. Bennett, S.K. Bhargava, E.C.C. Cheng, W.H. Lam, T.K.M. Lee, S.H. Privér, J. Wagler, A.C. Willis, V.W.W. Yam, Unprecedented near-infrared (NIR) emission in diplatinum(III) (d^7–d^7) complexes at room temperature, J. Am. Chem. Soc. 132 (2010) 7094–7103.

[72] M. Yoshida, N. Yashiro, H. Shitama, A. Kobayashi, M. Kato, A redox-active dinuclear platinum complex exhibiting multicolored electrochromism and luminescence, Chem. Eur. J. 22 (2016) 491–495.

[73] H. Leopold, M. Tenne, A. Tronnier, S. Metz, I. Münster, G. Wagenblast, T. Strassner, Binuclear C^C* cyclometalated platinum(II) NHC complexes with bridging amidinate ligands, Angew. Chem. Int. Ed. 55 (2016) 15779–15782.

[74] B. Ma, P.I. Djurovich, M. Yousufuddin, R. Bau, M.E. Thompson, Synthetic control of Pt···Pt separation and photophysics of binuclear platinum complexes, J. Am. Chem. Soc. 127 (2005) 28–29.

[75] M. Han, Y. Tian, Z. Yuan, L. Zhu, B. Ma, A phosphorescent molecular “butterfly” that undergoes a photoinduced structural change allowing temperature sensing and white emission, Angew. Chem. Int. Ed. 53 (2014) 10908–10912.

[76] C. Zhou, Y. Tian, Z. Yuan, M. Han, J. Wang, L. Zhu, M. S. Tameh, C. Huang, B. Ma, Precise design of phosphorescent structural change and dual emission, Angew, Chem. Int. Ed. 54 (2015) 9591–9595.

[77] R. Muñoz-Rodriguez, E. Buñuel, J.A.G. Williams, D.J. Cárdenas, Divergent luminescence bahviour from differential interactions in dinuclear Pt, Au, and mixed Pt–Au complexes built on a xanthene scaffold, Chem. Commun. 48 (2012) 5980–5982.

[78] S. Develay, J.A.G. Williams, Intramolecular excimers based on rigidly-linked platinum(II) complexes: intense deep-red triplet luminescence in solution, Dalton Trans. (2008) 4562–4564.

[79] J.A.G. Williams, The coordination chemistry of dipyridylbenzene: N-deficient terpyridine or panacea for brightly luminescent metal complexes? Chem. Soc. Rev. 38 (2009) 1783–1801.

[80] Z. Guo, S.M. Yiu, M.C.W. Chan, Shape-persistent (Pt-salphen)$_2$ phosphorescent coordination frameworks: structural insights and selective perturbations, Chem. Eur. J. 19 (2013) 8937–8947.

[81] S.W. Lai, M.C.W. Chan, T.-C. Cheung, S.M. Peng, C.-M. Che, Probing $d^8 - d^8$ Interactions in Luminescent Mono- and Binuclear Cyclometalated Platinum(II) Complexes of 6-Phenyl-2,2‘-bipyridines, Inorg. Chem. 38 (1999) 4046–4055.

[82] J.W. Steed, Supramolecular gel chemistry: developments over the last decade, Chem. Commun. 47 (2011) 1379–1383.

[83] Z. Zhao, J.W.Y. Lam, B.Z. Tang, Self-assembly of organic luminophores with gelation-enhanced emission characteristics, Soft Matter. 9 (2013) 4564–4579.

[84] A.Y.Y. Tam, V.W.W. Yam, Recent advances in metallogels, Chem. Soc. Rev. 42 (2013) 1540–1567.

[85] J. Mei, N.L.C. Leung, R.T.K. Kwok, J.W.Y. Lam, B.Z. Tang, Aggregation-induced emission: Together we Shine, united we soar!, Chem. Rev. 115 (2015) 11718–11940.

[86] N. Komiya, T. Muraoka, M. Iida, M. Miyanaga, K. Takahashi, T. Naota, Ultrasound-induced emission enhancement based on structure-dependent homo- and heterochiral aggregations of chiral binuclear platinum complexes, J. Am. Chem. Soc. 133 (2011) 16054–16061.

[87] N. Komiya, M. Okada, K. Fukumoto, D. Jomori, T. Naota, Highly phosphorescent crystals of vaulted trans-bis(salicylaldiminato)platinum(II) Complexes, J. Am. Chem. Soc. 133 (2011) 6493–6496.

[88] F. Gou, J. Cheng, X. Zhang, G. Shen, X. Zhou, H. Xiang, Unusual aggregation/gelation-induced phosphorescence of propeller-type binuclear platinum(II) enantiomers, Eur. J. Inorg. Chem. 30 (2016) 4862–4866.

[89] S. Liu, H. Sun, Y. Ma, S. Ye, X. Liu, X. Zhou, X. Mou, L. Wang, Q. Zhao, W. Huang, Rational design of metallophosphors with tunable aggregation-induced phosphorescent emission and their promising applications in time-resolved luminescence assay and targeted luminescence imaging of cancer cells, J. Mater. Chem. 22 (2012) 22167.

[90] L.-B. Xing, F. Qiao, Z. Yuan, J.-L. Zhang, R.-Y. Zhang, S. Zhuo, Z.-Y. Zhou, Binuclear alkynylplatinum(II) terpyridine complexes with flexible bridges behave as organogelators for several organic solvents, RSC Adv. 7 (2017) 14389–14394.

[91] V.W.W. Yam, R.P.L. Tang, K.M.C. Wong, K.K. Cheung, Synthesis, luminescence, electrochemistry, and ion-binding studies of platinum(II) terpyridyl acetylide complexes, Organometallics. 20 (2001) 4476–4482.

[92] T.K. Aldridge, E.M. Stacy, D.R. McMillin, Studies of the room-temperature absorption and emission Spectra of $[Pt(trpy)X]^+$ systems, Inorg. Chem. 33 (1994) 722–721.

[93] H. Achira, Y. Hoga, I. Yoshikawa, T. Mutai, K. Matsumura, H. Houjou, Effects of a semiflexible linker on the mechanochromic photoluminescence of bis(Pt-salen) complex, Polyhedron. 113 (2016) 123–131.

[94] H. Achira, M. Ito, T. Mutai, I. Yoshikawa, K. Araki, H. Houjou, Spontaneous helical folding of bis(Ni-salphen) complexes in solution and in the solid state: spectroscopic tracking of the unfolding process induced by Na^+ ions, Dalton Trans. 43 (2014) 5899–5907.

[95] Z.L. Gong, Y.W. Zhong, J. Yao, Regulation of intra- and intermolecular Pt–Pt and π–π interactions of a U-shaped diplatinum complex to achieve pseudo-polymorphic emissions in solution and crystalline states, J. Mater. Chem. C. 5 (2017) 7222–7229.

[96] F.D. Lewis, P. Daublain, G.B. Delos Santos, W. Liu, A.M. Asatryan, S.A. Markarian, T. Fiebig, M. Raytchev, Q. Wang, Dynamics and mechanism of bridge-dependent charge separation in pyrenylurea-nitrobenzene π-stacked protophanes, J. Am. Chem. Soc. 128 (2006) 4792–4801.

[97] T.A. Zeidan, Q. Wang, T. Fiebig, F.D. Lewis, Molecular wire behavior in π-stacked donor-bridge-acceptor tertiary arylureas, J. Am. Chem. Soc. 129 (2007) 9848–9849.

[98] A. Gross, T. Moriuchi, T. Hirao, A dinuclear alkynylplatinum(II) pyridinedicarboxamide: conformational change-induced switching of emission properties, Chem. Commun. 49 (2013) 1163–1165.

[99] F.K.W. Hau, H.S. Lo, V.W.W. Yam, Synthesis and Photophysical Studies of Calixarene-Based Alkynylplatinum(II) Terpyridine Complexes with Various Receptor Sites for Colorimetric and Luminescence Sensing of Anions, Chem. Eur. J. 22 (2016) 3738–3749.

[100] S.Y.L. Leung, A.Y.Y. Tam, C.H. Tao, H.S. Chow, V.W.W. Yam, Single-turn helix-coil strands stabilized by metal---metal and π---π interactions of the alkynylplatinum(II) terpyridyl moieties in meta -phenylene ethynylene foldamers, J. Am. Chem. Soc. 134 (2012) 1047–1056.

[101] S.Y.L. Leung, V.W.W.Yam, Hierarchical helices of helices directed by Pt···Pt and π–π stacking interactions: reciprocal association of multiple helices of dinuclear alkynylplatinum(II) complex with luminescence enhancement behavior, Chem. Sci. 4 (2013) 4228.

[102] S.Y.L. Leung, K.M.C. Wong, V.W.W. Yam, Self-assembly of alkynylplatinum(II) terpyridine amphiphiles into nanostructures via steric control and metal–metal interactions, Proc. Natl. Acad. Sci. 113 (2016) 2845–2850.

[103] P. Xu, H. Wu, H. Jia, S. Ye, P. Du, Linear bimetallic alkynylplatinum(II) terpyridyl complexes bearing p-phenylene ethynylene oligomers: Synthesis, characterization, aggregation, and photophysical properties, Organometallics. 33 (2014) 2738–2746.

[104] S. Huang, B. Yang, J. Zhong, H. Zhang, A theoretical investigation on the metal–metal interaction in a series of pyrazolate bridged platinum(II) complexes, Synth. Met. 205 (2015) 222–227.

[105] K. Ohno, H. Tanuma, Y. Kusano, S. Kaizaki, A. Nagasawa, T. Fujihara, Luminescence of tartrate bridged dinuclear 2,2′-bipyridine platinum(II) complexes: emission color controlled by intra- and inter-molecular interactions in the solid state, Dalt. Trans. 46 (2017) 7612–7618.

Captions to Figures

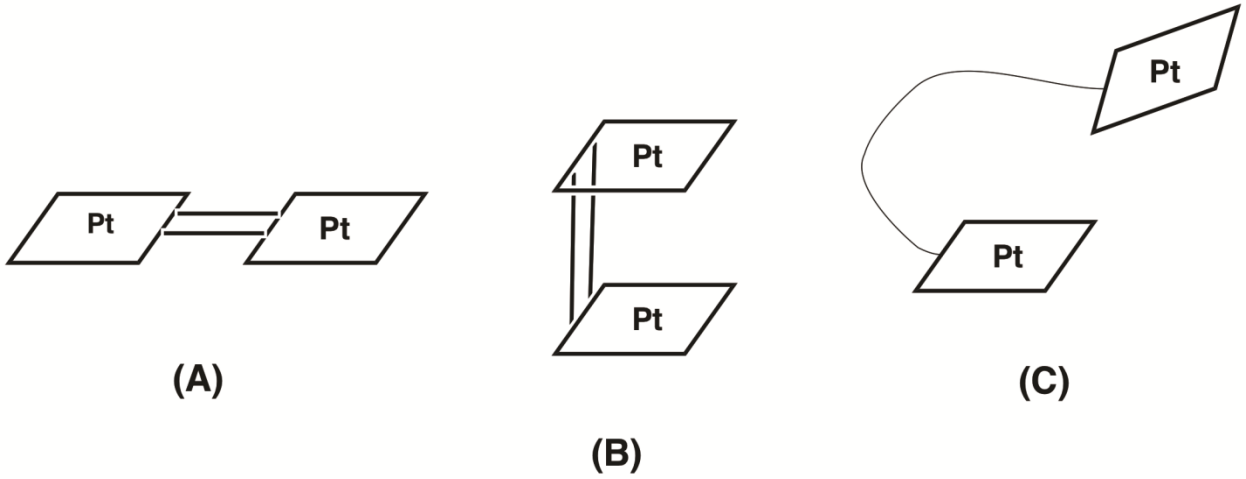

Figure 1 Schematic illustration of the three subdivisions of binuclear complexes as used in this review. **(A)** Complexes featuring rigid bridges that hold the Pt units in such a way that they cannot come together through *intramolecular* face-to-face interactions. **(B)** Complexes in which the Pt units are rigidly held in a conformation that favours face-to-face interactions between them, either in the ground state and/or the excited state. **(C)** Complexes with flexible bridges where the Pt units may behave as essentially independent units or interact with each other.

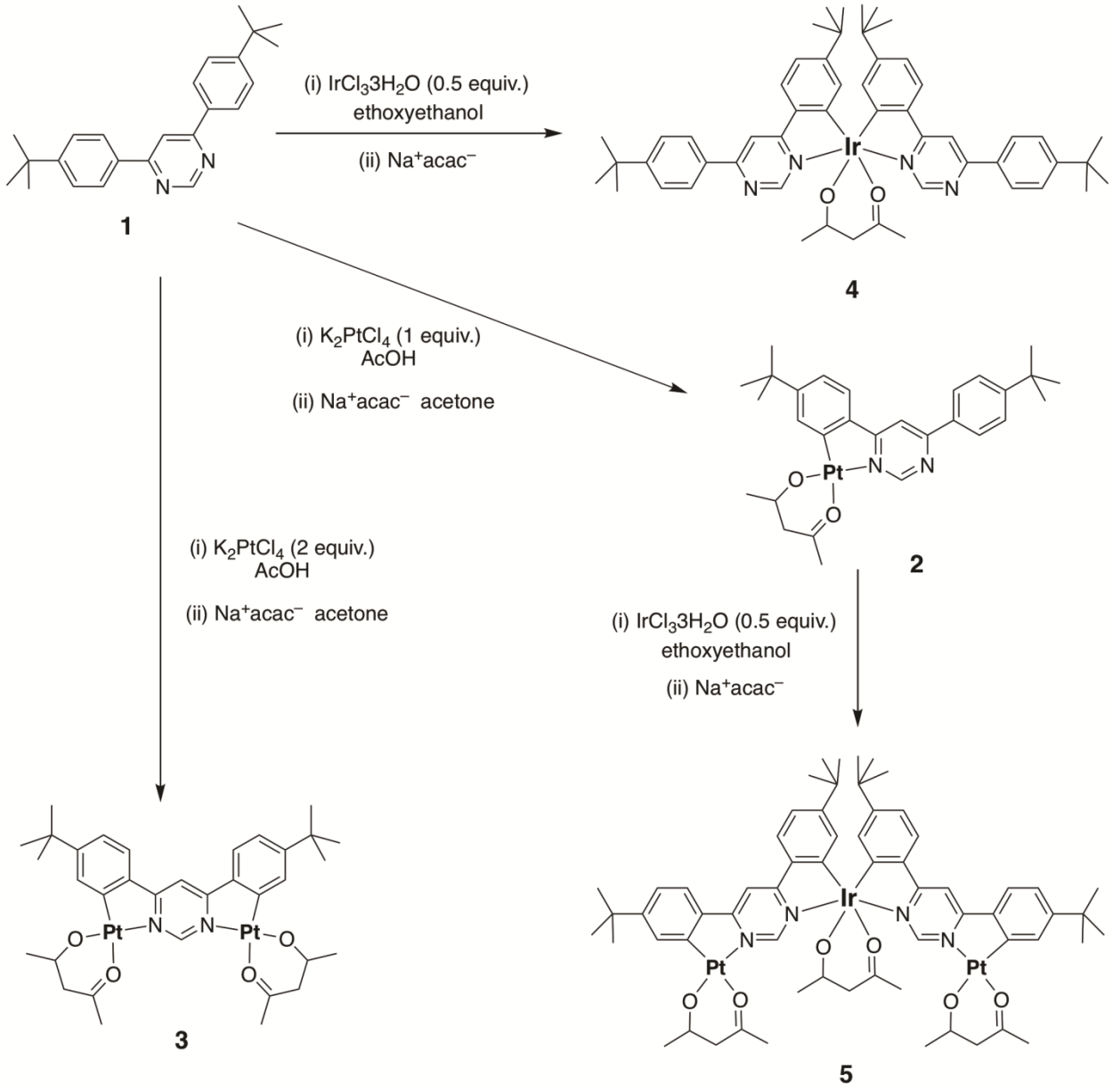

Figure 2 Structures and synthetic routes to the mono- and dinuclear Pt(II) complexes **2** and **3**, mononuclear iridium complex **4**, and the heterotrimetallic Pt_2Ir complex **5,** from the *bis*-N^C-cyclometallating proligand **1** [28].

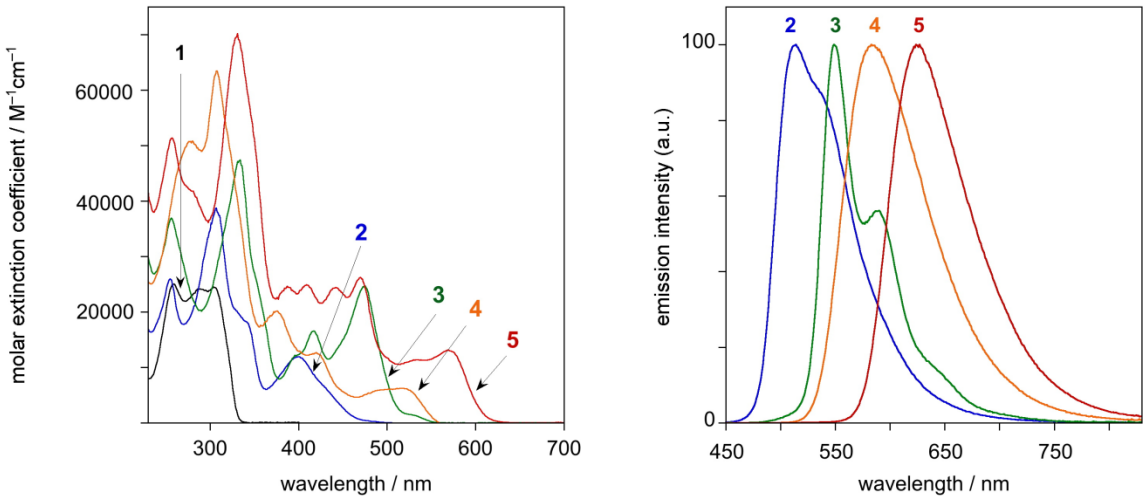

Figure 3 UV-visible absorption (left) and emission spectra (right) of **2**–**5** in CH_2Cl_2 at room temperature [28].

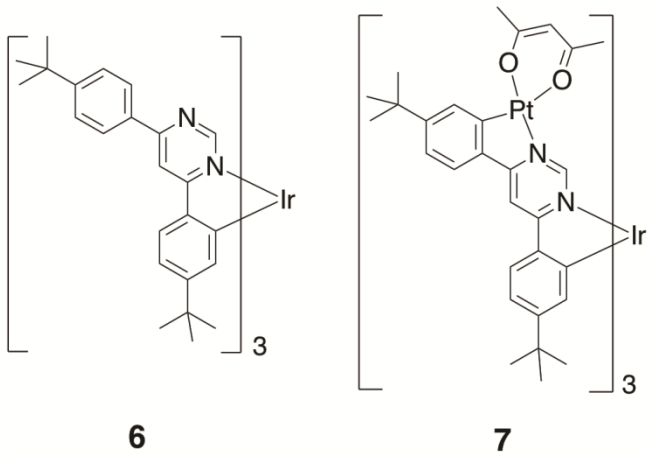

6 **7**

Figure 4 Structures of the Pt_3Ir complex **7** and the corresponding mononuclear iridium complex **6** [29].

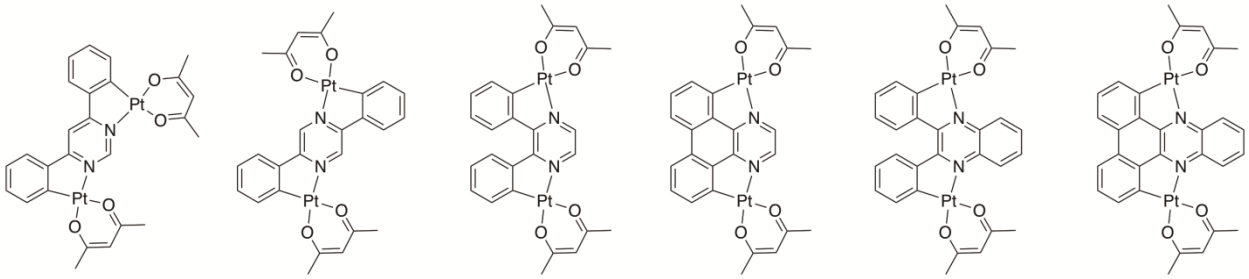

8 **9** **10** **11** **12** **13**

Figure 5 Structures of the dinuclear platinum(II) complexes **9–13** featuring diphenylpyrazine units, together with a diphenylpyrimidine analogue **8** [32].

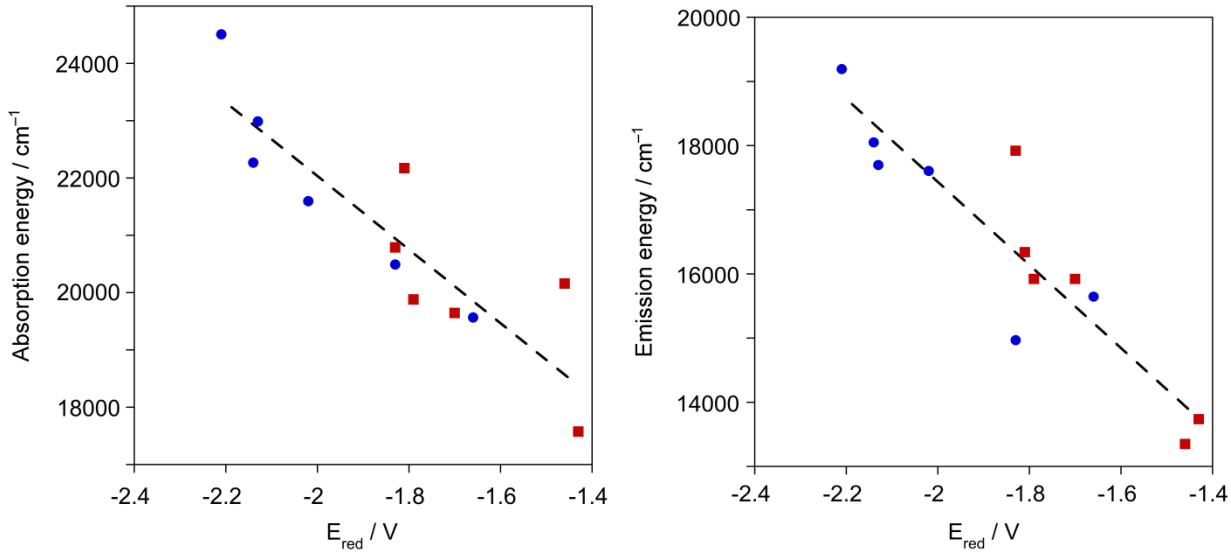

Figure 6 Left: plot of the lowest-energy absorption maximum in CH_2Cl_2 at 298 K (derived from λ_{max}) versus the reduction potential (values versus $Fc|Fc^+$) obtained by cyclic voltammetry for **8–13** (red squares), and for the corresponding mononuclear complexes (blue circles). Dashed line represents the best fit of the data for all 12 complexes; gradient = 6410 cm^{-1}/V. Right: corresponding plot for the emission maxima, under the same conditions; gradient of best-fit line = 6460 cm^{-1}/V [32].

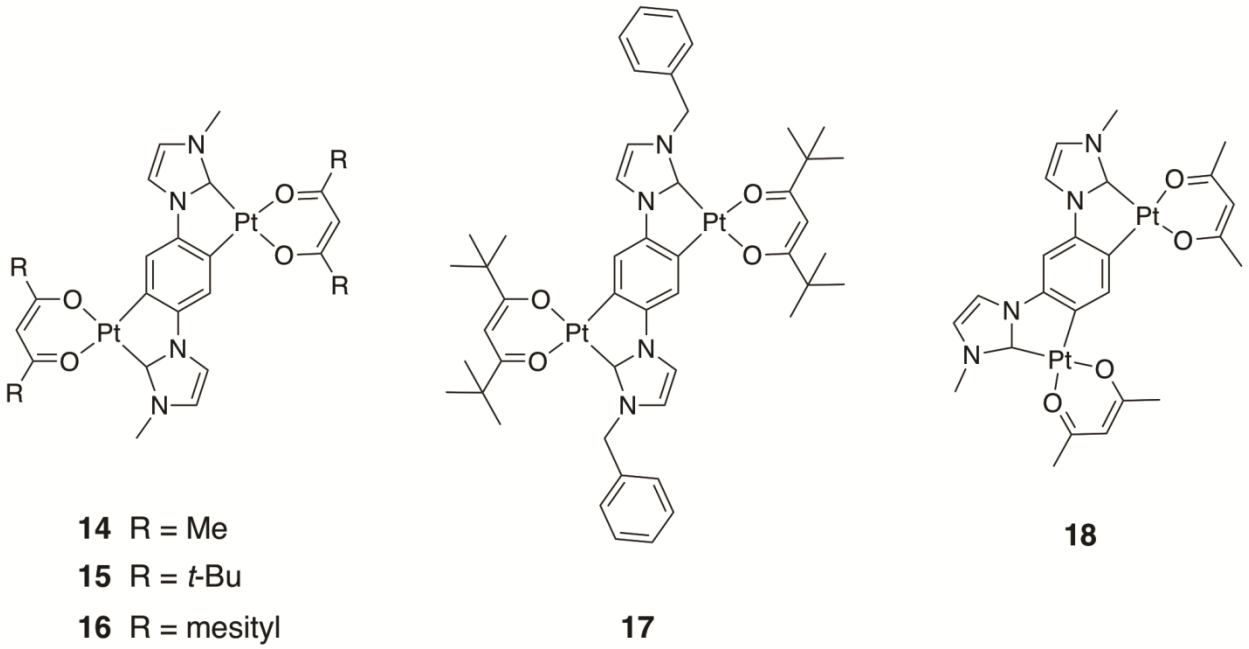

Figure 7 Diplatinum complexes **14**–**18** featuring N-heterocyclic carbene ligands [34].

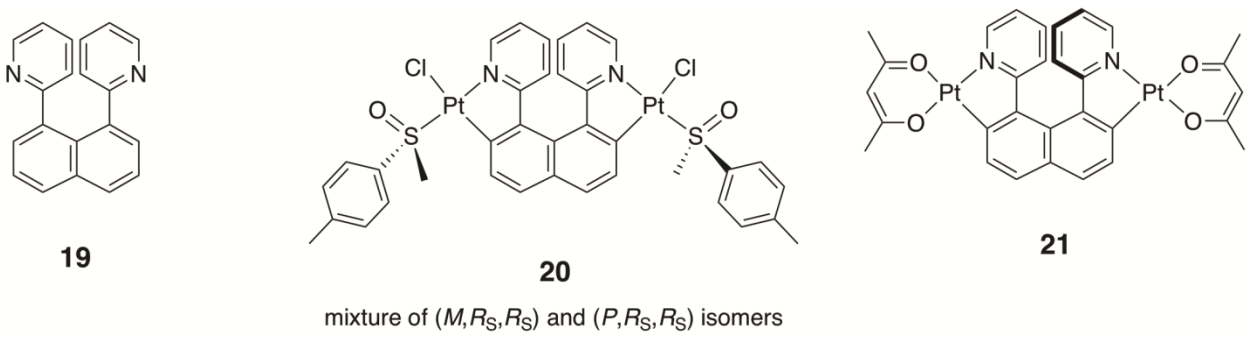

Figure 8 Enantiopure bis-platinahelicence **21** isolated following the resolution of diastersomeric complexes **20** containing chiral sulfoxide ligands, starting from 1,8-bis(2-pyridyl)naphathalene **19** [39].

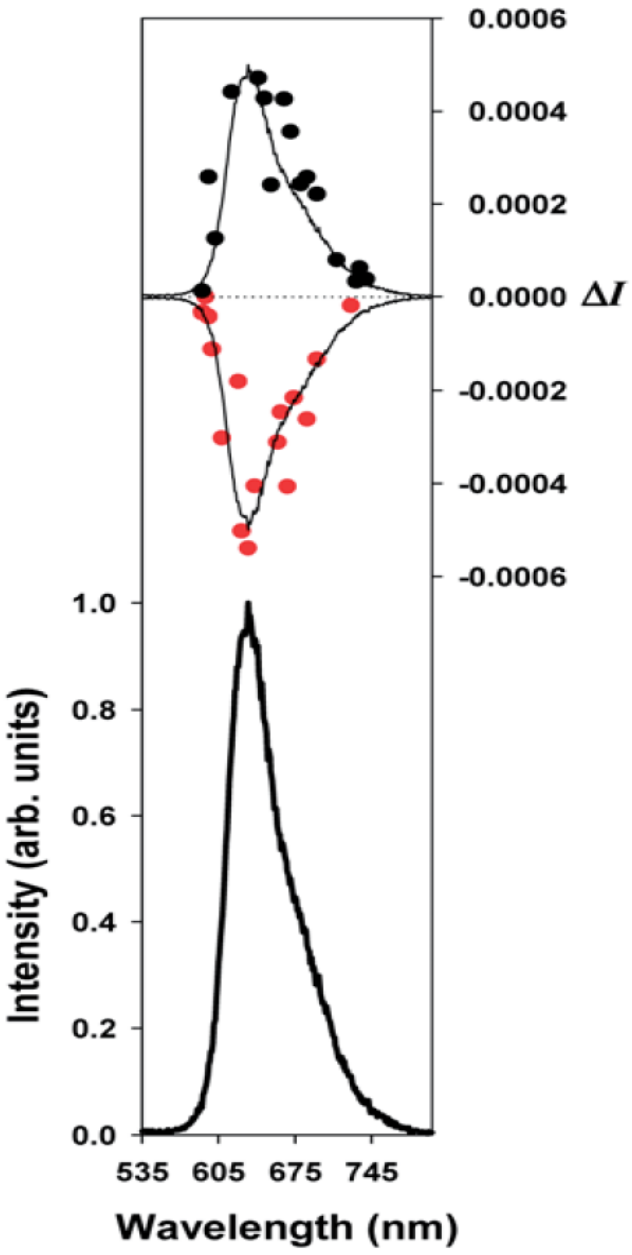

Figure 9 Cicurlarly polarized luminescence and total luminescence (upper and lower panels respectively) of *M*-**21** and *P*-**21** (red and black data points respectively) in degassed CH_2Cl_2 solution at 295 K. Reproduced from [39] by permission of The Royal Society of Chemistry.

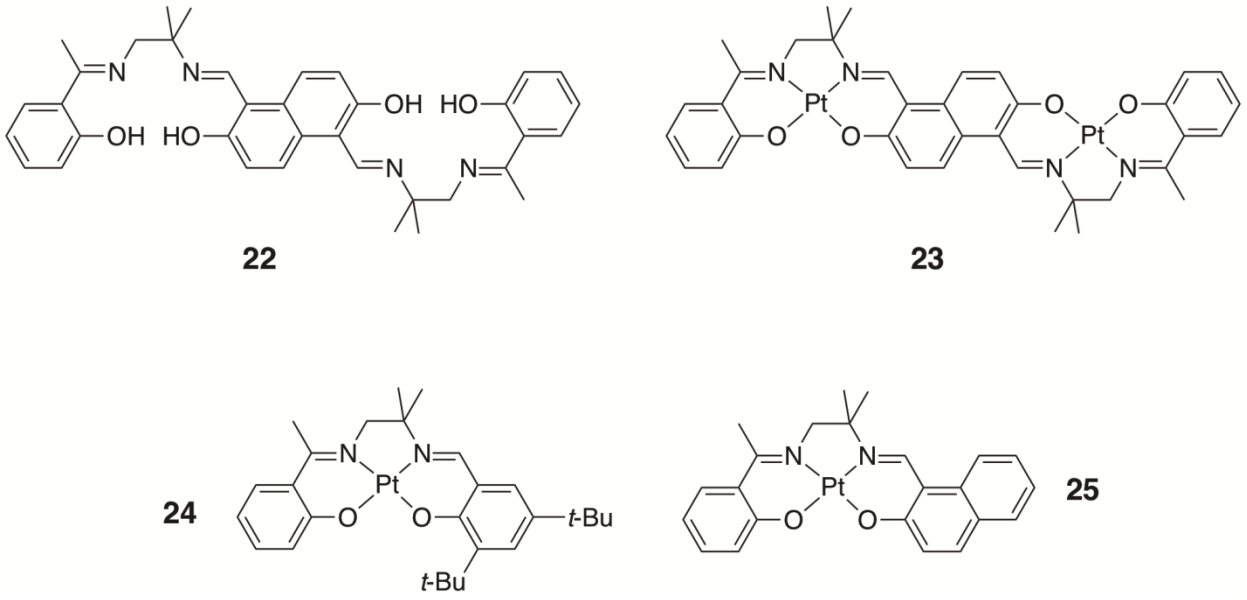

Figure 10 Structures of the *bis*-N_2O_2-coordinating bridging ligand **22** and its Pt_2 complex 23, with mononuclear models **24** and **25** [41].

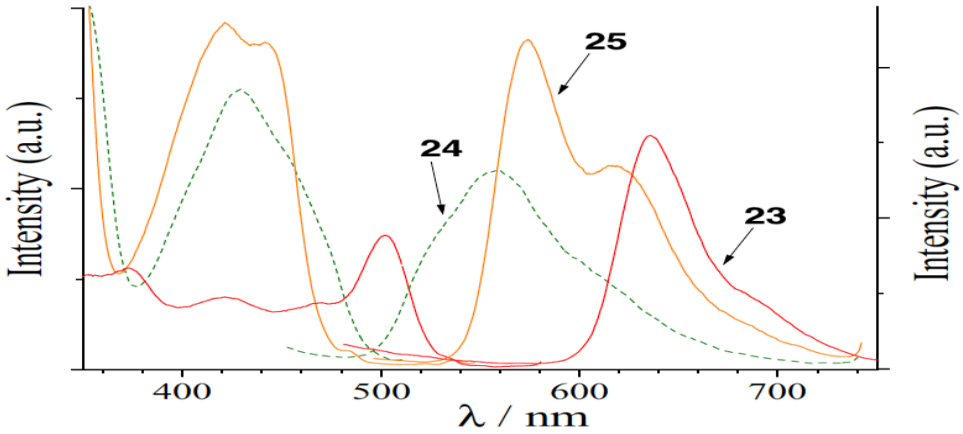

Figure 11 Emission and excitation spectra of **23**, **24**, and **25** in *o*-dichlorobenzene solution. Reprinted from [41] with permission of Elsevier.

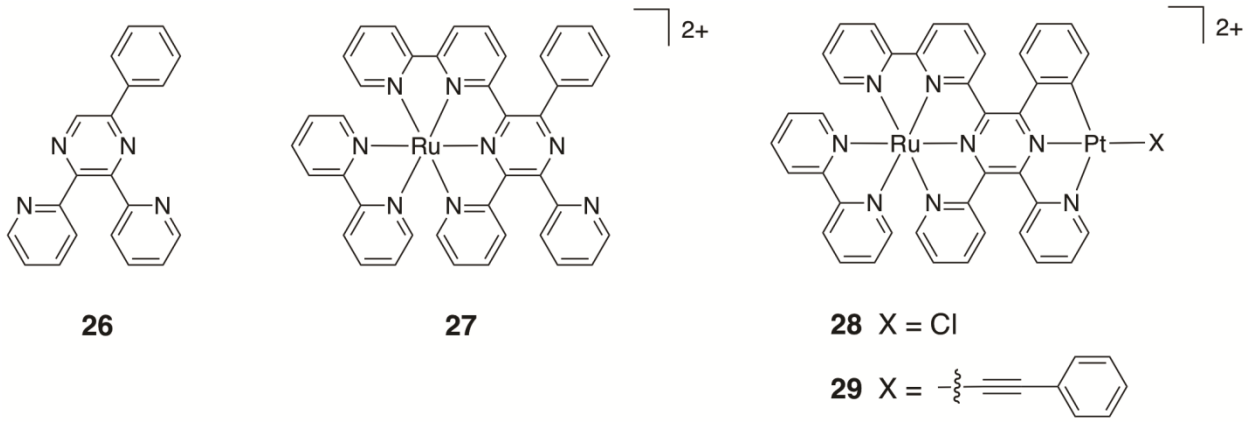

Figure 12 The NN–NNC bridging ligand **26** and the heterometallic RuPt complexes **28** and **29** isolated via the mononuclear Ru complex **27** [45].

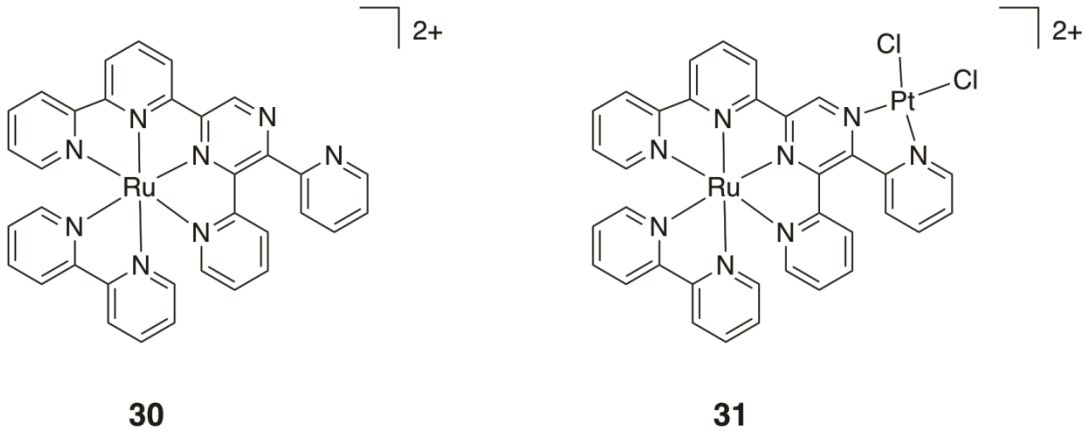

Figure 13 The bimetallic Ir-Pt complex **31** and its mono-iridium analogue **30** [51].

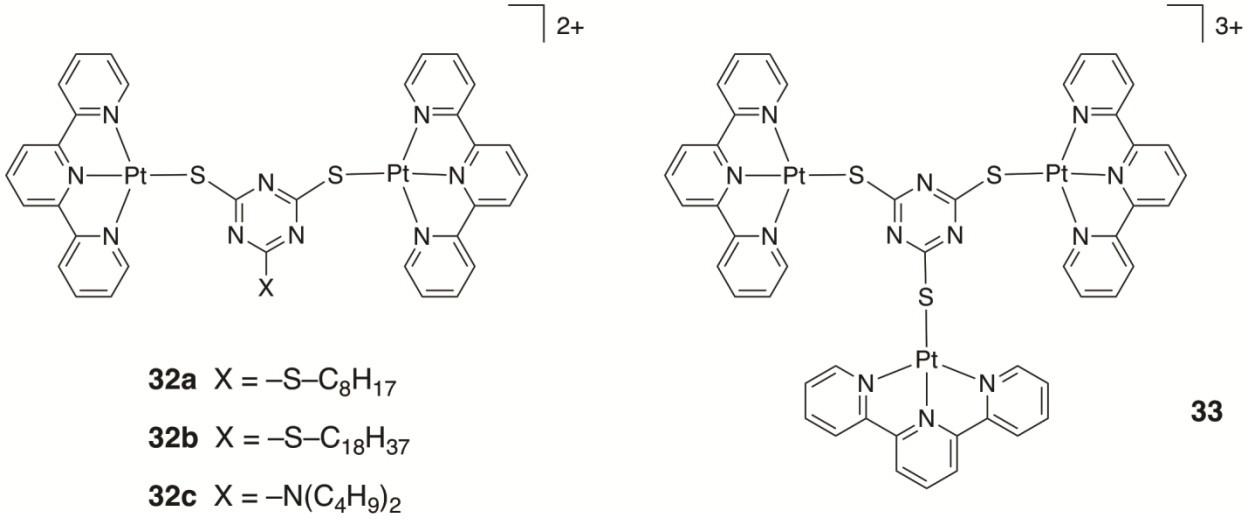

Figure 14 Multinuclear Pt(II) complexes **32a-c** and **33**, with triazine thiolate linkers [52].

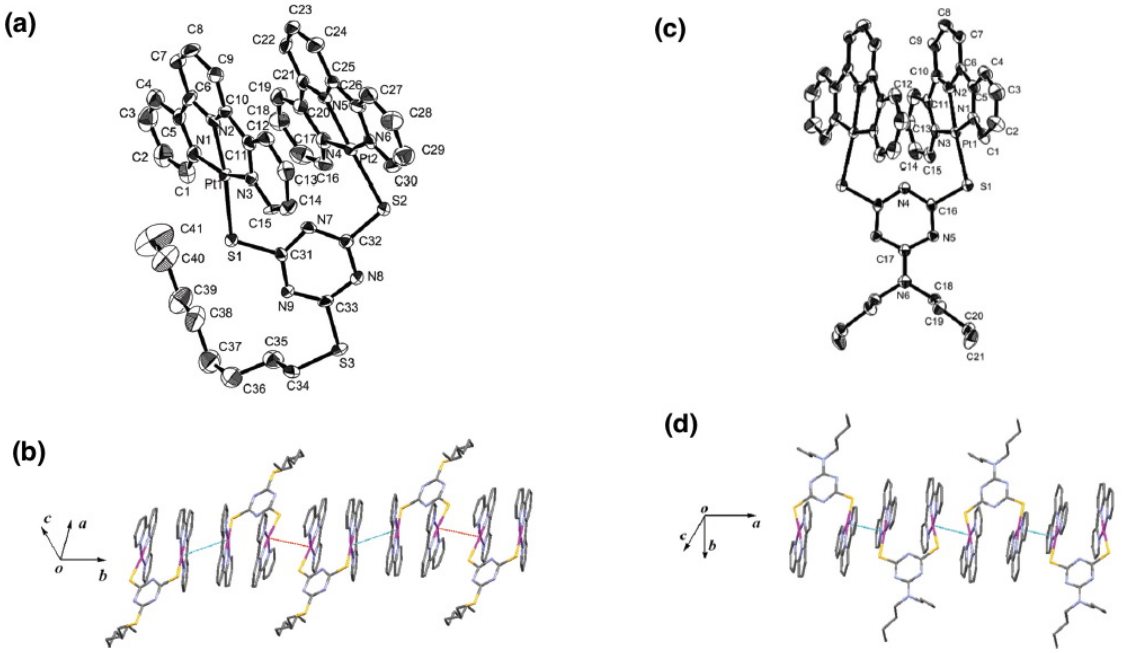

Figure 15 (a) Structure of **32a** in the crystal. (b) Crystal packing diagram of the cations in **32a**, with intermolecular Pt···Pt distances that are alternately short, 3.641(1) Å, and long, 4.352(1) Å. (c) Structure of **32c** in the crystal. (d) Crystal packing diagram of the cations in **32c**, with intermolecular Pt···Pt distances of 3.663(1) Å. Hydrogen atoms are omitted for clarity; thermal ellipsoids in (a) and (c) are shown at the 50% probability level. Reproduced from [52] by permission of The Royal Society of Chemistry.

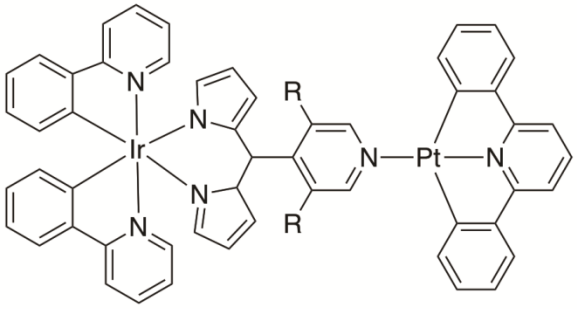

34 R = H
35 R = CH_3

Figure 16 Heterometallic Ir-Pt complexes **34** and **35** featuring a dipyrrin ligand bound to the $Ir(ppy)_2$ unit [56].

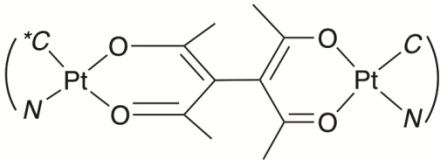

36

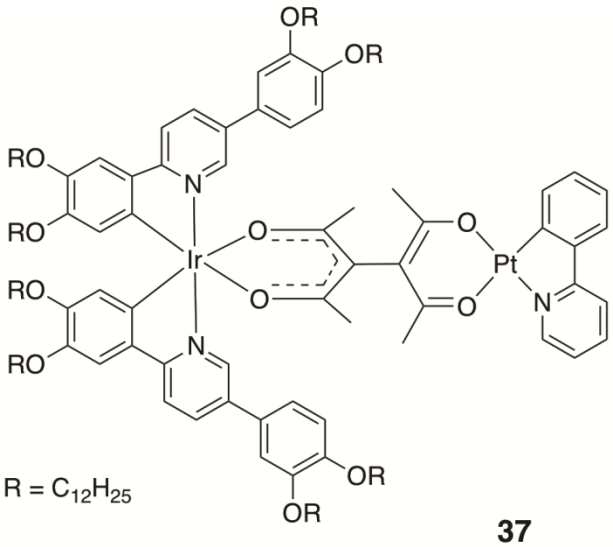

$R = C_{12}H_{25}$

37

Figure 17 Complexes with a *bis*-O^O-coordinating bridging ligand. Symmetrical (N^C* = N^C) and asymmetrical (N^C* ≠ N^C) complexes of type **36** reported by Thompson and co-workers [58], and the heterometallic Ir-Pt **37** synthesised by Bruce and co-workers for liquid crystalline properties [59].

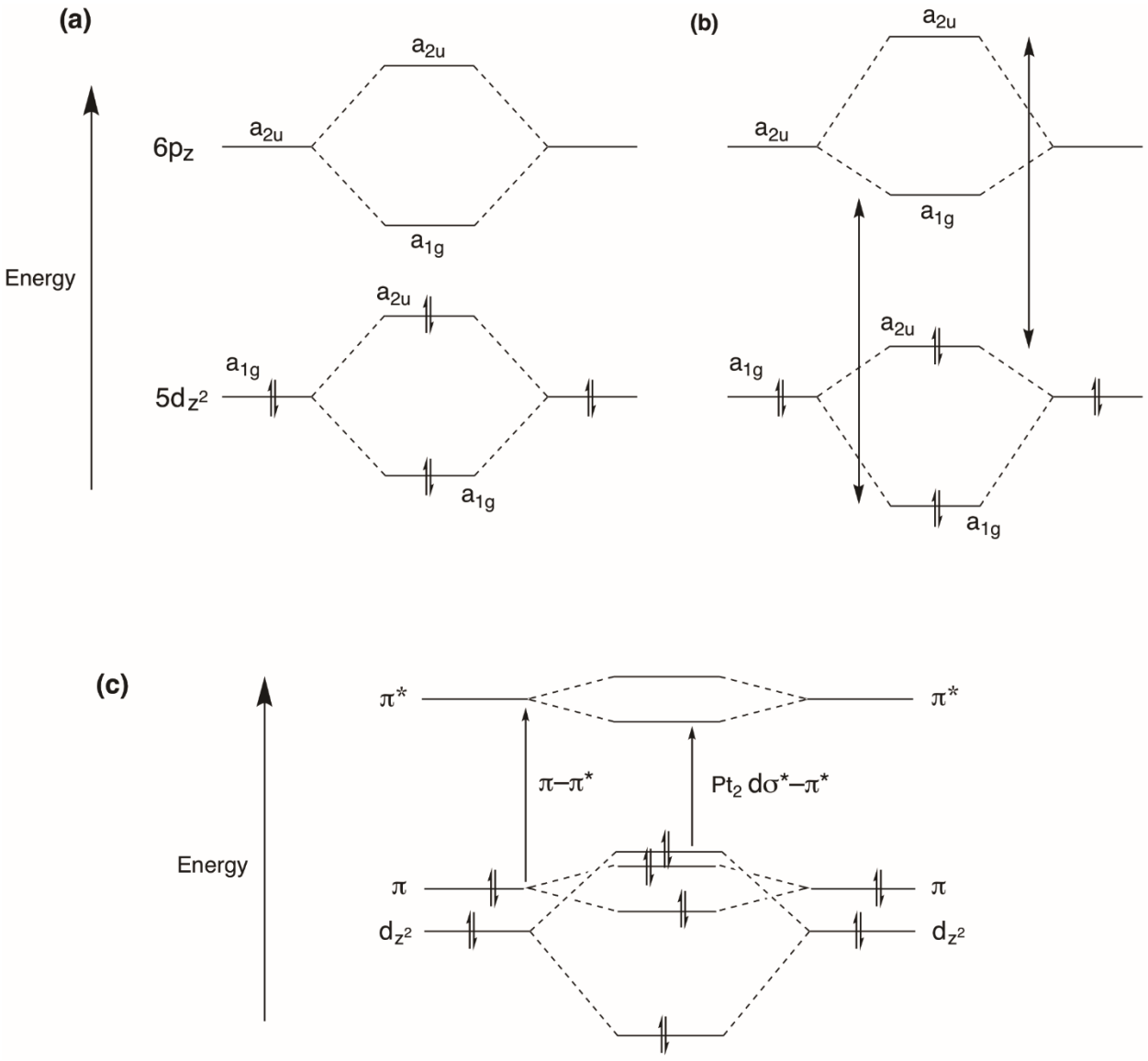

Figure 18 Molecular orbital scheme for a "dimer" consisting of two Pt(II) complexes interacting through Pt···Pt face-to-face interactions. (a) The interaction of the Pt centres through [vacant] $5d_{z2}$ and [filled] $6p_z$ orbitals without taking into account configuration interaction. (b) When configuration interaction between MOs of the same symmetry is taken into account, the resulting stabilisation becomes clear. (c) When conjugated aromatic ligands are present with

low-energy π* orbitals, the lowest-energy excited states are typically dσ*-π* (MMLCT), but note that π-π* transitions may also be significant.

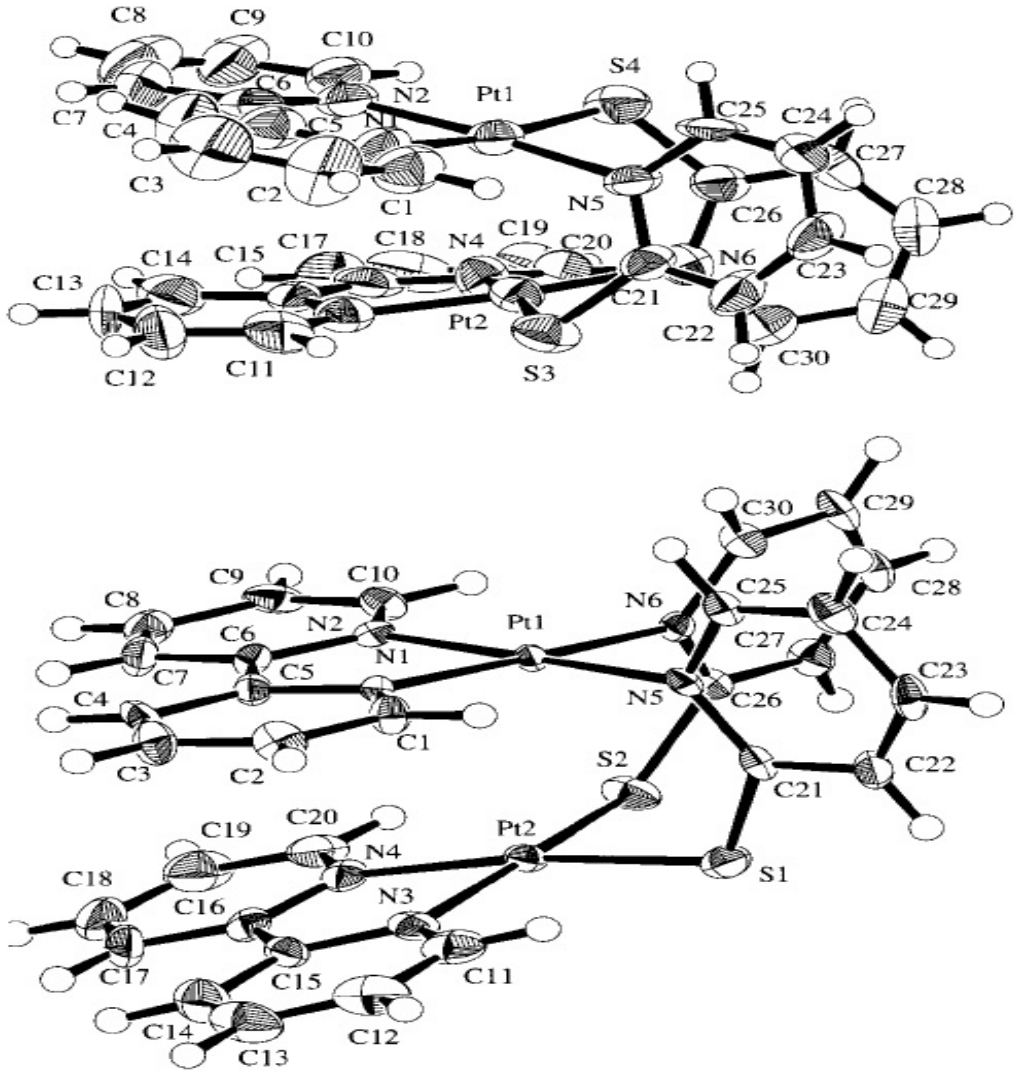

Figure 19 Isomers of $[Pt(bpy)(\mu\text{-pyS})]_2^{2+}$ **38** featuring an *anti* (top) or *syn* (bottom) arrangement of the bridging N^S ligands. Reproduced from [62] by permission of John Wiley & Sons Ltd.

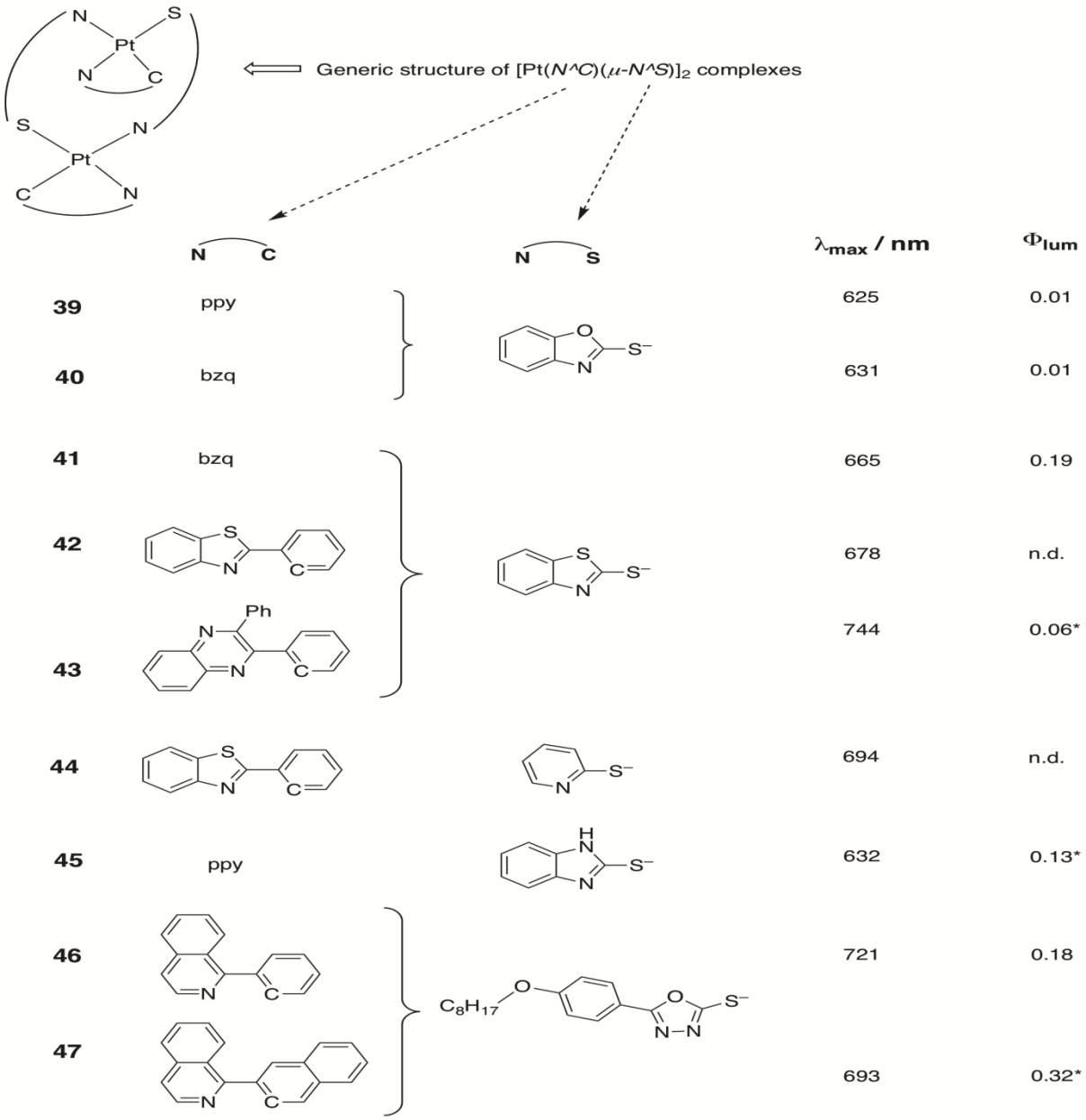

Figure 20 A selection of complexes of the type [Pt(*N*^*C*)(μ–*N*^*S*)]$_2$, together with luminescence λ_{max} and Φ_{lum} values in degassed CH_2Cl_2, except where indicated by an asterisk, for which the data refer to the complex doped into a thin film; **39**, **40** [65], **41** [67], **42** [63,64], **43** [68], **44** [63,64], **45** [68], **46** [69], **47** [70].

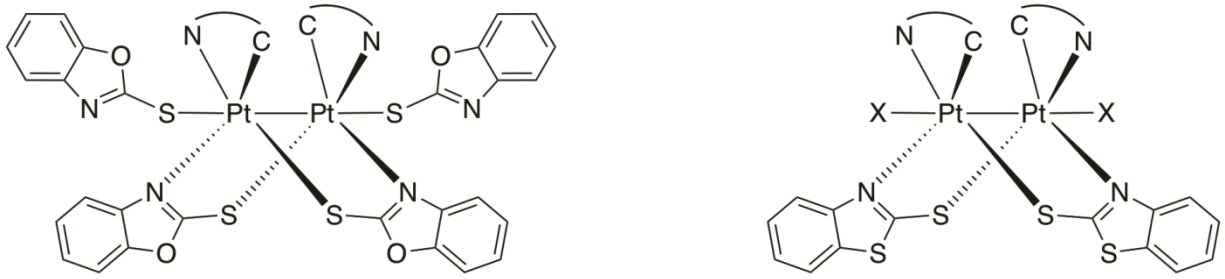

Figure 21 Examples of Pt(III)–Pt(III) dimers incorporating a Pt–Pt bond, formed through oxidation of corresponding *N^S*-bridged $Pt(II)_2$ complexes [65,67].

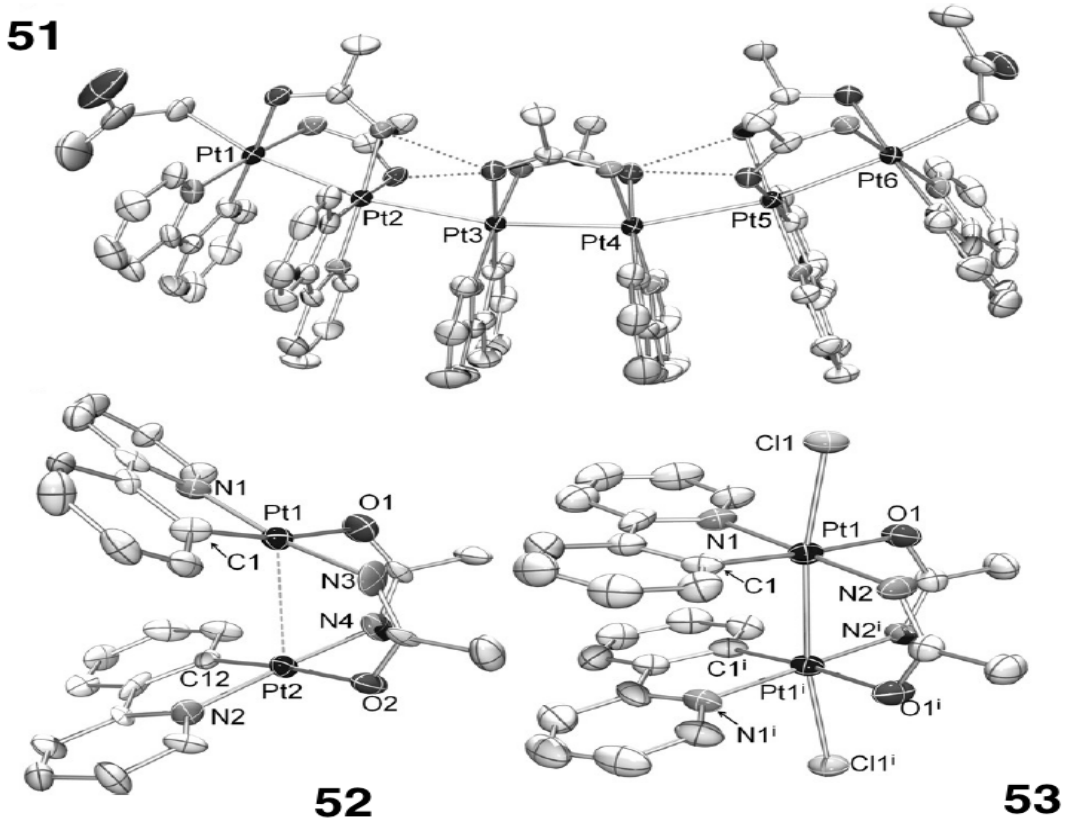

Figure 22 Molecular structures of **51**, **52**, and **53** in their respective crystals, in which the oxidation states of platinum are formally +2.33, +2, and +3 respectively. Ellipsoids are shown at the 50% probability level and hydrogen atoms are omitted for clarity. Reproduced from [72] by permission of John Wiley & Sons Ltd.

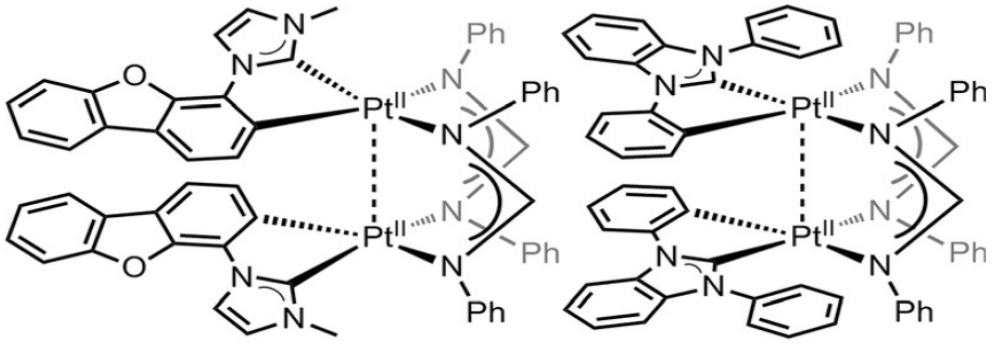

Figure 23 Amidinate-bridged $Pt(II)_2$ complexes with carbene ligands [73].

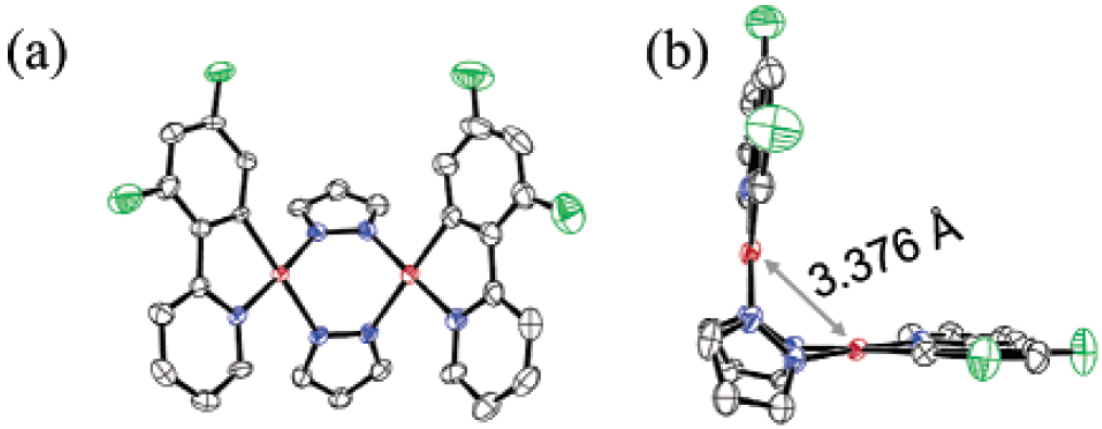

Figure 24 Two views of the molecular structure of $[Pt(dfppy)(\mu\text{-pz})]_2$ (**56** with *pz'* = pyrazole) in the crystal, showing the boat-like conformation that leads to short metal-metal separations. Reproduced with permission from [74]. Copyright 2005 American Chemical Society.

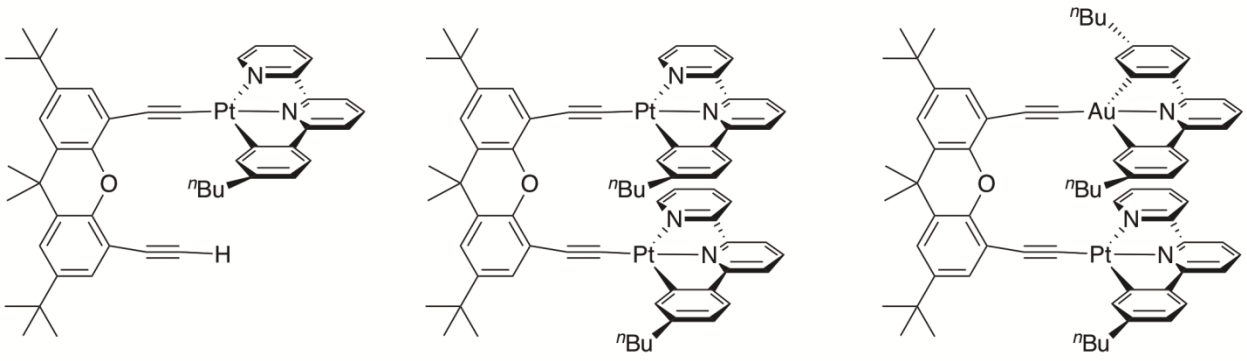

Figure 25 Dinuclear Pt(N^N^C) complex **58** with a bridging xanthene ligand and the structurally similar heterometallic Au-Pt complex **59**, together with the mononuclear model complex **57** [77].

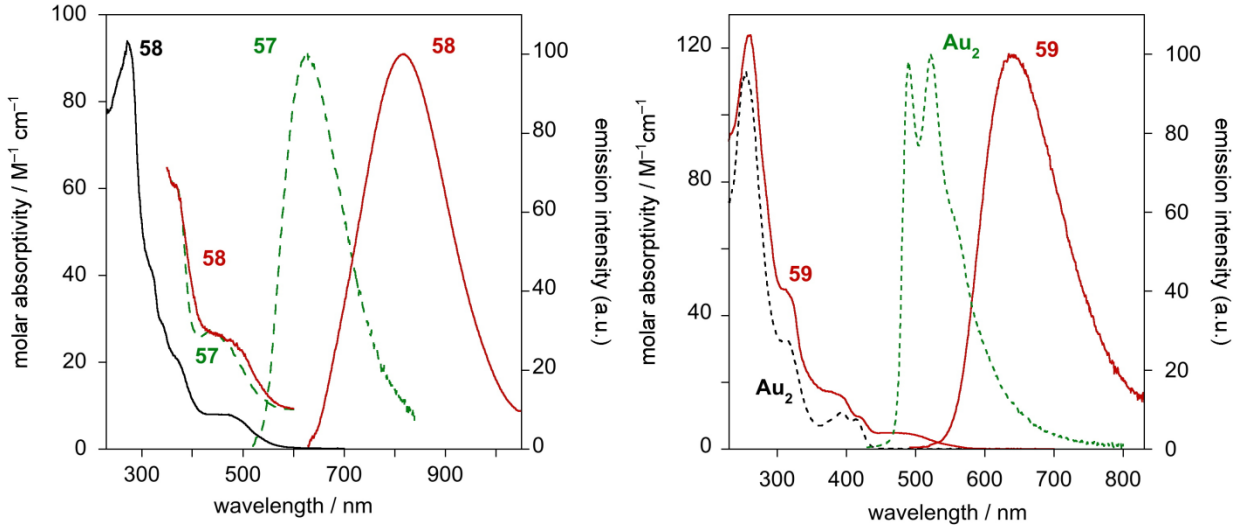

Figure 26 *Left:* Absorption spectrum of **58** and the emission and excitation spectra of **58** (solid lines) and **57** (dashed lines) in CH_2Cl_2 at room temperature. *Right:* Absorption and emission spectra of the heterometallic Au-Pt complex **59** (solid lines) together with the

corresponding spectra of the homo-dimetallic gold complex (dashed lines, labelled **Au_2**) in CH_2Cl_2 at room temperature [77].

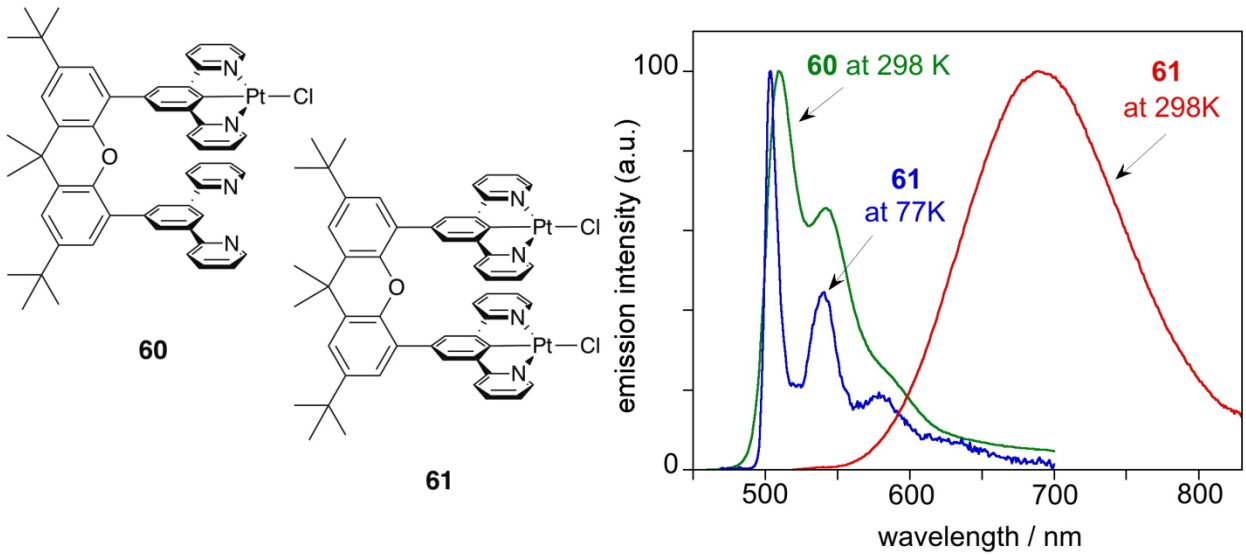

Figure 27 Mono- and diplatinum complexes **60** and **61**, their emission spectra in CH_2Cl_2 at room temperature, and the emission spectrum of **61** at 77 K (in diethyl ether / isopentane / ethanol, 2:2:1 v/v) [78].

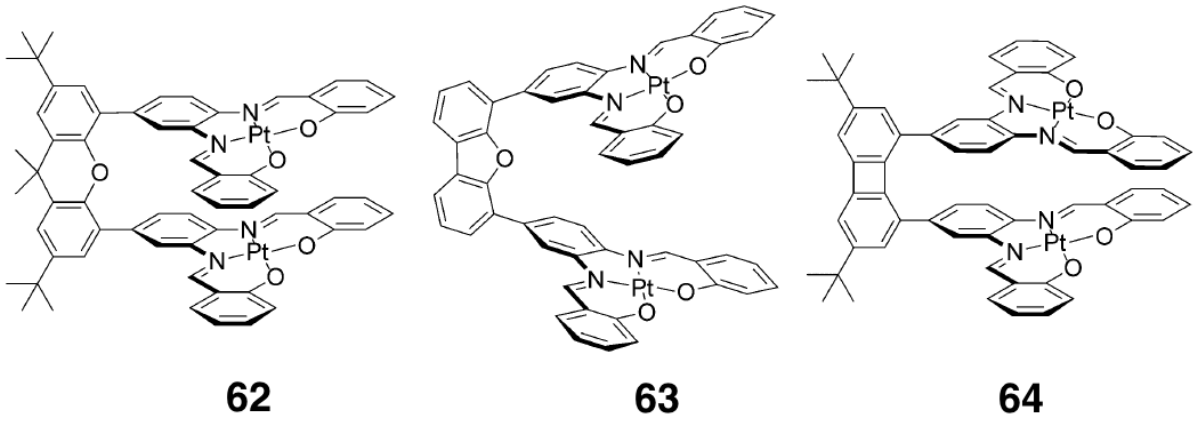

Figure 28 Dinuclear platinum(II) complexes **62**, **63** and **64** featuring Pt(salphen) units bridged by xanthene, dibenzofuran and biphenylene respectively. Reproduced from [80] by permission of John Wiley & Sons Ltd.

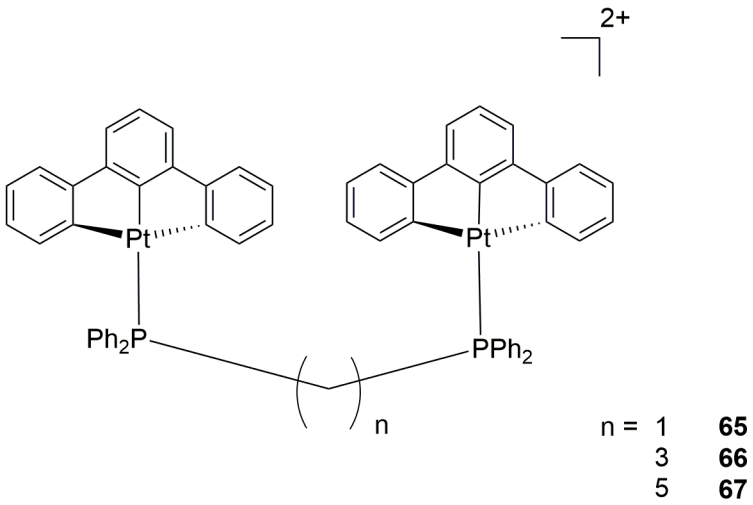

Figure 29 Structure of Pt complexes **65-67** linked by phosphino bridges.

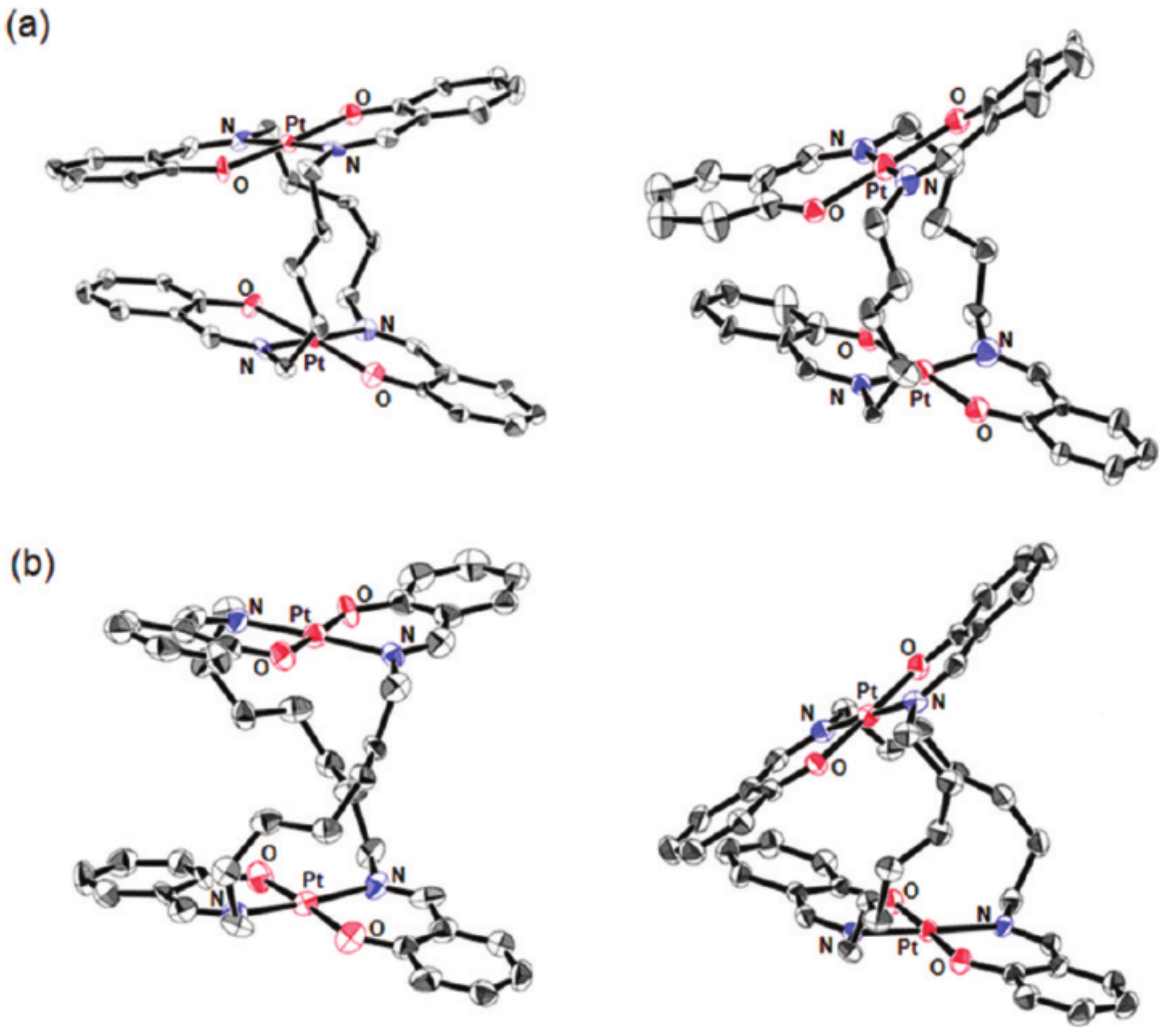

Figure 30 ORTEP representation of (a) (R) anti-**68a** and (b) (R) anti-**68c** as their racemic (left) and optically pure (right), (+) form crystals. Thermal ellipsoids are shown at the 50% probability level. Reproduced with permission from [86]. Copyright 2011 American Chemical Society.

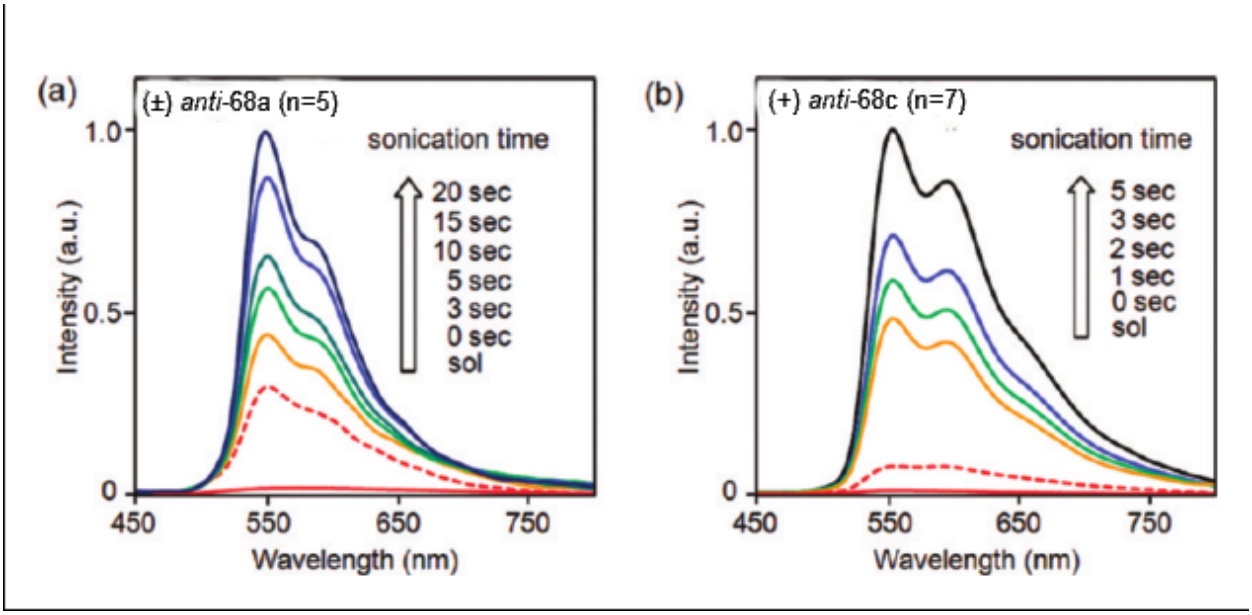

Figure 31 Emission spectra of gels of (a) (±) anti-**68a** (1.50×10^{-3} M) and (b) (+) anti-**68c** (2.20×10^{-3} M) in cyclohexane generated by sonication (44 kHz, 0.31 W/cm^2) for various sonication times ($\lambda_{ex} = 420$ nm, 293 K). Dashed line: a spontaneous gel formed by standing at room temperature for 1 h without sonication. Reproduced with permission from [86]. Copyright 2011 American Chemical Society.

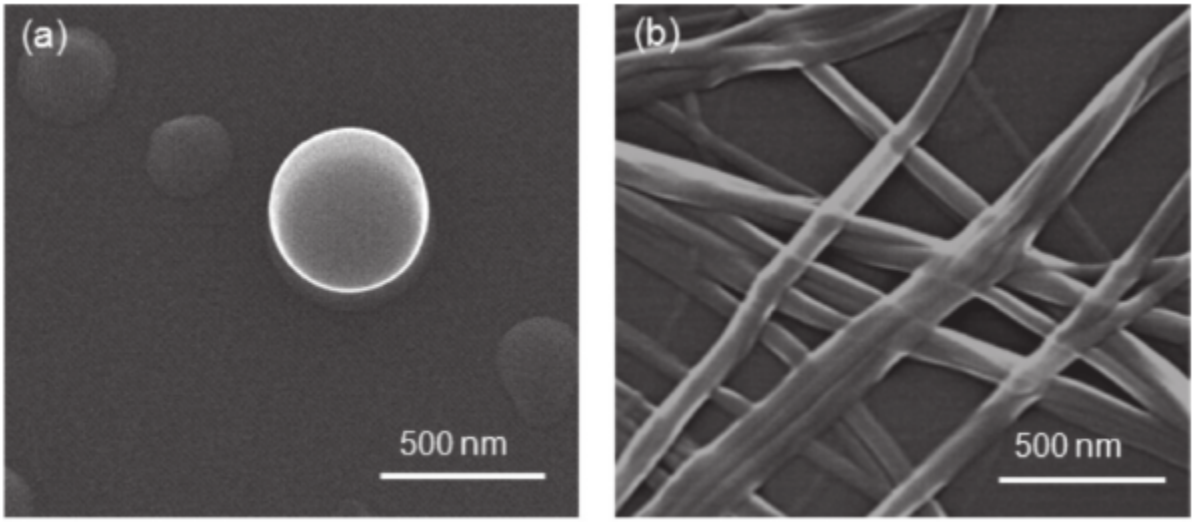

Figure 32 SEM images of dried ((±) anti-**68a** aggregates prepared from a 1.50×10^{-3} M solution in cyclohexane by various methods. (a) Solution prepared freshly; (b) gel just after brief sonication (44 kHz, 0.31W/cm^2, 3 s). Reproduced with permission from [86]. Copyright 2011 American Chemical Society.

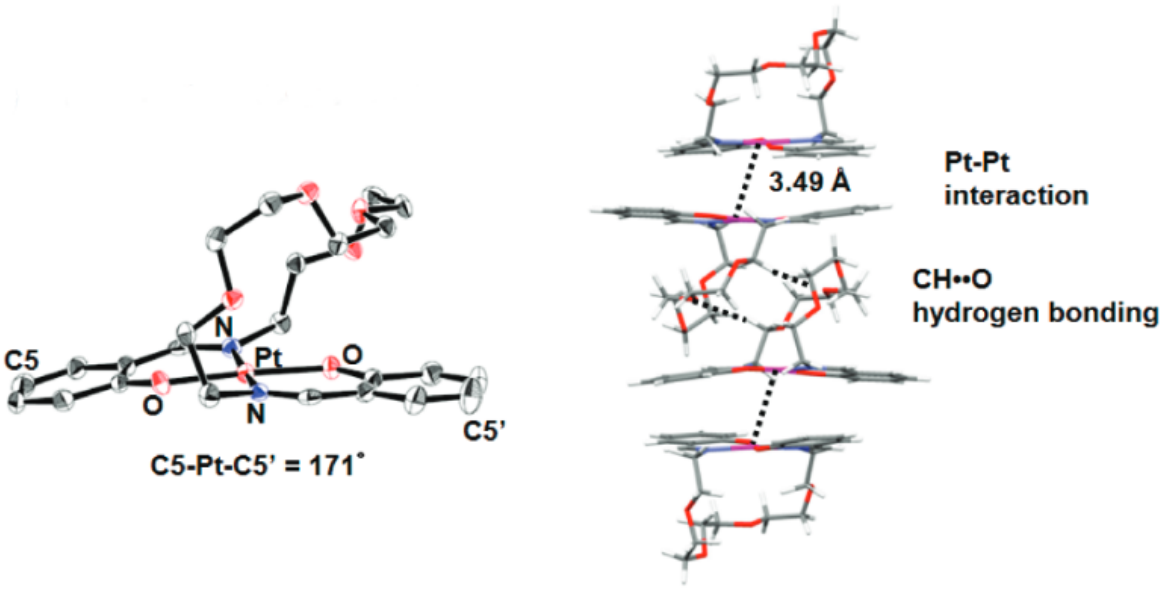

Figure 33 Molecular structure and packing of mononuclear complex **69**. Reproduced with permission from [87]. Copyright 2011 American Chemical Society.

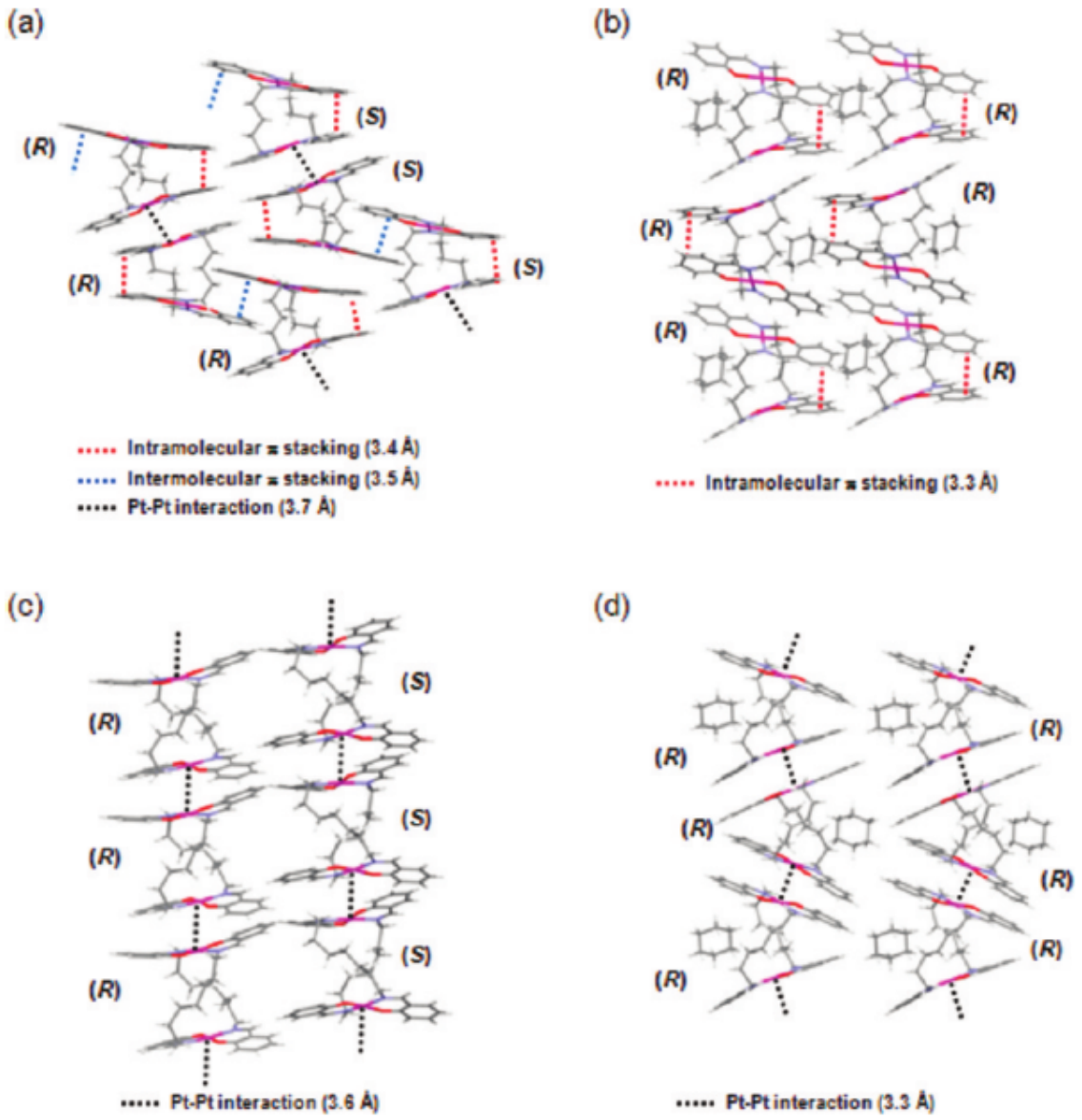

Figure 34 Packing of dinuclear complexes (a) (±) anti-**68a**, (b) (+) (R) anti-**68a**.C_6H_{12}, (c) (±) anti-**68c**, and (d) (+) (R) anti-**68c**.2.5C_6H_{12} in the crystalline state. Reproduced with permission from [86]. Copyright 2011 American Chemical Society.

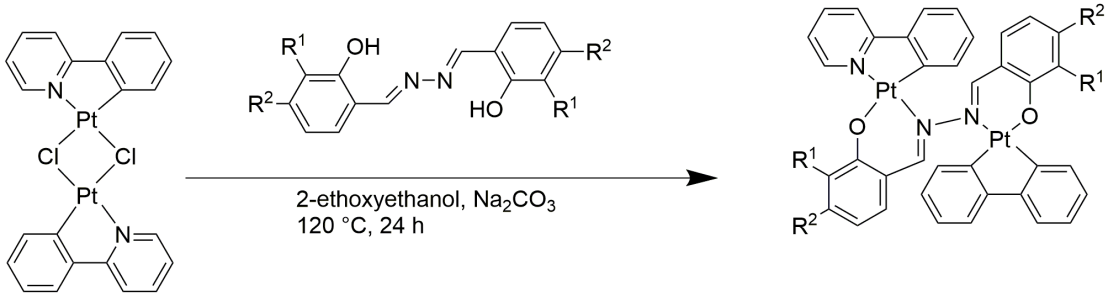

70: R^1=R^2=H	**QY (%) =**	10.5	**Lifetime (μs)** = 0.79
71: R^1=-OMe, R^2=H		15.0	1.23
72: R^1=H, R^2=-NEt_2		7.5	1.44

Figure 35 Synthesis of [(ppy)Pt(μ-SA)Pt(ppy)] complexes **70-72**. Quantum yield and lifetimes in powder form.

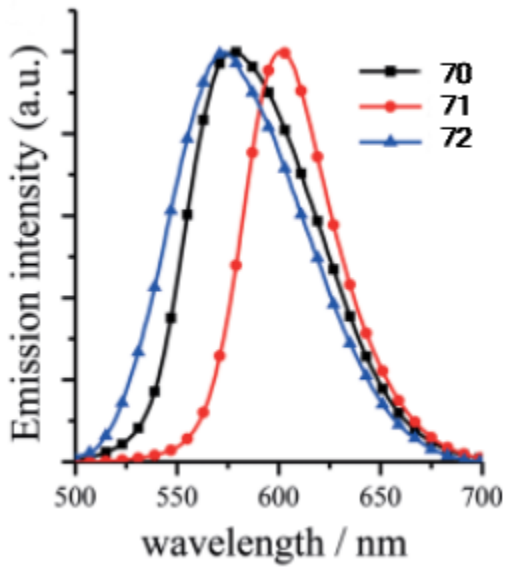

Figure 36 Normalized emission spectra of complex **70**–**72** powders. Reproduced from [88] by permission of John Wiley & Sons Ltd.

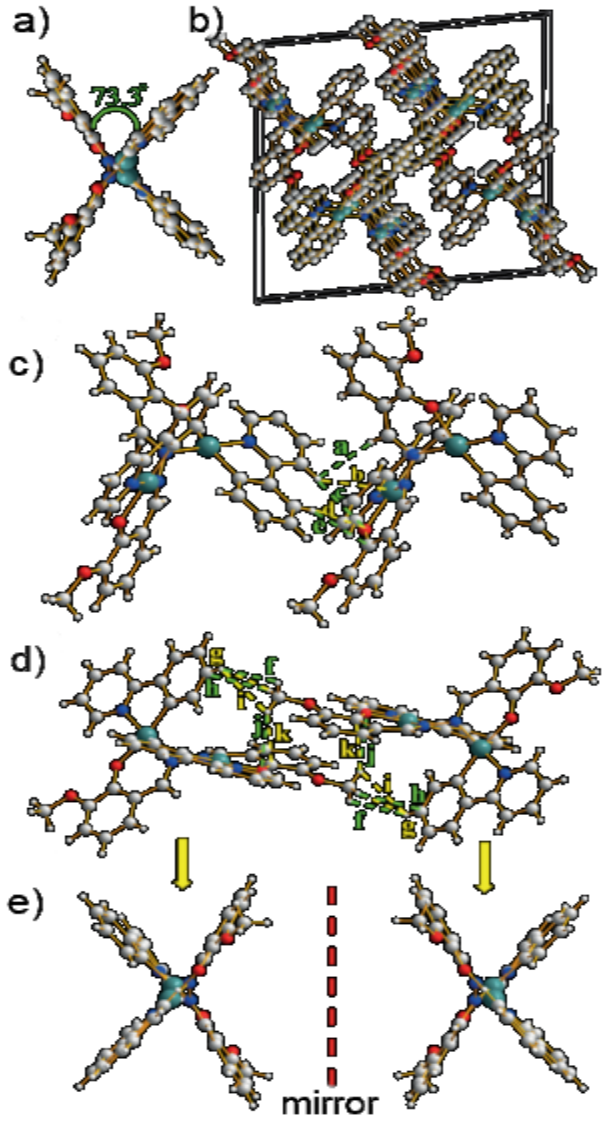

Figure 37 Single-crystal X-ray diffraction structure and packing of molecules of **71**: (a) side view; (b) packing (H atoms are omitted); (c,d) intermolecular interactions of the two closest enantiomers where a= 2.7844 Å, b= 2.9459 Å, c = 2.8566 Å, d= 2.7803 Å, e= 2.7085 Å, f= 2.6169 Å, g= 2.5737 Å, h = 2.9393 Å, i= 2.9639 Å, j= 2.9647 Å, k= 2.8314 Å; (e) enantiomers of **71**. Reproduced from [88] by permission of John Wiley & Sons Ltd.

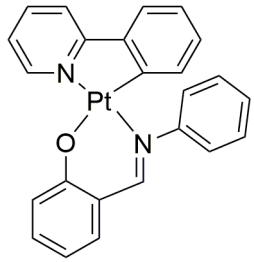

Figure 38 Structure of complex **73**.

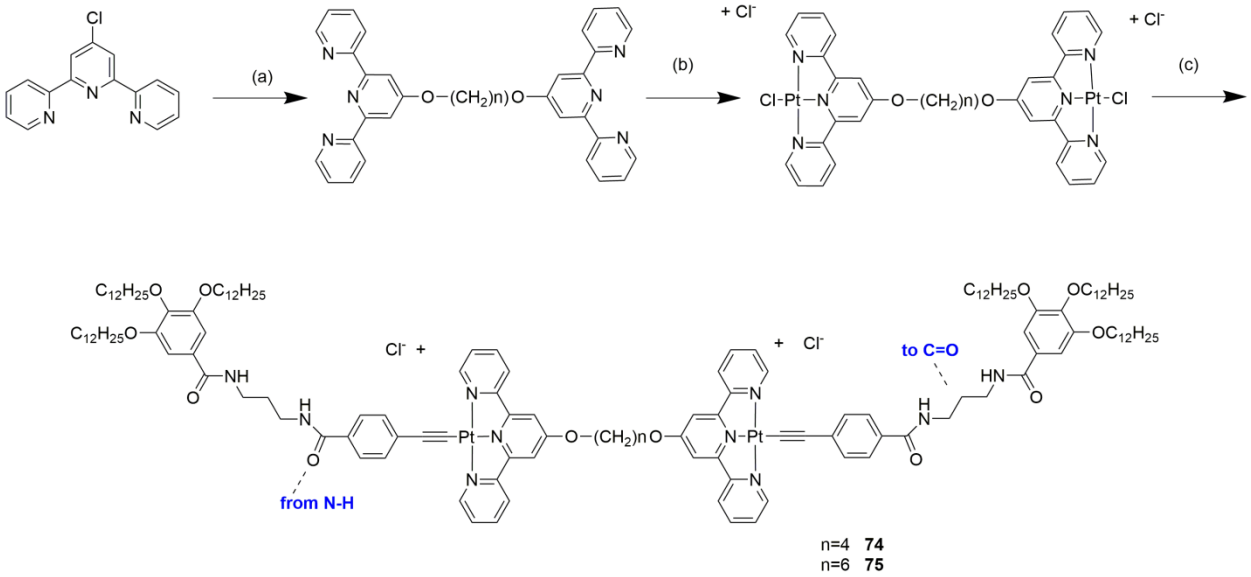

Figure 39 Chemical structures and synthesis routes of **74** and **75**. (a) 1,6- Hexanediol or 1,4-butanediol, DMSO, KOH; (b) K_2PtCl_4,CH_3CN, H_2O; (c) dodecyloxy-terminal alkyne, CuI, DMF, TEA.

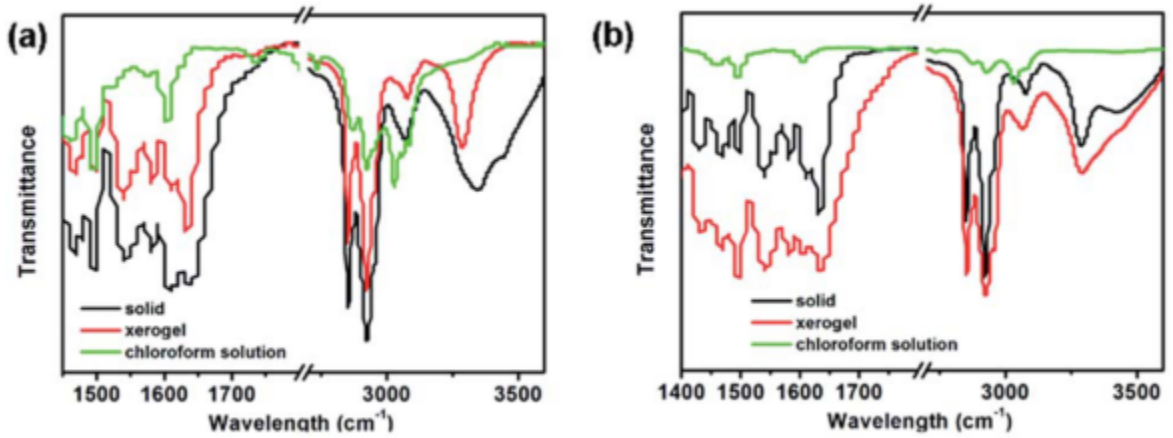

Figure 40 The FT-IR spectra **74** (a) and **75** (b) in solid, xerogel (obtained from toluene) and chloroform solution. Reproduced from [90] by permission of The Royal Society of Chemistry.

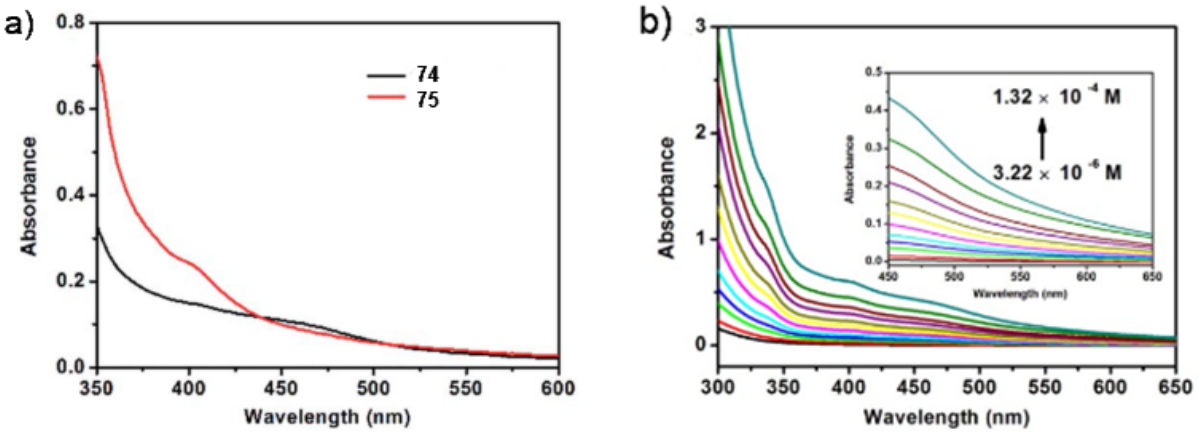

Figure 41 UV-vis absorption (a) comparison of **74** and **75** in DMSO solution at 2.2×10^{-5} M concentration (b) spectral changes of **74** in different concentrations of DMSO solution. Reproduced from [90] by permission of The Royal Society of Chemistry.

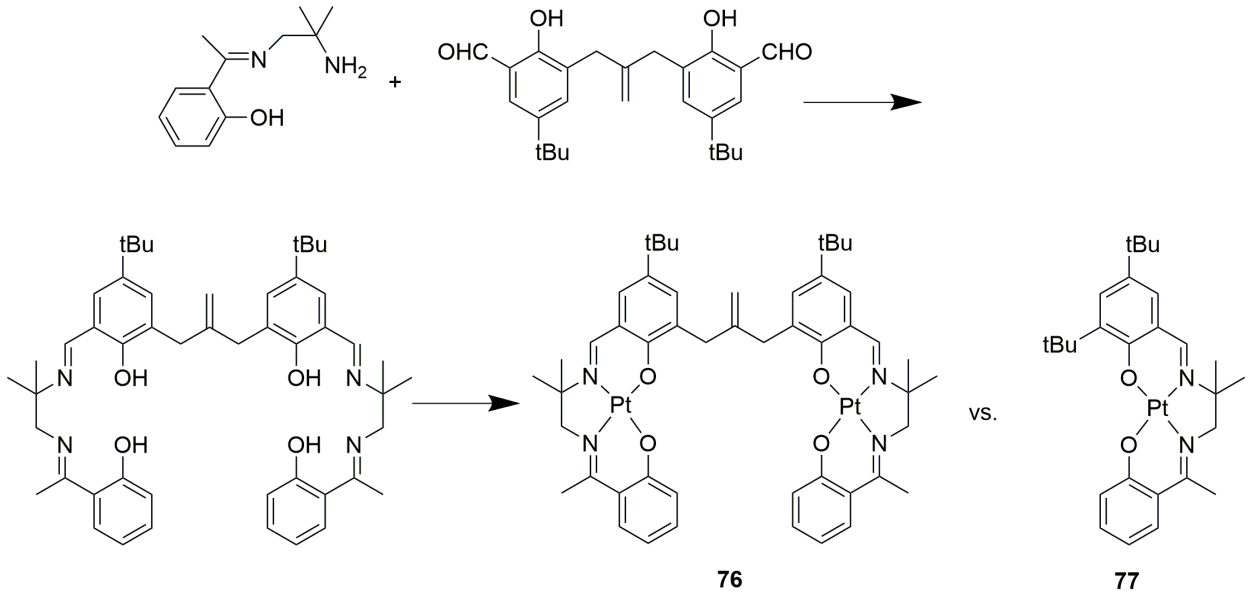

Figure 42 Synthesis of the dinuclear bis-salen complex **76** and the structure of the mononuclear complex **77**.

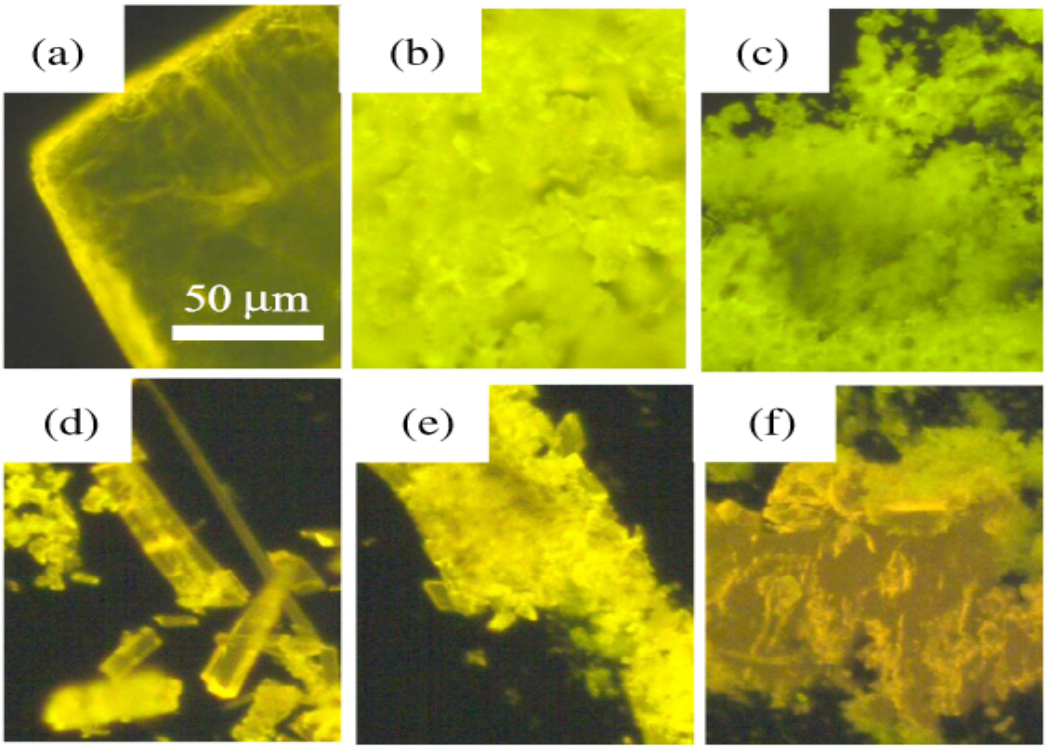

Figure 43 Microscopic fluorescence images of **77** (a–c) and **76** (d–f). (a, d) Microscale single crystals, (b, e) crushed microcrystals, and (c, f) samples smeared on a glass slide. Reproduced from [93] by permission of Elsevier.

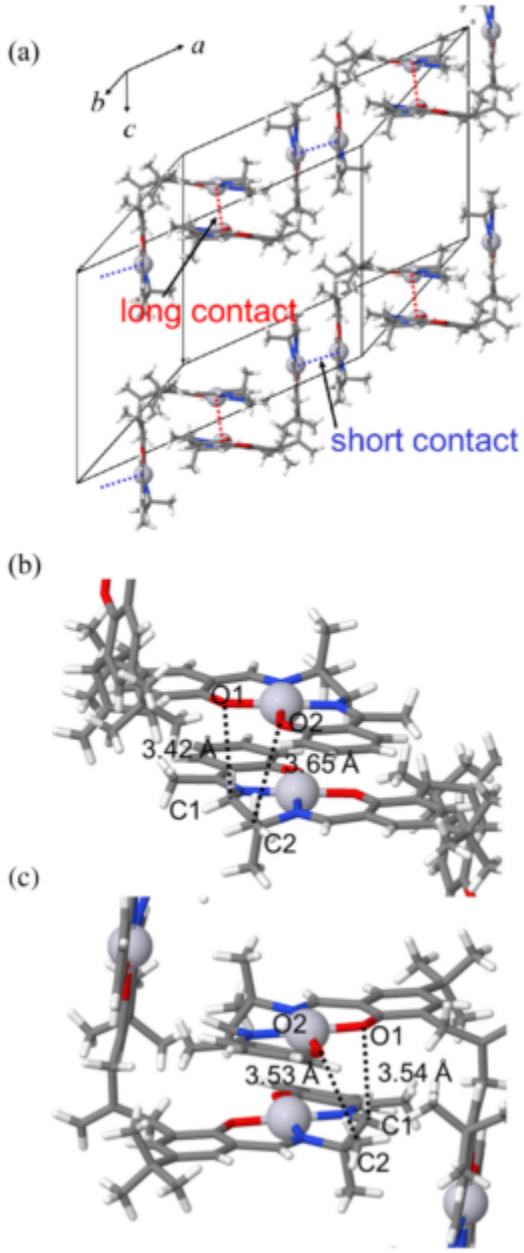

Fig. 44 Crystal structure of complex **76**. (a) The zigzag network composed of the stacked salen pair. A close-up of the (b) short contact and (c) long contact around the stacked pairs. Reproduced from [93] by permission of Elsevier.

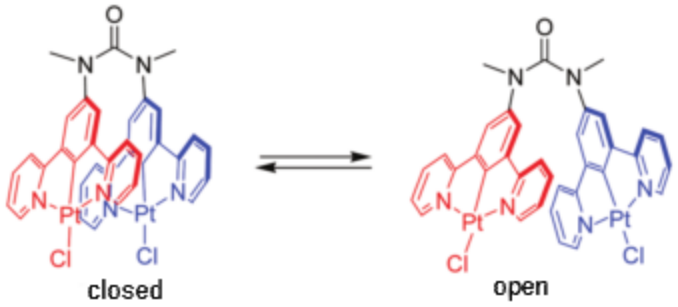

Figure 45 Diplatinum complex **78** that switches between the closed and the open form. Reproduced from [95] by permission of The Royal Society of Chemistry.

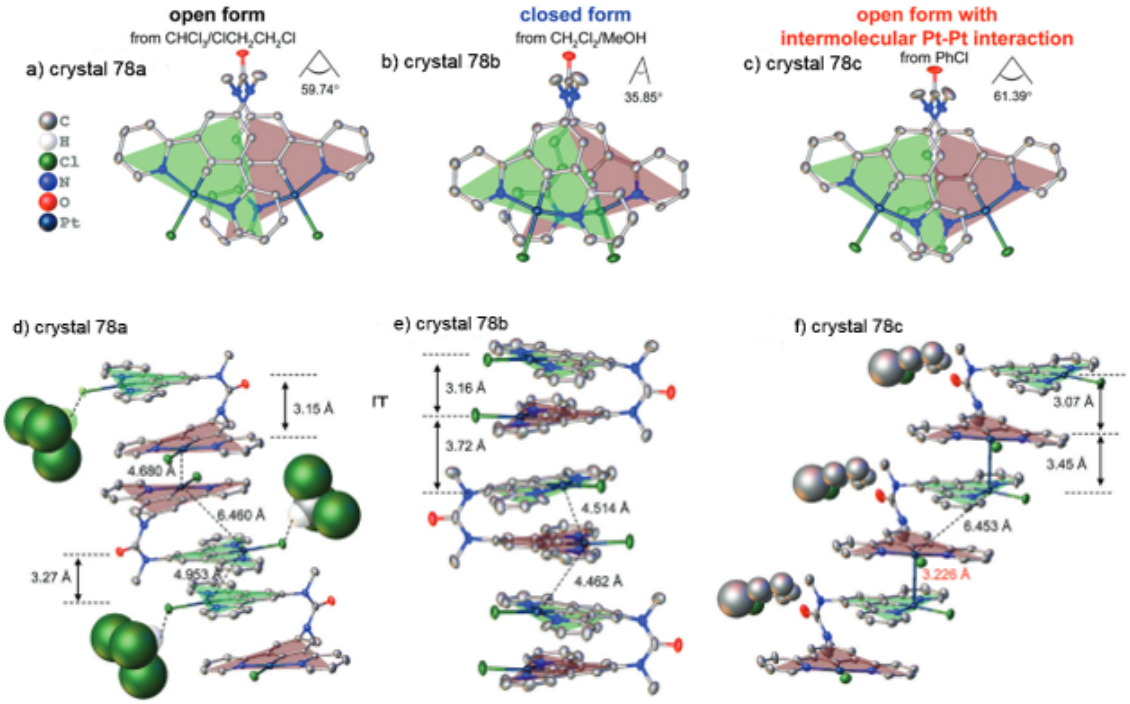

Figure 46 Thermal ellipsoid plots (a-c) and crystal packing (d-f) of three different single-crystal forms of complex **78** at 30 % probability. Reproduced from [95] by permission of The Royal Society of Chemistry.

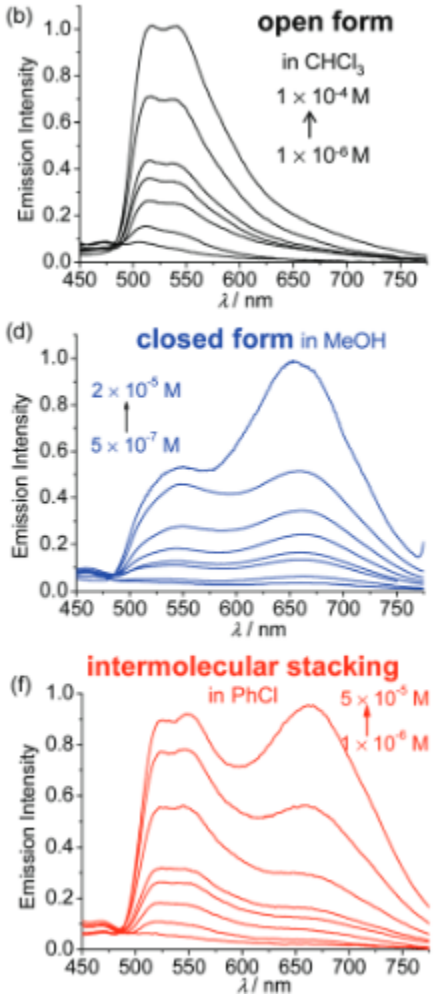

Figure 47 Emission spectral changes of complex **78** in (a) $CHCl_3$, (b) MeOH, and (c) PhCl, as a function of concentration. Reproduced from [95] by permission of The Royal Society of Chemistry.

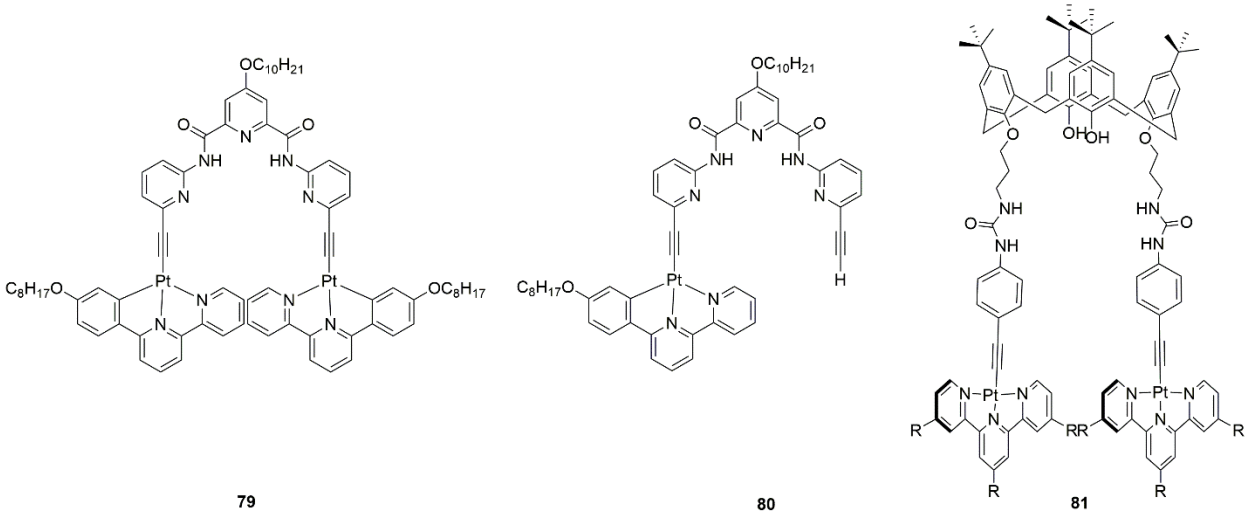

Figure 48 Pt complexes **79-81**.

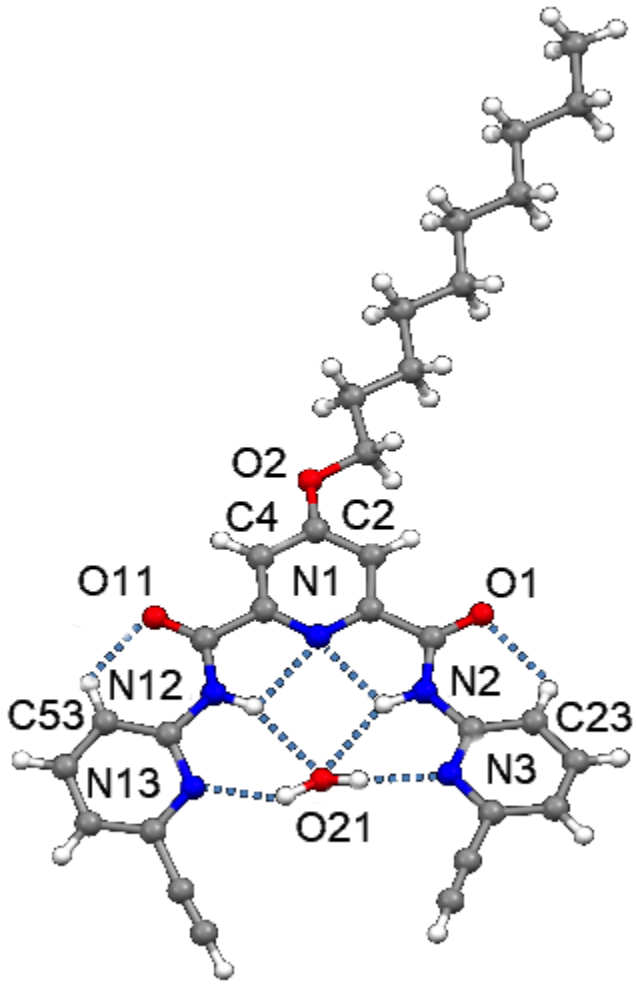

Figure 49 Crystal structure of the ligand for complex **79**. Reproduced from [98] by permission of The Royal Society of Chemistry.

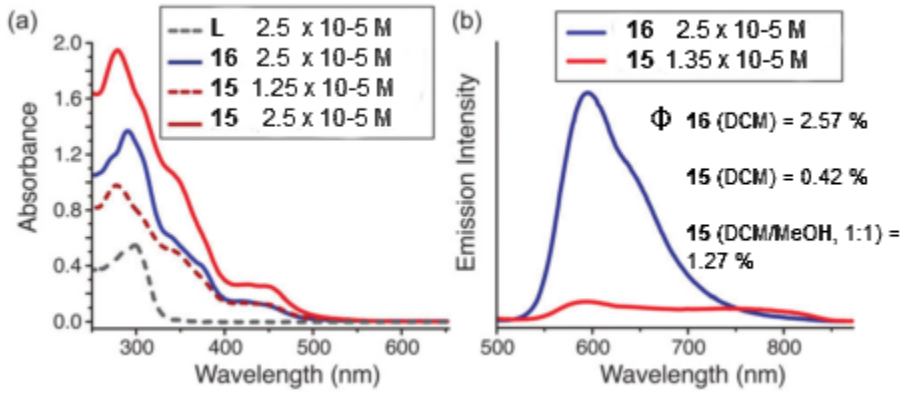

Figure 50 (a) UV-vis spectra of complexes **79** and **80** at different concentrations and (b) emission spectra of complexes **79** and **80** at different concentrations, all measured in DCM at 298 K. Reproduced from [98] by permission of The Royal Society of Chemistry.

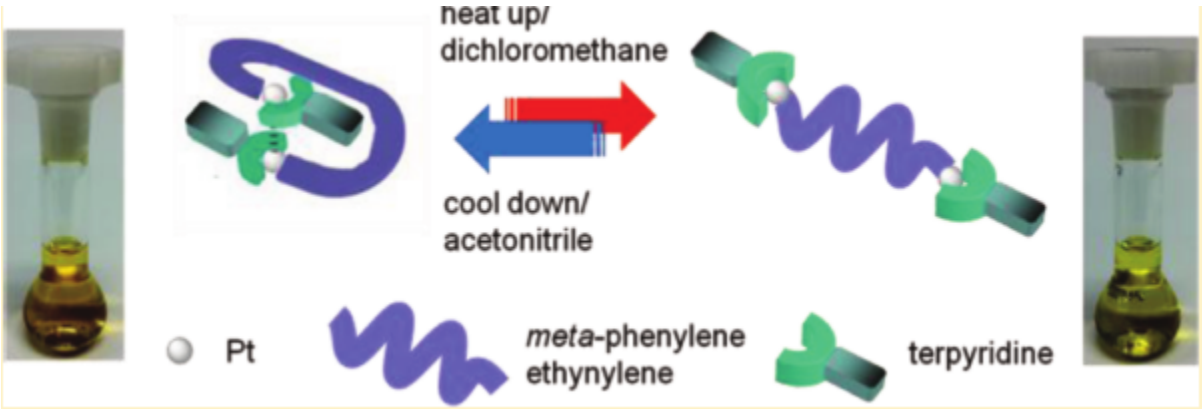

Figure 51 Folding and unfolding of complexes based on solvent and temperature modulation. Reproduced with permission from [100]. Copyright 2012 American Chemical Society.

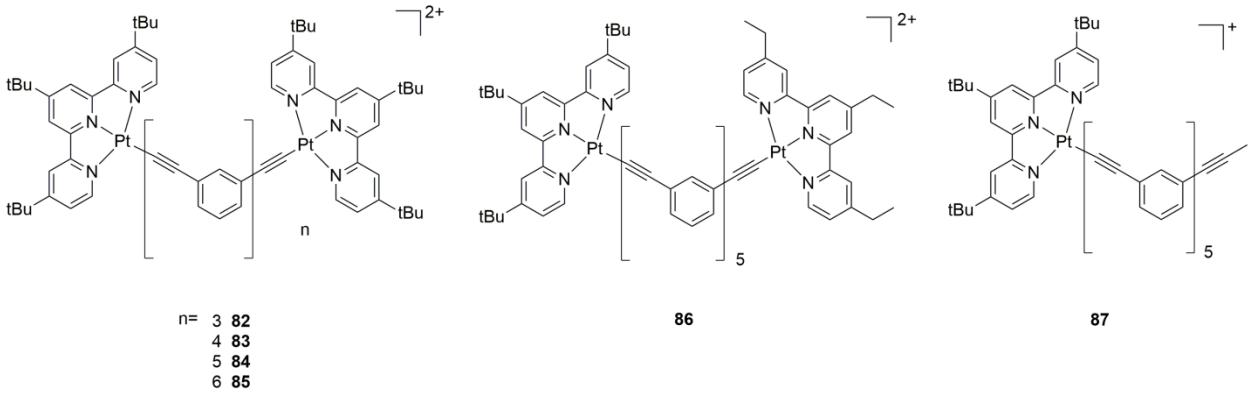

Figure 52 Structures of the dinuclear Pt complexes **84**-**86** and mononuclear Pt complex **87**.

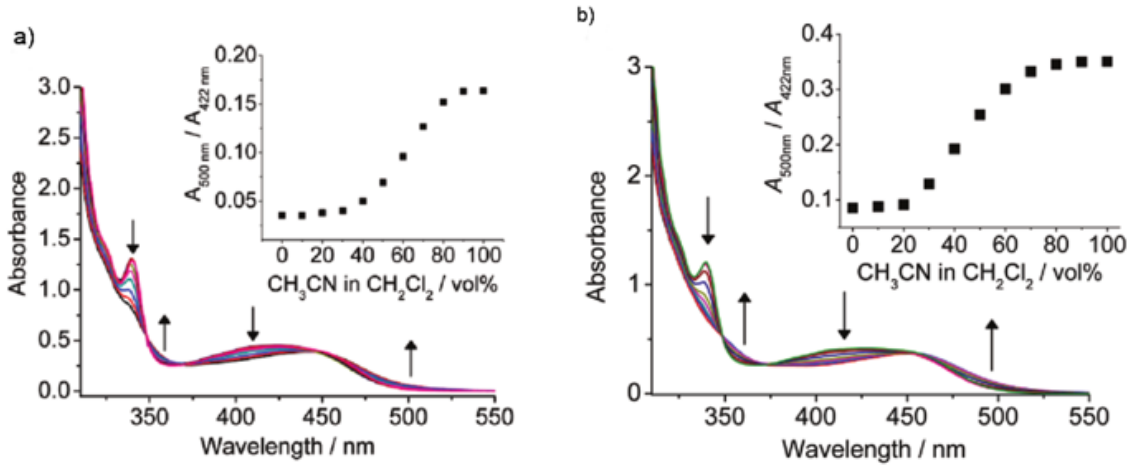

Figure 53 UV-vis absorption spectra of (a) complex **84** and (b) complex **86** with increasing CH_3CN content in DCM solution. The inset shows the absorbance ratio $A_{500\ nm}/A_{422\ nm}$ as a function of solvent compositions. Reproduced with permission from [100]. Copyright 2012 American Chemical Society.

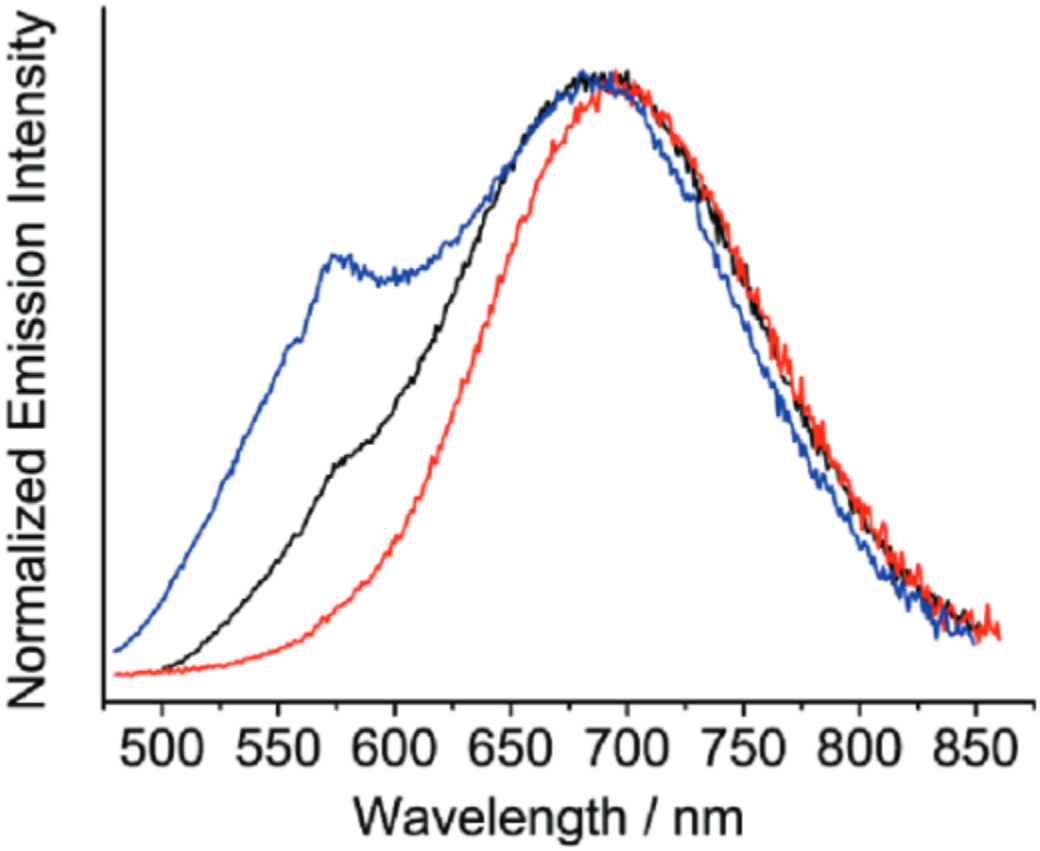

Figure 54 Emission spectra of CH_3CN for **84** (black), **85** (blue), and **86** (red) at 298 K in DCM. Reproduced with permission from [100]. Copyright 2012 American Chemical Society.

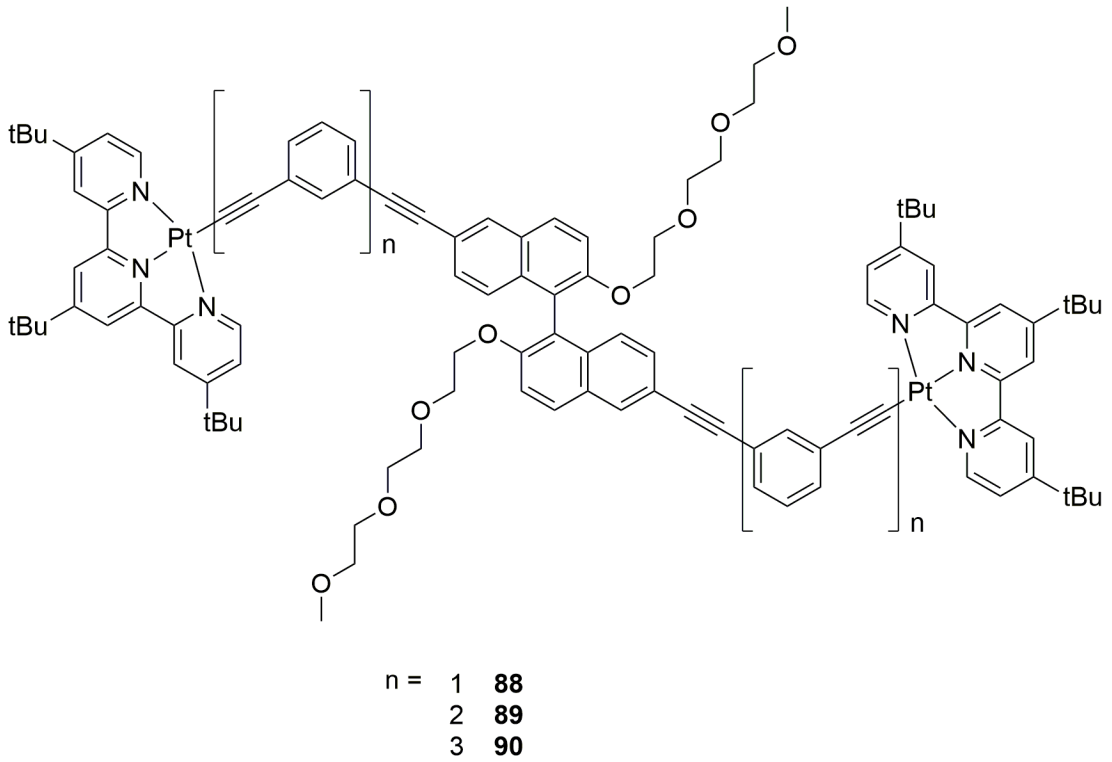

n = 1 **88**
2 **89**
3 **90**

Figure 55 Structure of dinuclear Pt complexes **88-90** with modified mPE bridges.

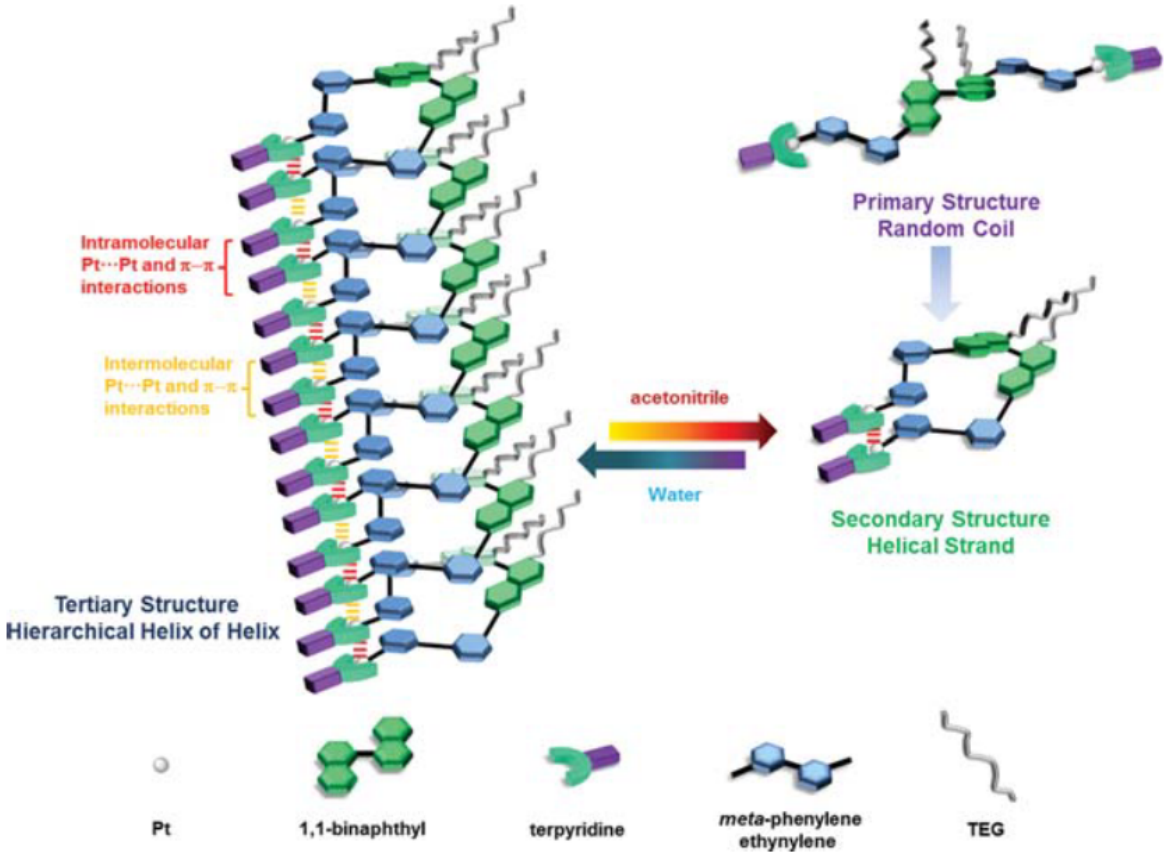

Figure 56 Helical arrangement of complexes **89** and **90**. Reproduced from [101] by permission of The Royal Society of Chemistry.

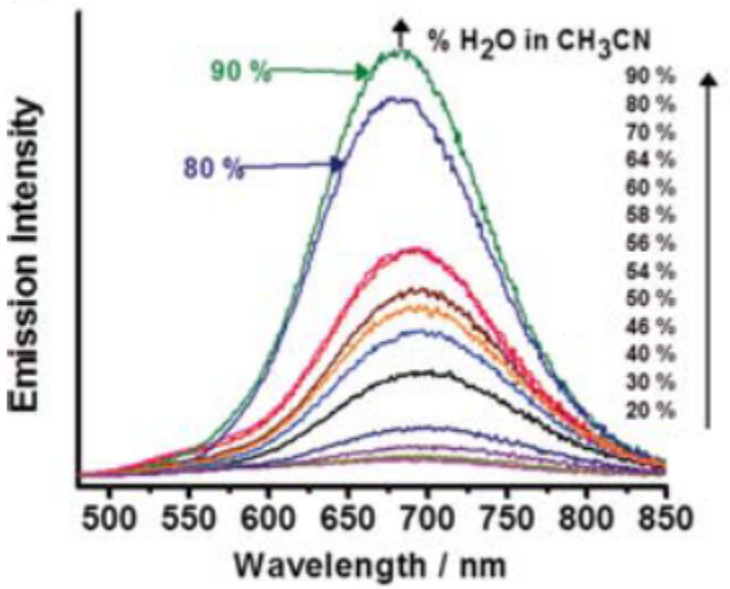

Figure 57 Luminescence enhancement of complex **89** on increasing the water content of solutions. Reproduced from [101] by permission of The Royal Society of Chemistry.

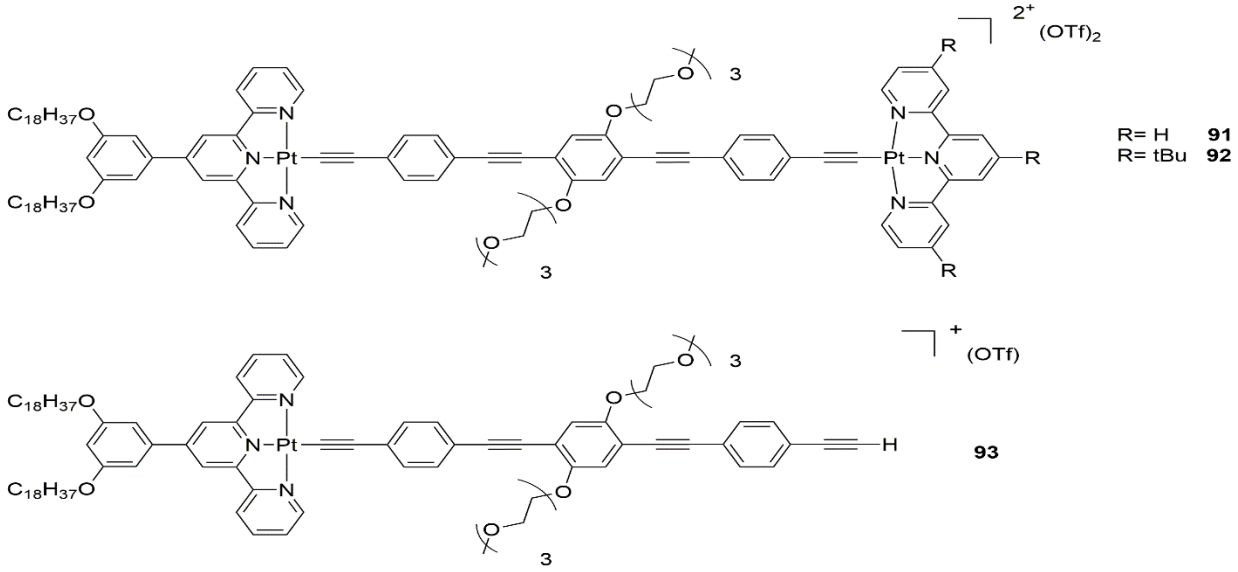

Figure 58 Structures of complexes **91**-**93**.

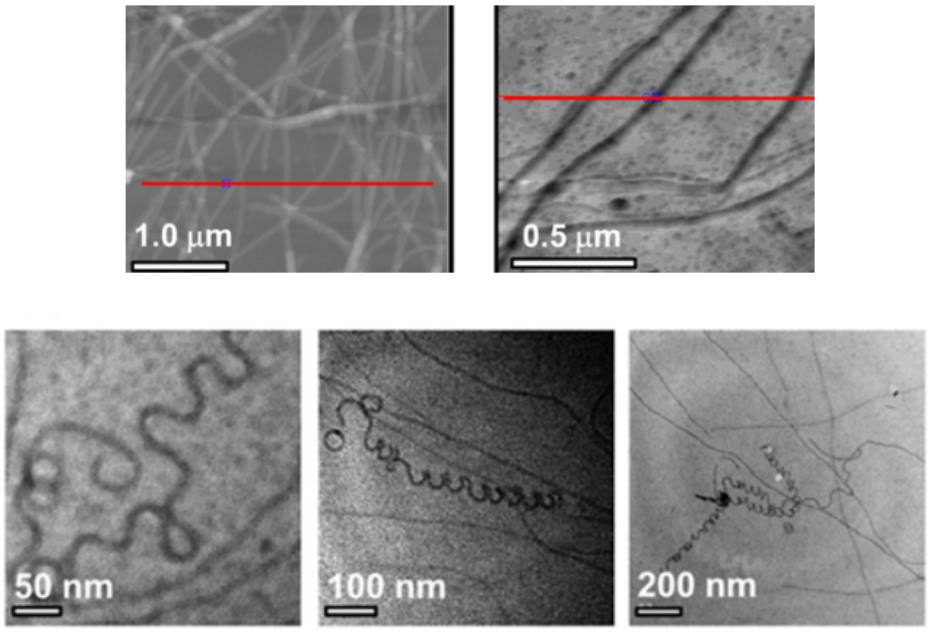

Figure 59 AFM images of complex **91** (upper) and complex **92** (lower). Reproduced from [102] by permission of Proceedings of the National Academy of Sciences of the United States of America.

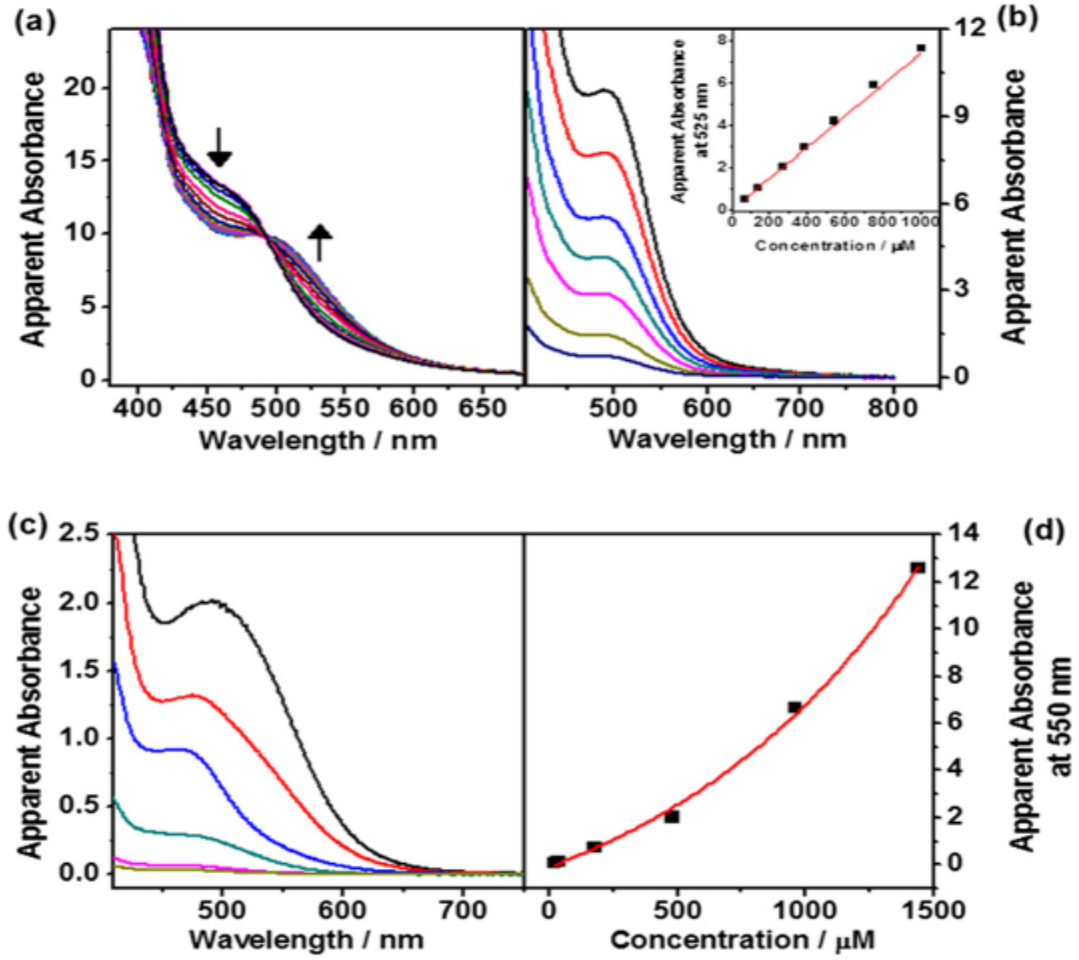

Figure 60 (a) UV-vis absorption spectral traces of **93** in DMSO ([Pt]=843 μM) on increasing temperature. (b) UV-vis absorption spectral changes of **93** in DMSO as the concentration is increased from 69 to 1,005 μM. (Inset) A plot of the apparent absorbance of **93** at 525 nm as a function of concentration. (c) UV-vis absorption spectral changes of **91** in DMSO as the concentration is increased from 17 to 1,442μM. (d) A plot of the apparent absorbance of **27** at 550 nm as a function of concentration. Reproduced from [102] by permission of Proceedings of the National Academy of Sciences of the United States of America.

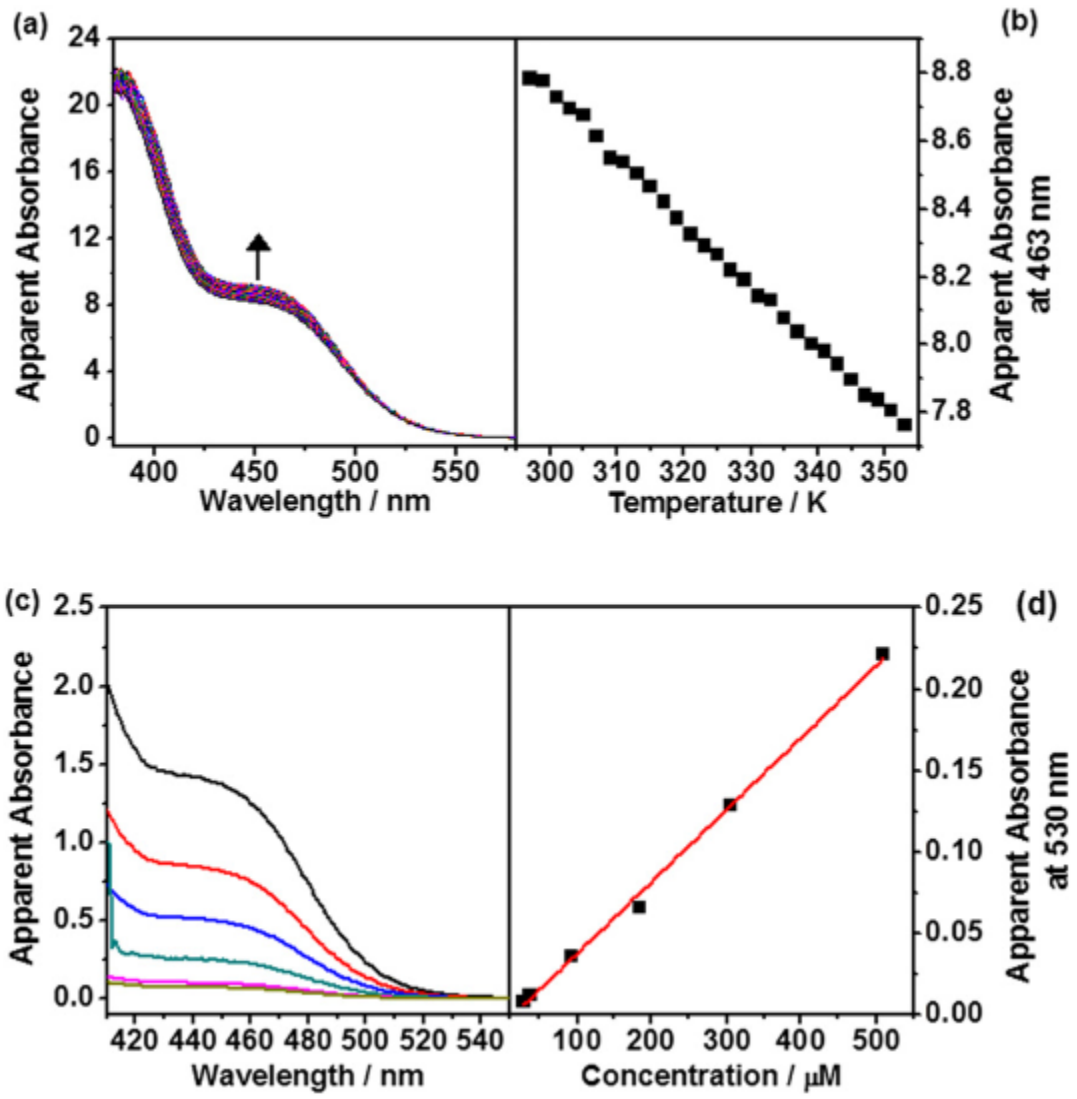

Figure 61 (a) UV-vis absorption spectral traces of **92** in DMSO ([Pt]=360 μM) on decreasing temperature and (b) plot of absorbance at 463 nm vs. Temperature from 353 to 297 K. (c) UV-vis absorption spectral changes of **92** in DMSO as the concentration is increased from 28 to 510μM. (d) A plot of the apparent absorbance at 530 nm as a function of concentration. Reproduced from [102] by permission of Proceedings of the National Academy of Sciences of the United States of America.

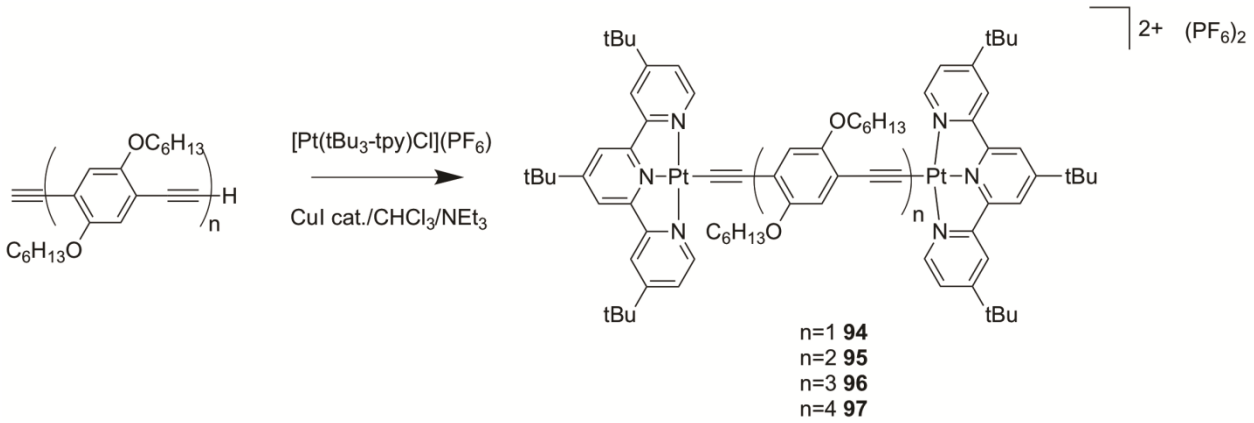

Figure 62 Synthesis of Pt terpyridyl complexes **94-97** reported by Du et al.

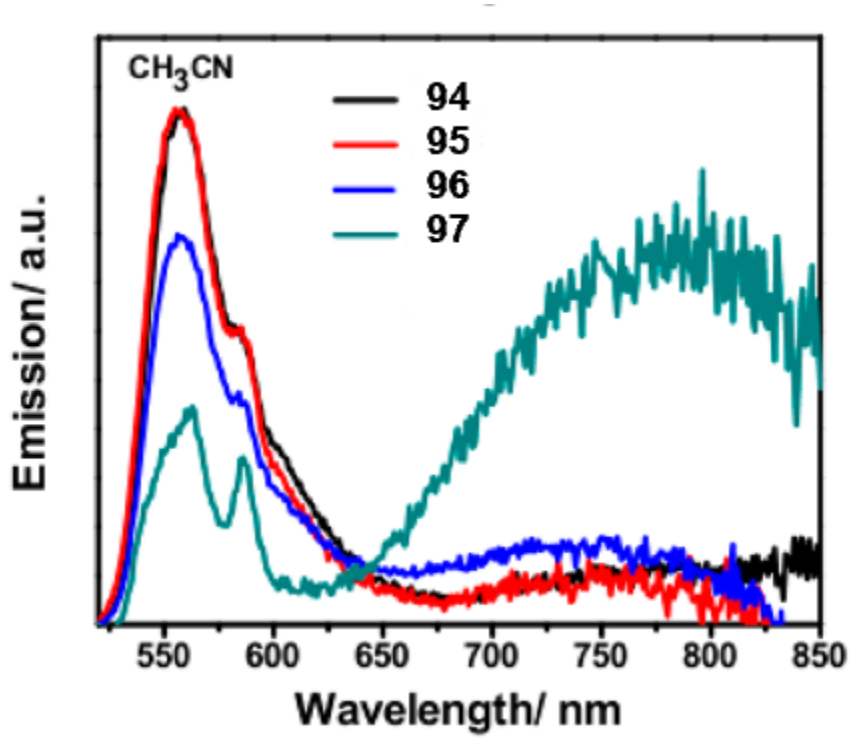

Figure 63 Emission spectra of complexes **94–97** in CH_3CN at 298 K (concentration 1×10^{-5} M, λ_{ex} 500 nm. Reproduced with permission from [103]. Copyright 2012 American Chemical Society.

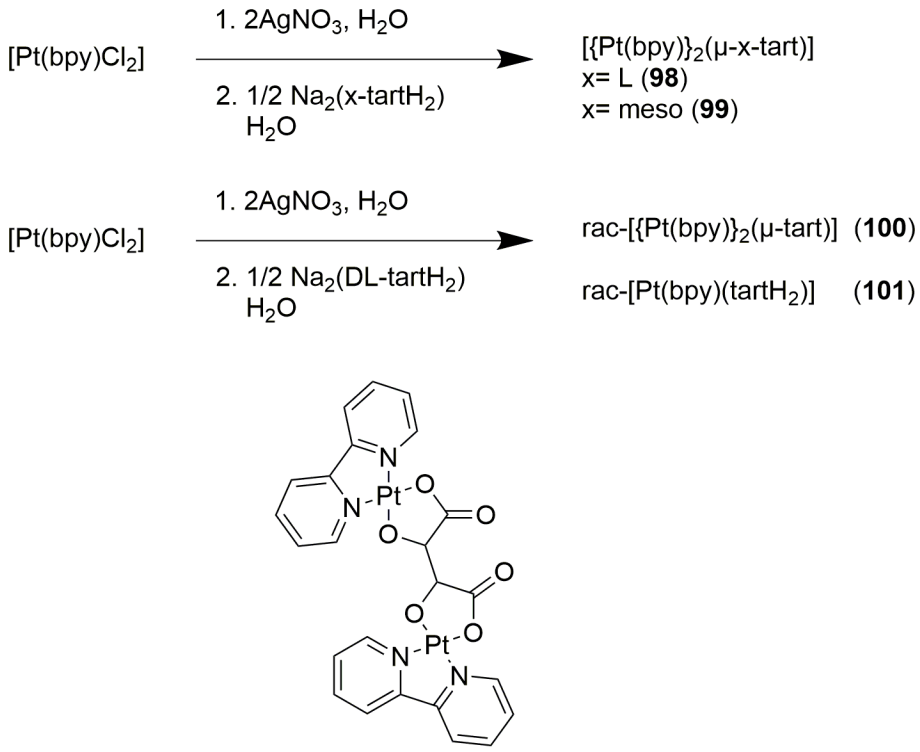

Figure 64 Synthesis of complexes **98**-**101**.

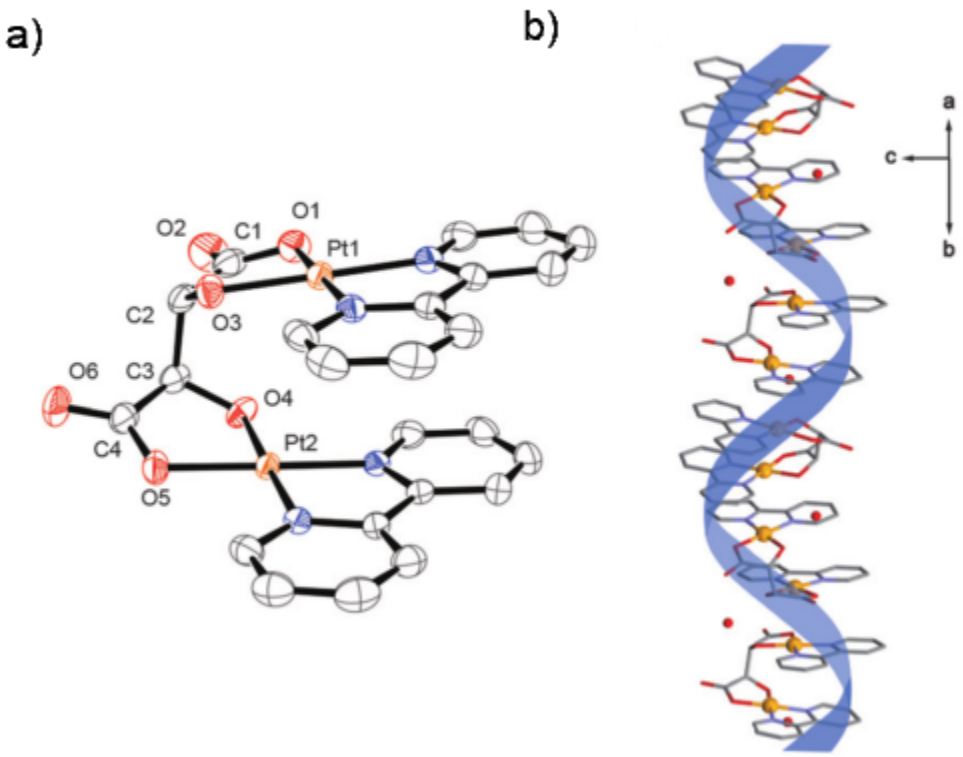

Figure 65 (a) Clamshell-like form of the dinuclear complex **98**, (b) crystal structures of the right-handed helical structure **98α**. Reproduced from [105] by permission of The Royal Society of Chemistry.

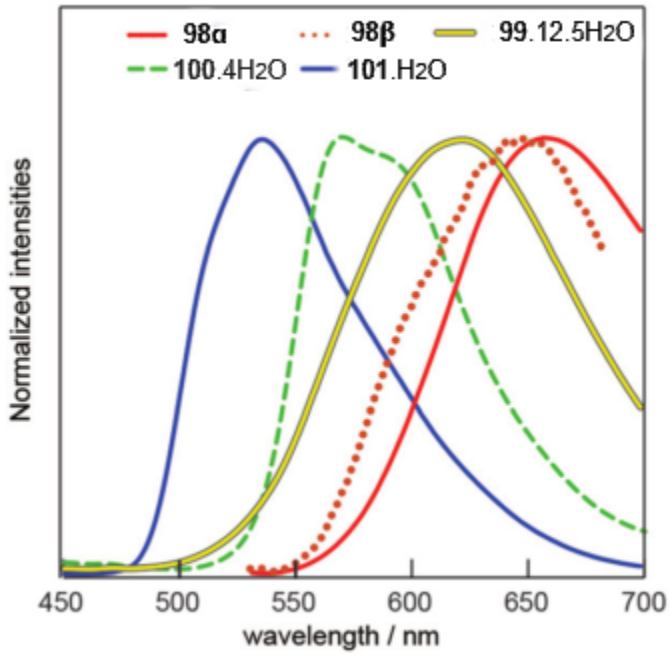

Figure 66 Luminescence spectra (λ_{ex} = 365 nm) of **98α**, **98β**, **99**·12.5H_2O, **100**·4H_2O, and **101**·H_2O at room temperature. Reproduced from [105] by permission of The Royal Society of Chemistry.